



January 2019

## Supercritical Water Desalination: Model-Predicted NaCl Concentration Comparison

Sebastian David Gardner

Follow this and additional works at: <https://commons.und.edu/theses>

---

### Recommended Citation

Gardner, Sebastian David, "Supercritical Water Desalination: Model-Predicted NaCl Concentration Comparison" (2019). *Theses and Dissertations*. 2849.  
<https://commons.und.edu/theses/2849>

This Thesis is brought to you for free and open access by the Theses, Dissertations, and Senior Projects at UND Scholarly Commons. It has been accepted for inclusion in Theses and Dissertations by an authorized administrator of UND Scholarly Commons. For more information, please contact [zeineb.yousif@library.und.edu](mailto:zeineb.yousif@library.und.edu).

SUPERCRITICAL WATER DESALINATION:  
MODEL-PREDICTED NaCl CONCENTRATION COMPARISON

by

Sebastian David Gardner  
Bachelor of Arts, Concordia College, 2015  
Bachelor of Arts, Concordia College, 2015


A Thesis  
Submitted to the Graduate Faculty  
of the  
University of North Dakota  
in partial fulfillment of the requirements  
for the degree of  
Master of Science

Grand Forks, North Dakota

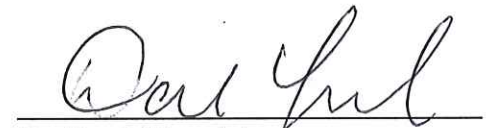
December  
2019

© 2019 Sebastian David Gardner

This thesis, submitted by Sebastian Gardner in partial fulfillment of the requirements for the Degree of Master of Science from the University of North Dakota, has been read by the Faculty Advisory Committee under whom the work has been done and is hereby approved.

  
Dr. Michael Mann

  
Dr. Edward Kolodka

  
Dr. Daniel Laudal

This thesis is being submitted by the appointed advisory committee as having met all of the requirements of the School of Graduate Studies at the University of North Dakota and is hereby approved.

  
Chris Nelson  
Dean of the School of Graduate Studies

11/20/19  
Date

## PERMISSION

Title                                      Supercritical Water Desalination: Model-Predicted NaCl  
Concentration Comparison

Department                              Chemical Engineering

Degree                                      Master of Science

In presenting this thesis in partial fulfillment of the requirements for a graduate degree from the University of North Dakota, I agree that the library of this University shall make it freely available for inspection. I further agree that permission for extensive copying for scholarly purposes may be granted by the professor who supervised my thesis work or, in his absence, by the Chairperson of the department or the dean of the School of Graduate Studies. It is understood that any copying or publication or other use of this thesis or part thereof for financial gain shall not be allowed without my written permission. It is also understood that due recognition shall be given to me and to the University of North Dakota in any scholarly use which may be of any material in my thesis.



\_\_\_\_\_  
Sebastian Gardner

12/2/19

\_\_\_\_\_  
Date

## **ACKNOWLEDGMENTS**

I wish to express my sincere appreciation to the members of my advisory committee: Dr. Michael Mann, Dr. Edward Kolodka, and Dr. Dan Laudal, for their guidance and support during my time in the master's program at the University of North Dakota. I would like to express my gratitude to the members of the Institute for Energy Studies for assisting me along the way in my research and coursework, especially, Harry Feilen, Nic Dyrstad-Cincotta, Teagan Nelson, Joshua Oluwayomi, Junior Nasah, and Nolan Theaker. I would also like to extend a sincere thank you to Dr. Srivats Srinivasachar of Envergex for his technical guidance and support throughout my work here at the University of North Dakota. This thesis would not have been possible had it not been for the generous efforts of those aforementioned as well as others not mentioned here.

For Taylor, always.

## **ABSTRACT**

Freshwater availability is increasingly becoming a concern for various parts of the world. Seawater desalination is becoming more commonplace as a source for freshwater in water-stressed regions such as California and the Middle East. Reverse osmosis is the most commonly employed technology for seawater desalination thanks to its ability to operate at a large scale, producing freshwater from seawater with relative ease. There are other sources of water which need to be desalinated, however, which reverse osmosis systems cannot effectively treat.

Unconventional oil and gas extraction, commonly known as fracking, produces vast amounts of wastewater with high TDS levels (approximately 100,000-300,000 mg/L) and dissolved organics, known as produced water, which cannot be effectively treated by conventional desalination technologies. Supercritical water desalination is currently being explored as a solution produced water desalination. Supercritical water desalination takes advantage of water's unique properties beyond its critical pressure and temperature which result in substantially lower solubility for inorganic salts.

Designing a supercritical desalination system requires extensive knowledge of fluid properties as well as salt solubilities across a wide temperature and pressure range. Obtaining this information experimentally is expensive and time-consuming. Utilizing a high fidelity model to produce key system properties can improve desalination system design in an efficient manner.



This research aims to evaluate various concentration models, and thus their underlying formulation methods, and determine which model yields the most accurate concentration results for a produced water sample across the temperature range 25-450 °C at 240 bar. It is hypothesized that an empirically-derived model will outperform a conventional thermodynamic-based model for concentration determination at these elevated conditions.

This research was accomplished by comparing the predicted concentrations of a NaCl-H<sub>2</sub>O solution produced by the concentration models: HSC, PHREEQC, AspenPlus, and SoWat to experimental data across the aforementioned process conditions. The predicted NaCl concentration produced by each model was evaluated to determine its ability to accurately predict concentration at elevated conditions.

The empirically-derived SoWat model predicted NaCl concentration curve outperformed the concentration curves produced HSC, PHREEQC, and AspenPlus when comparing with experimental data. This model can be confidently utilized to develop a supercritical water desalination system as its predicted results are accurate. The employment of a high fidelity model such as SoWat will drastically reduce the cost and time required to develop an effective supercritical water desalination system.

## TABLE OF CONTENTS

ACKNOWLEDGEMENTS.....	v
ABSTRACT.....	vi
LIST OF FIGURES.....	xii
LIST OF TABLES.....	xiv
1 INTRODUCTION, OBJECTIVE, and OUTLINE.....	1
1.1 Introduction.....	1
1.2 Objective.....	2
1.3 Outline.....	3
1.4 References.....	4
2 CURRENT TECHNOLOGIES.....	5
2.1 Background.....	5
2.2 The Problem.....	6
2.3 Current Technologies.....	8
2.3.1 Reverse Osmosis.....	8
2.3.2 Thermal Desalination.....	12
2.3.2.1 Vapor Compression (VC).....	12
2.3.2.2 Multi-effect Distillation (MED).....	15
2.3.2.3 Multi-stage Flash Distillation (MSF).....	18
2.4 Supercritical Water Desalination.....	21
2.4.1 Theory.....	21

2.4.2	Barriers to Implementation.....	25
2.5	References.....	26
3	PREVIOUS SOLUBILITY WORK.....	28
3.1	Introduction.....	28
3.2	Bischoff and Pitzer NaCl Solubility.....	28
3.2.1	Background.....	29
3.2.2	Methods.....	29
3.2.3	Results.....	31
3.2.4	Discussion.....	35
3.3	Driesner NaCl-H <sub>2</sub> O Empirical Property Model.....	36
3.3.1	Background.....	38
3.3.2	Methods.....	40
3.3.3	Results.....	47
3.3.4	Discussion.....	54
3.4	Leusbrock Dissertation.....	55
3.4.1	Background.....	55
3.4.2	Methods.....	60
3.4.3	Results.....	61
3.4.4	Discussion.....	65
3.5	References.....	65
4	COMPARISON OF CONCENTRATION MODELS.....	69
4.1	Introduction.....	69
4.2	HSC Equilibrium Modeling.....	70

4.2.1	Theory.....	70
4.2.2	Methods.....	71
4.2.3	Results.....	72
4.2.4	Discussion.....	76
4.3	PHREEQC Species Distribution Modeling.....	76
4.3.1	Theory.....	77
4.3.2	Methods.....	78
4.3.3	Results.....	79
4.3.4	Discussion.....	82
4.4	AspenPlus Electrolyte Modeling.....	83
4.4.1	Theory.....	84
4.4.2	Methods.....	86
4.4.3	Results.....	87
4.4.4	Discussion.....	91
4.5	SoWat Empirical NaCl-H <sub>2</sub> O Property Model.....	92
4.5.1	Theory.....	92
4.5.2	Methods.....	93
4.5.3	Results.....	94
4.5.4	Discussion.....	99
4.6	Comparison of Models.....	100
4.6.1	Methods.....	101
4.6.2	Results.....	102
4.6.3	Discussion.....	104

4.7	References.....	106
5	SUMMARY AND FUTURE WORK.....	108
5.1	Summary of Work Performed.....	108
5.1.1	HSC Equilibrium Modeling.....	108
5.1.2	PHREEQC Species Distribution Modeling.....	109
5.1.3	AspenPlus Electrolyte Modeling.....	110
5.1.4	SoWat Empirical NaCl-H <sub>2</sub> O Property Modeling.....	110
5.1.5	Comparison of Models.....	111
5.2	Summary of Findings.....	111
5.3	Future Work.....	113
5.4	References.....	116
	APPENDIX.....	117
	Appendix A: Raw Simulation Data.....	A1-A8

## LIST OF FIGURES

2.1: Water Distribution on Earth.....	6
2.2: Reverse Osmosis Process Schematic.....	9
2.3: Reverse Osmosis Plant Layout.....	11
2.4: MVC and TVC Process Schematic.....	14
2.5: MED Process Schematic.....	17
2.6: MSF Process Schematic.....	19
2.7: Pure Water Phase Diagram.....	22
2.8: Hypothetical SCWD Process Schematic.....	24
3.1: Bischoff and Pitzer Experimental Apparatus.....	30
3.2: Isobar P-T-x Diagram for 3.2 wt% NaCl-H <sub>2</sub> O Solution.....	31
3.3: Isotherm P-T-x Diagram in Subcritical Region.....	33
3.4: Isotherm P-T-x Diagram in Supercritical Region.....	34
3.5: T-P-x Diagram of H <sub>2</sub> O-NaCl.....	39
3.6: Driesner Model-Predicted NaCl Vapor Pressure.....	47
3.7: Driesner Model-Predicted NaCl Melting Curve.....	48
3.8: Driesner Model-Predicted Critical Pressure.....	49
3.9: Driesner Model-Predicted Critical Composition.....	50
3.10: Driesner Model-Predicted Density.....	51
3.11: Driesner Model-Predicted Isobaric Specific Heat Capacity.....	53
3.12: Density and Dielectric Constant as a Function of Temperature.....	56

3.13: NaCl Solubility as a Function of Temperature.....	57
3.14: Solubility of NaCl as a Function of Density.....	58
3.15: Leusbrock Experimental Apparatus.....	60
3.16: Na <sub>2</sub> SO <sub>4</sub> Solubility as a Function of Density.....	61
3.17: NaNO <sub>3</sub> Solubility as a Function of Density.....	62
3.18: NaCl Solubility as a Function of Density.....	63
3.19: KCl Solubility as a Function of Density.....	64
4.1: HSC-Predicted NaCl Concentration for a 10 wt% Solution.....	73
4.2: HSC-Predicted Ion Concentration for a Produced Water Sample.....	74
4.3: HSC-Predicted Concentration for Produced Water (Less Prevalent Ions).....	75
4.4: PHREEQC-Predicted NaCl Concentration for a 10 wt% Solution.....	79
4.5: PHREEQC-Predicted Ion Concentration for Produced Water.....	81
4.6: AspenPlus-Predicted NaCl Concentration for a 10 wt% Solution.....	87
4.7: AspenPlus-Predicted Ion Concentration for Produced Water.....	89
4.8: AspenPlus-Predicted Concentration for Produced Water (Less Prevalent Ions).....	90
4.9: SoWat-Predicted NaCl Concentration for a 10 wt% Solution.....	95
4.10: SoWat-Predicted NaCl Concentration with Predicted Phases Present.....	96
4.11: SoWat-Predicted Density for a 10 wt% NaCl-H <sub>2</sub> O Solution.....	97
4.12: SoWat-Predicted Specific Heat Capacity for a 10 wt% NaCl-H <sub>2</sub> O Solution.....	98
4.13: Comparison of Predicted NaCl Concentration for a 3.2 wt% NaCl Solution.....	102
5.1: Leusbrock Experimental Apparatus.....	115

## LIST OF TABLES

2.1: Summary of Current Desalination Technologies.....	20
3.1: Parameters for NaCl Melting, Boiling, and Sublimation Curve.....	42
3.2: Parameters for Critical Curve.....	43
3.3: Parameters for Critical Composition.....	44
3.4: Parameters for NaCl Density.....	45
3.5: Parameters for Enthalpy and Isobaric Heat Capacity.....	46
3.6: Properties of Water.....	55
3.7: Fitting Parameters for Equation 3.16.....	61
4.1: Produced Water Sample Composition.....	72
A.1: HSC 10 wt% NaCl Raw Simulation Data.....	A1
A.2: HSC Produced Water Raw Simulation Data.....	A2
A.3: PHREEQC 10 wt% NaCl Raw Simulation Data.....	A3
A.4: PHREEQC Produced Water Raw Simulation Data.....	A4
A.5: AspenPlus 10 wt% NaCl Raw Simulation Data.....	A5
A.6: AspenPlus Produced Water Raw Simulation Data.....	A6
A.7: SoWat 10 wt% NaCl Raw Simulation Data (Part 1).....	A7
A.8: SoWat 10 wt% NaCl Raw Simulation Data (Part 2).....	A8



# **Chapter 1: Introduction, Objective, and Outline**

## **1.1 Introduction**

Unconventional oil and gas extraction techniques such as fracking have drastically altered the freshwater availability across the United States. A single fractured well uses approximately 5,600,000 gallons of fresh water during the initial drilling and hydraulic fracturing phase of the well's life [1]. The amount of freshwater required for a single basin where hydraulic fracturing is being utilized is astronomical when considering that there are over 12,000 wells operating in the Bakken basin in western North Dakota alone [2].

Hydraulically fractured wells produce a hyper saline waste product known as produced water. Produced water contains total dissolved solids (TDS) levels of 100,000-300,000 mg/L, depending on each well site. In 2007, the Argonne National Laboratory estimated that the total volume of produced water was 882,000,000,000 gallons [3]. This number has likely grown substantially in the last decade thus increasing the importance of developing technologies to deal with these large volumes of waste water.

Traditional desalination technologies are unable to effectively treat produced water streams thus deep well injection is being utilized as the most economical alternative. Supercritical water desalination is currently being investigated as a unique technological approach to treating produced water.

Supercritical water desalination takes advantage of the unique solubility characteristics of water near/above its critical pressure and temperature. In order to effectively and efficiently design technologies which can exploit supercritical water's solubility properties at these conditions, information regarding various inorganic salts' solubilities at these conditions is needed.

Experimental work can be performed to obtain the necessary solubility information however this can be expensive and time consuming. High fidelity models which can accurately predict the concentration behavior of a wide range of inorganic salts at high temperatures and pressures can be employed which drastically reduce the costs and time required for designing technologies. Certain models available today don't accurately predict concentration behavior at the near-critical and supercritical region of water; thus it is important to know what models perform best at these conditions so engineers can properly employ models with high accuracy.

## **1.2 Objective**

This work aims to determine the best modeling technique for predicting the concentrations of constituents of produced water across a range of temperatures in order to best design a supercritical water desalination system. This work hypothesizes empirical models which are derived from experimental data will outperform conventional models which utilize techniques such as "Gibbs energy minimization" with regards to model accuracy.

This work will be accomplished by comparing the predicted concentrations produced by the modeling programs HSC (Gibbs energy minimization), PHREEQC (utilizes a combination of experimental data and derived equilibrium constants), SoWat

(experimentally-derived empirical model), and AspenPlus (ELECNRTL property method) to experimental data. A sample of produced water sourced from the Bakken formation in western North Dakota has been analyzed for a full ion composition. This sample composition will serve as the modeled solution composition in the model comparison.

### **1.3 Outline**

Outside of the brief introduction presented in this chapter of the thesis, Chapter 2 will present current desalination technologies and their shortfalls with regards to treating produced water. This technology review includes reverse osmosis, vapor compression, multi-effect distillation, multi-stage flash distillation, and supercritical water desalination.

Chapter 3 of this thesis summarizes key relevant work in salt solubility in the near-critical and supercritical region of water. This summary of key solubility work includes work produced by Bischoff and Pitzer, Thomas Driesner, and Ingo Leusbrock. Their work was all summarized in context of the stated goals of this thesis.

Chapter 4 of this thesis contains results from various model predictions as well as their respective comparison to experimental data. The goal of this chapter is to present model variability and to identify the most accurate model for predicting the concentration of various constituents of produced water as a function of temperature.

Chapter 5 of this thesis serves as a summary of the modeling work completed. This chapter also looks ahead at what future work ought to be completed to gain a greater understanding of the problem being investigated.

#### 1.4 References

- [1] Ogden, D. D., and Trembly, J. P., “*Desalination of hypersaline brines via Joule-heating: Experimental investigations and comparison of results to existing methods,*” in *Desalination*, **2017**, vol. 424, pp. 149-158.
- [2] “*Current Active Drilling Rig List,*” Sourced from [dmr.nd.gov/oilgas/riglist.asp](http://dmr.nd.gov/oilgas/riglist.asp), accessed January 2019.
- [3] Veil, J., Clark, C., et al., “*Produced water volume estimates and management practices,*” in *SPE Prod. Oper.*, **2011**, vol 26, pp. 234-239.

## Chapter 2: Current Technologies

### 2.1 Background

Water is the foundation of life. A single statistic that supports this statement is this: approximately 351,000,000 L freshwater is consumed globally every second [1]. This number is likely to increase as the world's population has doubled in the last 40 years and is estimated to reach 9,000,000,000 by 2050 [2]. Demand for freshwater is growing at twice the projected population rate. Globally, approximately 70% of all freshwater consumed is due to agriculture, 20% is due to industry, and the remaining 10% is due to domestic use.

Nearly 40% of the world's population currently faces water shortages and this is expected to grow to 60% by 2050 [1]. As we consume more and more freshwater and in turn produce contaminated wastewater, new technologies are going to need to be utilized to effectively treat this contaminated water and yield consumable water in order to meet global demand. Water for use can be sourced from several different types of environments. The world's current distribution of water can be seen in **Figure 2.1**.

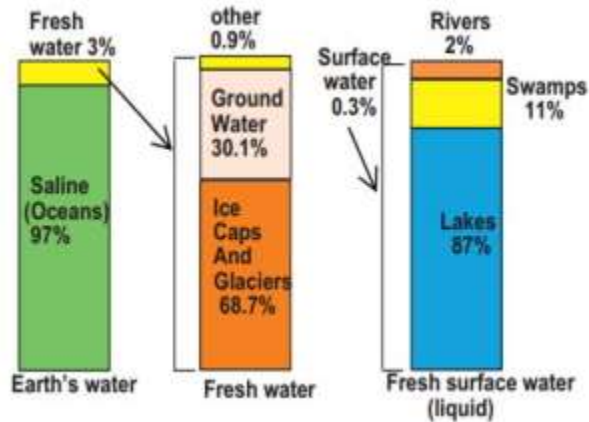


**Figure 2.1:** Water distribution on Earth [3]

As is seen in **Figure 2.1**, freshwater only makes up approximately 3% of the available water on Earth. When we disaggregate that 3% further, we can see that most of that water is currently locked up in ice caps and glaciers, thus not readily accessible for use. The ability to tap into the wealth of ocean water available on Earth and effectively treat it for a specified end-use would greatly improve our global water circumstances. Several desalination technologies in use today aim to tackle this problem and have managed to do so with some success. However, sea water isn't the only source of high-salinity water that needs to be treated.

## 2.2 The Problem

Adequate water treatment and purification are growing issues that the world faces today. Water shortages in more arid regions of the world have historically been the most common scenario in which the desalination of water was employed to seawater. The advent of unconventional oil/gas recovery methods which produce large quantities of

hypersalinated brines bring about new challenges and requirements to water desalination on top of existing seawater desalination.

The oil/gas industry is a large producer of hypersalinated brines due to fracking in unconventional reservoirs. Fracking yields approximately 3.8 million gallons of hypersalinated produced/flowback water per well with TDS levels of 200,000 mg/L and organics concentrations of ~2000 mg/L [4,5]. There are currently approximately 12,800 fracking wells operating in the Bakken in ND alone [6]. This means there are approximately  $4.9 \times 10^{10}$  gallons of hypersalinated water in the Bakken alone that must be treated by unconventional methods as its TDS levels are >45,000 mg/L and its organics concentrations are ~2,000 mg/L.

Currently this water is disposed of using deep well injection as it is the most economic method to deal with the water. However, some areas where this occurs have reportedly experienced increased seismic activity and many are pointing the finger at deep well injection as the reason why. With increased public scrutiny, an impending freshwater crisis, substantial environmental concerns, and constantly changing federal guidelines and mandates, companies are looking for new, more economic and environmentally benign methods for dealing with the large amounts of produced water from these well sites. In order to understand the new types of treatment methods being explored today, it's important to first understand how current desalination technologies work, and how they may fall-short with regards to effective produced water treatment.

## **2.3 Current Technologies**

### **2.3.1 Reverse Osmosis**

The most common method of water desalination is reverse osmosis (RO). There are approximately 18,000 reverse osmosis treatment plants operating worldwide [7]. RO plants can successfully treat inlet streams with total dissolved solids (TDS) levels of approximately 45,000 mg/L without substantial fouling which reduces their effectiveness. RO plants have an upper efficiency of approximately 45% for seawater feed streams which yield reject streams with TDS levels of approximately 100,000 mg/L [8]. These reject streams are unable to be recycled and treated by the RO system as the high TDS levels rapidly foul the membranes and thus they are dispensed back into the ocean, creating potential adverse environmental effects.

Reverse osmosis works by taking advantage of the diffusive nature of water. Water will move from areas of high concentration to low concentration, thus when a semi-permeable membrane is utilized to hold back inorganic salts, brines can be desalinated using osmosis. This phenomenon can be visualized in **Figure 2.2**.



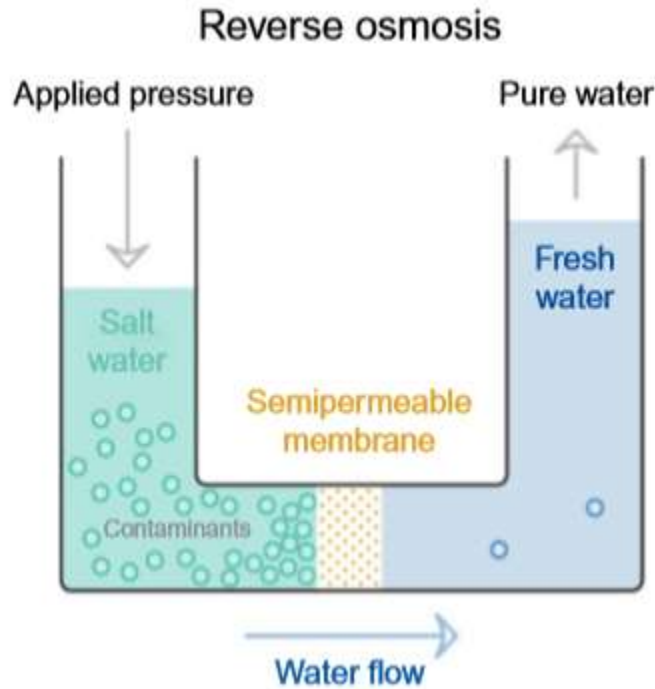


**Figure 2.2:** Process schematic of reverse osmosis desalination [9]

Reverse osmosis currently dominates the world’s desalination market, with only a few thermal desalination methods following behind. Together, reverse osmosis and thermal desalination methods generate 90% of the world’s desalinated water [10]. Reverse osmosis systems require a substantial energy input in order to adequately treat seawater. The energy requirement for a real-scale reverse osmosis plant is approximately 3.5-4.5 kWh/m<sup>3</sup> of water treated [11]. This substantial energy requirement would normally serve as a barrier to implementation of reverse osmosis plants at a greater scale, however, as more and more areas become stressed for fresh water there will be no choice but construct more RO capacity regardless of financial burden incurred.

Reverse osmosis plants begin operation by pumping a feed brine, most commonly seawater, through a pretreatment step. The pretreatment most commonly consists of filtering and chemical addition in order to remove larger particles that would quickly foul

the RO membranes. After pretreatment, the feed stream is brought to high pressure, typically 50-80 bar for seawater, using high pressure pumps prior to entering the RO membranes [12]. The high pressure is required in order for the feed stream to overcome the high osmotic pressure caused by the high salinity of the stream, and thus allow for desalination.

The high pressure feed stream is brought into the RO system and is pushed through the semi-permeable membrane resulting in a desalinated “clean” stream and a high concentrated “reject” stream. The clean stream exits the RO system and is sent through an end-use specific post treatment if necessary. The high concentrate reject streams can have TDS levels at approximately 100,000 mg/L which are too high for the RO membranes to handle without rapid fouling thus they cannot be recycled. Thus the reject stream, still at high pressure, is run through a pressure exchanger in order to recover as much work as possible from the process prior to being discharged back into the environment. A full reverse osmosis plant layout can be seen in **Figure 2.3**.

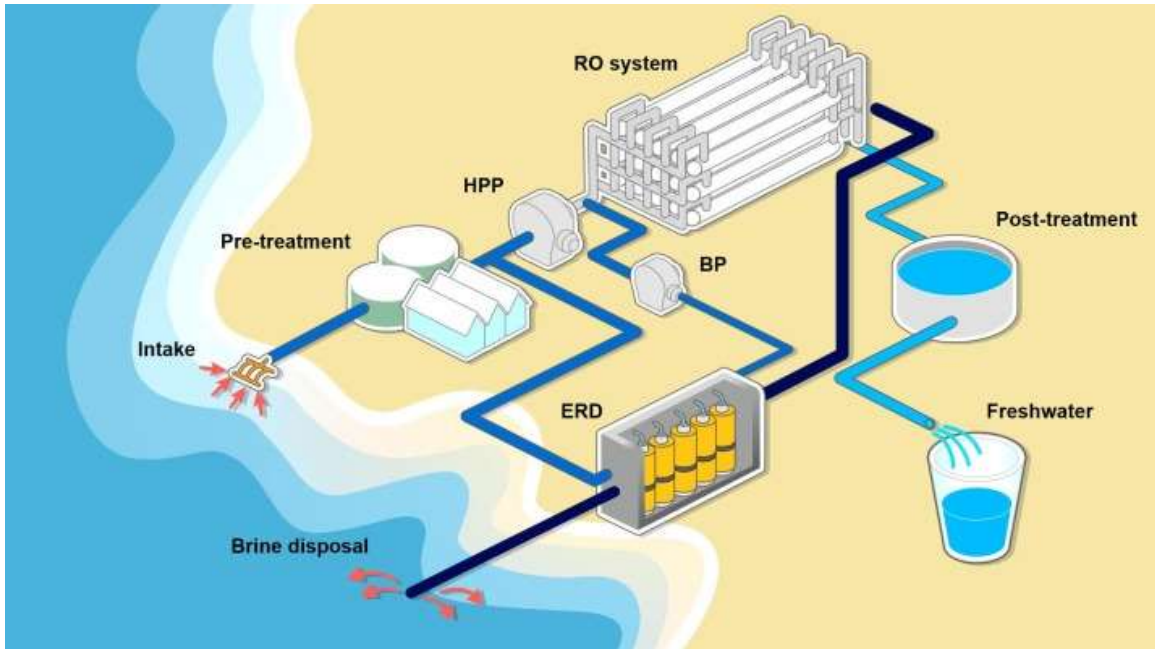


**Figure 2.3:** Typical reverse osmosis plant layout [11]

As previously mentioned, produced water streams have TDS levels of approximately 200,000 mg/L which is substantially above the upper threshold of what RO systems can effectively treat. RO membranes would be subjected to rapid fouling and eventual failure if employed to untreated produced water, thus rendering the technology ineffective in treatment.

Reverse osmosis doesn't provide chemical treatment to the water it desalinates thus the dissolved organic acids with concentrations of approximately 2,000 mg/L would not be effectively treated using this technology.

Reverse osmosis system's inability to recycle and treat the produced reject streams, their inability to effectively desalinate untreated produced water, and their inability to remove dissolved organics from produced water renders this technology ineffective at treating produced water.

### **2.3.2 Thermal Desalination**

Thermal desalination systems constitute a large part of the desalination market, behind reverse osmosis. Reverse osmosis dominates the world market due to its well established technology and its effectiveness at treating brackish water and sea water. Thermal desalination is a nice alternative when harsh operating conditions are present which reverse osmosis systems cannot handle (i.e. higher salinity brines) thanks to the system's exhibited robustness [13]. A large benefit of thermal desalination systems is their ability to recover low-grade heat from industrial plants that would otherwise be lost to the environment, thus maximizing the use of energy from operating plants. The most common types of thermal desalination are vapor compression, multi-effect distillation, and multi-stage flash distillation.

#### **2.3.2.1 Vapor Compression (VC)**

Vapor compression (VC) is one of the main types of thermal desalination. Vapor compression desalination is accomplished via either mechanical vapor compression (MVC) or thermal vapor compression (TVC). These methods are most likely employed in conjunction with other large-scale industrial processes in which both high salinity brines are created and waste heat/electricity is available.

Vapor compression desalination starts with a feed brine stream being fed into a cross exchanger to preheat the stream prior to entering the vaporization chamber. If needed, a supplemental heat exchanger is utilized to add enough heat to partially vaporize the process stream. The now pre-heated two-phase stream is fed into a vaporization chamber allowing a clean vapor stream and a concentrated liquid brine stream to separate, with the salts remaining in the concentrated liquid brine stream.

The clean vapor stream is removed from the concentrated liquid process stream and recompressed into a liquid via either mechanical or thermal means. The process of recompressing the clean vapor stream results in a substantial temperature increase of the stream. The heat from this clean stream is recovered and used to heat the inlet feed brine stream.

The high-concentrate liquid brine stream exits the vaporization chamber. Any available heat is recovered from the high-concentrate liquid brine and then the brine is disposed of.

Mechanical vapor compression and thermal vapor compression operate similarly, only diverging in the manner in which the clean vapor streams are compressed into a heating fluid. MVC utilizes mechanic compressors powered by electricity whereas TMC utilizes a steam jet ejector which creates a vacuum in order to compress the clean vapor stream [12]. A typical MVC system can process 100-3,000 m<sup>3</sup> brine/day whereas a TVC system can process 10,000-30,000 m<sup>3</sup>/day [12]. Both mechanical and thermal vapor compression process schematics can be seen in **Figure 2.4**.

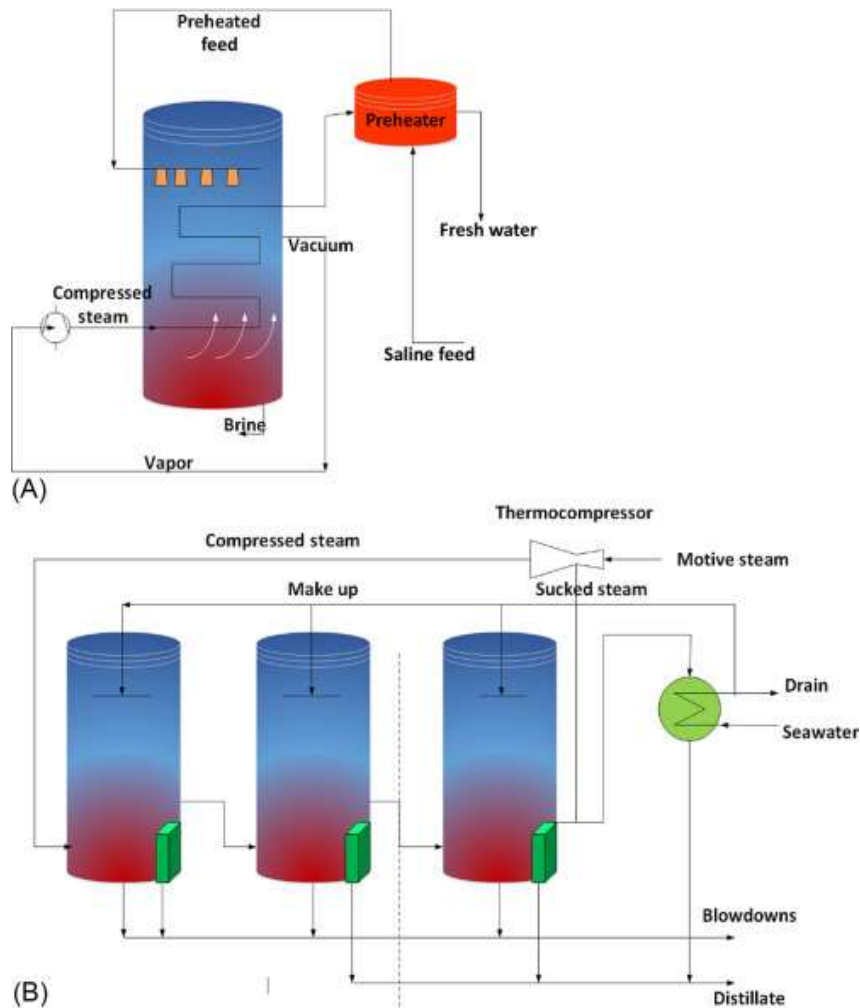


**Figure 2.4:** A) MVC system process schematic. B) TVC system process schematic. [12]

A major drawback of this desalination method is the production of a high-concentrate liquid brine stream. This is similar to reverse osmosis in that treatment process solves a problem, yet also creates one as well. The high-concentrate liquid brine stream is not recycled to the process and thus will cause environmental disruptions over time as more and more brine is disposed of, increasing local ion concentrations and disturbing delicately balanced ecosystems.

Another drawback of this treatment method is the inability to oxidize and destroy dissolved organics. The process of partially vaporizing a hypersalinated brine, thus

leaving the dissolved inorganic salts behind and producing a clean vapor stream doesn't account for the presence of dissolved organics. Some organics may stay behind in the high-concentrate liquid brine while others will leave in the vapor phase with the "clean vapor" stream. Regardless, the organics aren't being adequately oxidized and destroyed, rendering the technology ineffective in treating produced water.

The inability for both mechanical vapor compression and thermal vapor compression process systems to treat the high-concentrate liquid brine streams as well as destroy the dissolved organics in them renders the technology ineffective at treating produced water to the standards needed.

#### **2.3.2.2 Multi-effect Distillation (MED)**

Multi-effect distillation (MED) is the least energy intensive form of thermal desalination when paired with thermal vapor compression [1]. Multi-effect distillation was the most commonly employed desalination technology until the development and subsequent commercialization of multi-stage flash distillation in the 1960s. However, thanks to new advancements in technology, multi-effect distillation is making a comeback and is being employed more frequently in today's desalination market. Compared with multi-stage flash distillation, multi-effect distillation systems consume less electricity with their pumping schemes (1.5-2 kW/ton of water) [12]. A typical multi-effect distillation system contains ten units and can treat anywhere from 600-30,000 m<sup>3</sup> water/day [12].

Multi-effect distillation systems desalinate water using a series of chambers with decreasing pressure known as "effects". The inlet brine stream is fed into the system and

cross-exchanged with “clean” vapor stream to preheat the brine before entering the first effect. The preheated brine is sprayed into a pressure-controlled effect with a series of steam-heated tube bundles assembled within. As the brine comes into contact with the heated tube bundles, the brine partially vaporizes, resulting in a “clean” vapor stream and a concentrated liquid brine stream.

The clean vapor stream exits the top of the first effect and serves as the heating fluid in the heating bundles in the second effect. As the clean vapor stream relinquishes its heat energy by partially vaporizing the concentrated brine in the second effect, it is condensed into a clean distillate stream and is removed from the system. Each effect contributes clean distillate to the total distillate stream header, culminating in the distillate produced by the final effect clean vapor stream which preheats the incoming feed brine.

The concentrated liquid brine stream that results from partial vaporization of the feed brine on the steam-heated tube bundles in the first effect is collected onto a tray and moved into the second effect. The concentrated liquid brine is once again fed into the effect through a series of spray nozzles and onto a series of heated tube bundles. Once the concentrated brine is brought into contact with the heated bundles, it is again partially vaporized, resulting in a clean vapor stream and a further concentrated liquid brine stream. The concentrated liquid brine stream is then moved into the next effect and the process repeats itself until the final effect. The concentrated liquid brine stream that is collected in the final effect is removed from the system and discarded as a waste stream.



The pressure in the multi-effect distillation system is controlled using vacuum ejectors. The system is set up in such a way that the pressure is highest in the first effect and decreases with each subsequent effect. By decreasing pressure in each subsequent effect, the brine stream can be coaxed into vaporizing with lower temperatures by utilizing the thermodynamic properties of the process fluid. A process schematic of a typical multi-effect distillation system is seen in **Figure 2.5**.

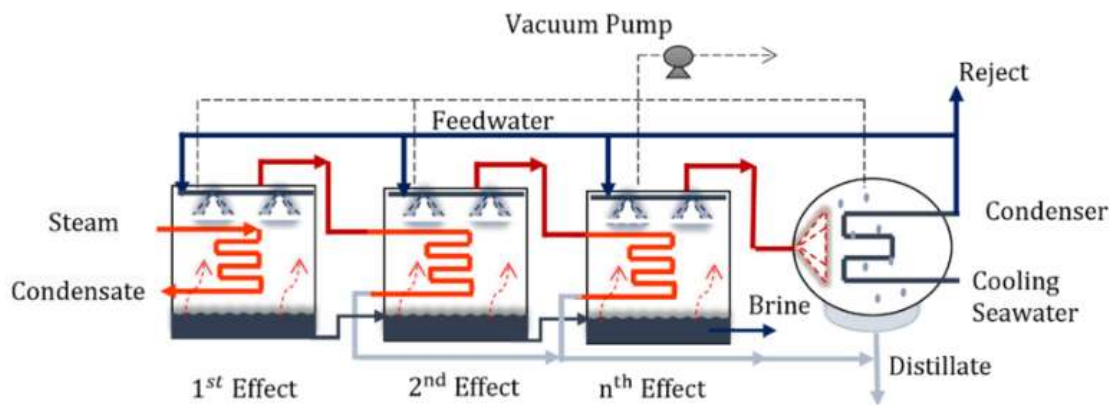


**Figure 2.5:** Process schematic of a typical MED system. [14]

Multi-effect distillation systems typically operate as a single-pass system which means it requires less electricity for pumping than other systems which use large recycle streams. MED systems are able to operate at lower temperatures such as 70°C which leads to reduced corrosion and sedimentation [14].

The drawbacks of MED systems are very similar to those experienced in VC systems. MED systems produce a highly concentrated liquid brine stream that is not able to be treated by the system due to rapid fouling of the process equipment. This reject stream is thus disposed of into the environment which can lead to serious adverse effects. Another drawback of this treatment process is the inability of the process to destroy

dissolved organics. These shortfalls in the MED system render it ineffective at properly treating produced water.

### **2.3.2.3 Multi-stage Flash Distillation (MSF)**

Multi-stage flash distillation is the most widely applied non-membrane desalination process today. Nearly 26% of all the desalination processes worldwide are multi-stage flash distillation [12]. Typical multi-stage flash distillation systems can treat approximately 10,000-40,000 m<sup>3</sup> water/day using anywhere from 4-40 stage systems [12]. Typical MSF systems are operated alongside power plants due to the availability of low-grade heat sources and electricity [15]. Most MSF systems operate as a once-through system however they can also include brine recirculation streams in order to increase treatment efficiency. A drawback of including the recirculation systems is the increased electrical demand for new pumping schemes which can be deemed untenable for smaller systems, thus a once-through system is operated instead.

Multi-stage flash distillation systems operate in a series of stages/vessels in which successive stages are held at decreasing temperatures and pressures using steam and vacuum pumps. A brine feed stream is preheated and is fed into the first stage under vacuum. Upon entering the first stage the brine stream “flashes” and produces a “clean” vapor stream and a concentrated brine stream. The clean vapor stream is allowed to condense and is collected in trays in the tops of each stage before exiting as a separate clean stream.

The concentrated brine stream moves to the next stage which is held at a lower pressure and temperature and thus the brine stream flashes again, producing a clean vapor

stream which is collected in trays at the top of the stage, leaving behind a more concentrated brine stream at the bottom of the stage. The concentrated brine stream then moves to the next stage(s) where the process is repeated as many times as required to reach the desired water treatment target. A process schematic for a typical MSF system can be seen in **Figure 2.6**.

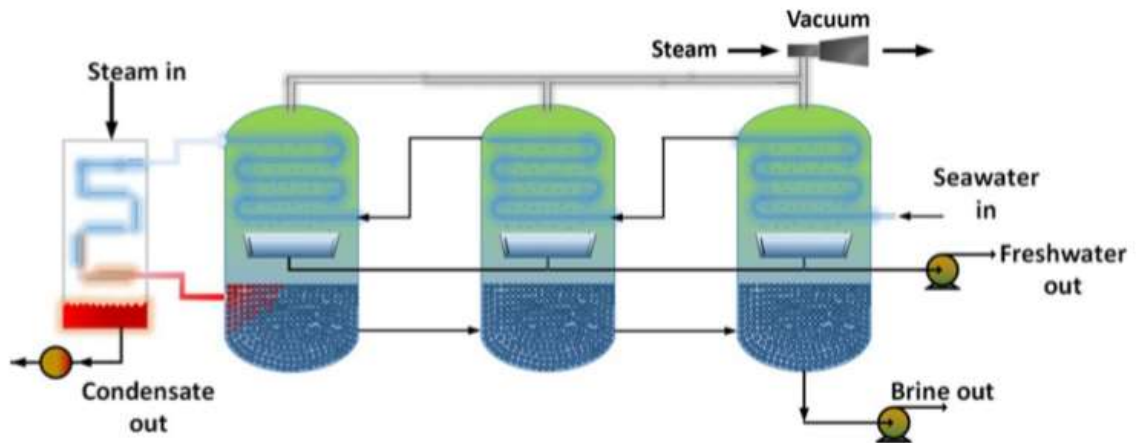


**Figure 2.6:** Process schematic of a typical multi-stage flash distillation system [12]

An advantage of multi-stage flash distillation is the limited amount of scaling that occurs. This is due in large part because the evaporation of the brine doesn't occur on the heating tube bundles, it "flashes" in the vessel [3]. MSF systems typically require approximately  $3.5 \text{ kWh/m}^3$  water treated which is less than reverse osmosis ( $3.5\text{-}4.5 \text{ kWh/m}^3$  water treated) which allows these systems to own more market share than other desalination processes [15,11].

A drawback of MSF systems is that they produce a high concentrate brine waste stream that is disposed of into the environment. Even when part of this stream is recycled back into the system, there is still a substantial risk incurred when high-salinity brines are discharged into the environment [16]. Similar to previously discussed technologies, MSF

doesn't treat dissolved organics which renders the technology inadequate at treating produced water.

The large amounts of high salinity discharge streams as well as the inability to treat dissolved organics shows that MSF is unable to adequately treat produced waters. This conclusion, as shown in **Table 2.1**, has been reached for all previously discussed desalination technologies.

**Table 2.1:** Summary of current desalination technologies

<b>Technology</b>	<b>Typical Unit Capacity</b>	<b>Energy Demand</b>	<b>Concentration Limit of Incoming Brine</b>	<b>Does it treat organics?</b>	<b>Reject Stream Concentration</b>
Reverse Osmosis	24,000 m <sup>3</sup> /day [17]	3.5-4.5 kWh <sub>e</sub> /m <sup>3</sup>	~45,000 mg/L	No	~100,000 mg/L
Vapor Compression	10,000-30,000 m <sup>3</sup> /day	7-12 kWh <sub>e</sub> /m <sup>3</sup> [17]	~35,000 mg/L	No	~200,000 mg/L [18]
Multi-effect Distillation	600-30,000 m <sup>3</sup> /day	1.5-2 kWh <sub>e</sub> /m <sup>3</sup>	~35,000 mg/L	No	~200,000 mg/L [18]
Multi-stage Flash Distillation	10,000-40,000 m <sup>3</sup> /day	3.5 kWh <sub>e</sub> /m <sup>3</sup>	~35,000 mg/L	No	~75,000 mg/L [15]

It is evident upon review of **Table 2.1** that current desalination technologies are not equipped to adequately treat produced water. The inability for these technologies to treat organics renders their treatment of produced water incomplete. The production hypersalinated reject streams which cannot be recycled presents an ecological hazard as well as a technical challenge as produced water streams have TDS levels well beyond the concentrations of the produced reject streams. The need for a new technology to handle these hypersalinated brines with dissolved organics is where supercritical water desalination comes in.

## 2.4 Supercritical Water Desalination

Supercritical water desalination is a very promising technological approach to water treatment. The crux of this technology is using the unique physical characteristics of water above its critical pressure and temperature to leverage its thermodynamics in removing dissolved inorganic salts. The use of fluids above their critical temperatures and pressures is not new and has been exploited heavily with supercritical CO<sub>2</sub>.

Supercritical CO<sub>2</sub> becomes an excellent solvent at conditions above its critical temperature and pressure (31.1 °C, 73.9 bar) whereas at conditions below these points it is not. This is most commonly employed when extracting caffeine from coffee beans using supercritical CO<sub>2</sub>, and then once back at standard conditions, the caffeine readily falls out of solution as it is no longer soluble in CO<sub>2</sub>. By manipulating the conditions under which the solvent (CO<sub>2</sub>) is placed under, we can see substantially different physical properties manifest. Thus, applying this concept to water, the world's "universal solvent", offers unique opportunities for technological advances in water treatment.

### 2.4.1 Theory

Salt solubility in supercritical water ( $T > 374$  °C,  $P > 221$  bar) decreases drastically due to the substantial decrease in water density (approximately 997 kg/m<sup>3</sup> → approximately 100 kg/m<sup>3</sup>) as well as the decrease in water's polarity [19,20]. **Figure 2.7** shows a phase diagram of pure water as a function of pressure and temperature.

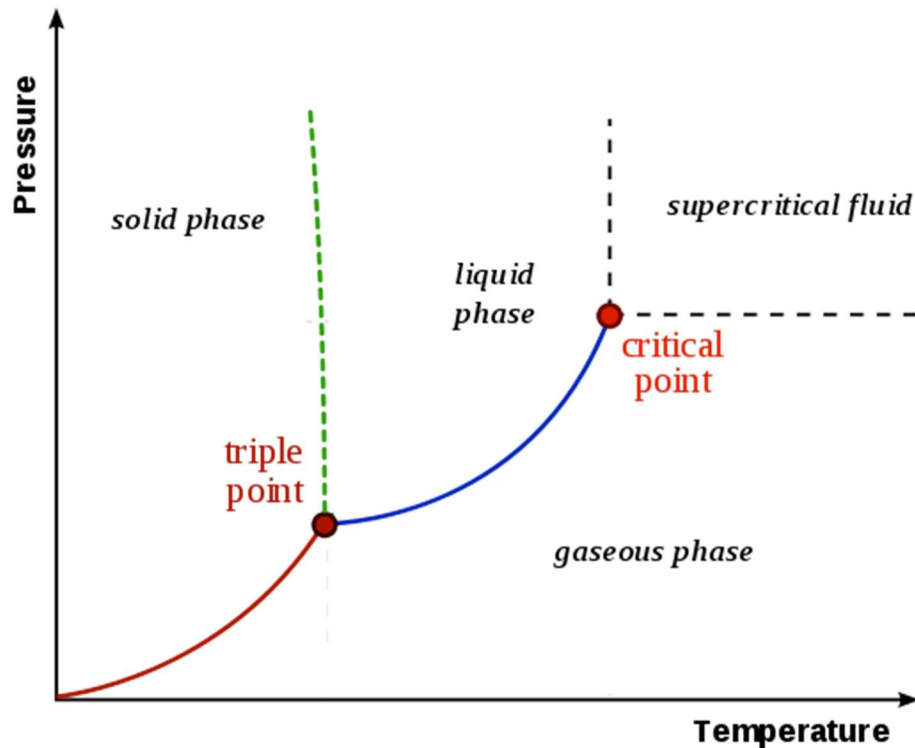


**Figure 2.7:** Pure water phase diagram [21]

As can be seen in **Figure 2.7**, water maintains a distinct vapor, liquid, or solid phase at conditions beneath its critical pressure and temperature. However, as these conditions are met and/or surpassed, water behaves neither as a distinct vapor nor as a liquid but instead as an amalgam of both.

The dissociation constant of water ( $K_w$ ) decreases by roughly nine orders of magnitude in the supercritical zone as compared to ambient conditions [20]. In other words, water is less polar and thus polar solutes are no longer as soluble, and non-polar solutes become more soluble in the supercritical region. This allows us to exploit these properties to precipitate out large quantities of inorganic salts, which are polar. The thermodynamic properties of supercritical water dictating inorganic salt solubility will be discussed in greater detail in chapter three of this thesis.

Another benefit of the unique supercritical water properties is that the decrease in the dissociation constant of water allows organic reactions to progress faster as water becomes more non-polar, thus better facilitating mass transfer of the non-polar organics. This allows increased reaction rates for oxidation of dissolved organics in supercritical water which is necessary when treating complex high-salinity brine streams with significant concentrations of dissolved organics (i.e. produced water).

Supercritical water desalination systems currently under development vary widely and many feature proprietary technology. All processes however contain the same fundamental steps that must occur in order to achieve desalination and thus effective treatment.

In a theoretical supercritical water desalination system, an inlet brine stream would first be sent through a pre-treatment step to remove large particulates or key scale-forming components (depending on inlet stream) using filtration or chemical treatment. The pretreated stream would then be brought to pressure, approximately 240 bar, using high pressure pumps. Now at pressure, the pretreated brine stream would be brought to temperature ( $> 374\text{ }^{\circ}\text{C}$ ) using the most efficient heat source available.

Now at supercritical conditions, the unique thermo-physical properties of supercritical water can be exploited and the polar inorganic salts will fall out of the solution as the solvent is now quasi-nonpolar. The precipitated salts can be separated from the supercritical water using a separation method which best suits the entire process. The key to whatever separation process is utilized is that it must occur at temperature and pressure otherwise the inorganic salts will re-dissolve into solution as the solvent regains its polar properties.

The separated solids can be removed from the system and separated as desired based on value or end-use. The production of a solid waste stream rather than a high-concentrate brine stream is unique from other desalination technologies as it can be used as a by-product with potential value rather than an environmental hazard.

The clean supercritical fluid stream can be re-condensed and brought back to atmospheric conditions while recovering energy from the stream through the use of cross heat exchangers and pressure exchangers. This step is important as it is necessary to make the process as economically competitive as possible. A generic supercritical desalination process diagram can be seen in **Figure 2.8**.

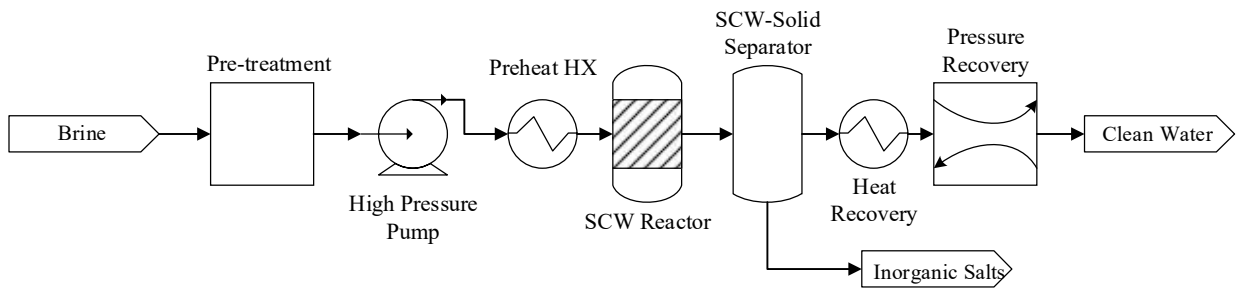


**Figure 2.8:** Hypothetical supercritical water desalination system process schematic.

As seen in **Figure 2.8**, the inlet brine is pretreated (as necessary for each specific inlet composition) and brought up to process pressure using high pressure pumps. Heat exchangers will be used to bring the process stream up to just below the critical temperature prior to entering the SCW reactor. The SCW reactor will bring the process stream above the critical temperature and the inorganic salts will drop out of solution. It is also in the SCW reactor that the organics destruction will occur. Next (while still at the desired process conditions) the solids will be separated from the clean process stream using a SCW-Solid separator. Following this unit operation, as much heat and pressure will be recovered from the clean process stream as possible to maximize efficiency.



#### **2.4.2 Barriers to implementation**

Implementation of supercritical water desalination technology faces a few main barriers. The high energy requirement of this technology, the high capital cost of the technology, and the lack of experimental data available to inform the technology's development are all areas which currently impede the deployment of this technology.

The energy cost of treating hypersalinated brines with this method is roughly 4.5 times higher than the most efficient reverse osmosis systems operating today. This gap is likely to decrease as more research is performed in the field of supercritical water desalination.

The capital costs for equipment that can handle supercritical water conditions as well as scaling and corrosion are also significantly higher than traditional desalination methods. Stainless steel, which commonly is used for standard desalination technologies is not sufficiently able to handle the corrosion conditions experienced at supercritical conditions. Hastelloy c276 is the recommended material for construction for supercritical reactors and piping, which yields approximately a 5x increase in cost compared to 316 stainless steel. An increased understanding in the phenomena occurring at these conditions as well as the solubility of the more corrosive inorganic salts being treated will likely allow for a reduction in equipment costs through a more targeted employment of expensive materials.

The current economics of this process do not favor this technology's employment, however as clean water availability becomes more scarce and research continues to improve the efficiency of this technology, it will likely become more commonly utilized [22].

## 2.5 References

- [1] Datsgerdi, H.R. and Chua, H.T.; *"Thermo-economic analysis of low-grade heat driven multi-effect distillation based desalination processes,"* in Desalination, **2018**, vol 448, pp 36-48
- [2] Cosgrove, W. and Rijsberman, F.; *"World Water Vision: Making Water Everybody's Business,"* published by Earthscan, **2014**.
- [3] Lilane, A., Saifaoui, D., Jenkal, H., and Chouiekh, M.; "Modeling and simulation of the performances of the reverse osmosis membrane," in Materials Today: Proceedings, **2019**.
- [4] A. J. Kondash, E. Albright, & A. Vengosh, *"Quantity of flowback and produced waters from unconventional oil and gas exploration,"* in Science of the Total Environment, **2017**, vol 574, pp 314–321.
- [5] Rosenblum et al. *"Organic Chemical Characterization and Mass Balance of a Hydraulically Fractured Well: From Fracturing Fluid to Produced Water over 405 Days,"* in Environmental Science and Technology, **2017**, vol 51, pp. 14006-14015.
- [6] *"Current Active Drilling Rig List,"* Sourced from: [dmr.nd.gov/oilgas/riglist.asp](http://dmr.nd.gov/oilgas/riglist.asp), accessed January 2019.
- [7] Voutchkov, N., *"Desalination-Past, Present and Future,"* in International Water Association, August 2016, Sourced from: <https://iwa-network.org/desalination-past-present-future/>, accessed January 2019.
- [8] C. Charcosset; *"A review of membrane processes and renewable energies for desalination,"* in Desalination, **2009**, pp 214-231.
- [9] Alsehli, M., Alzahrani, M., and Choi, J.K.; *"A novel design for solar integrated multi-effect distillation driven by sensible heat and alternate storage tanks,"* in Desalination, **2019**, vol 468.
- [10] *"30<sup>th</sup> GWI/International Desalination Association Worldwide Desalting Plant Inventory,"* in Desalination, **2017**.
- [11] Kim, J., Park, K., Yang, D.R., and Hong, S.; *"A comprehensive review of energy consumption of seawater reverse osmosis desalination plants,"* in Applied Energy, **2019**, vol 254
- [12] Rabiee, H. Khalilpour, K. R., Tapper, Nigel.; *"Energy-Water Nexus: Renewable-Integrated Hybridized Desalination Systems,"* in Polygeneration and Polystorage: For Energy and Chemicals, **2019**, pp 409-458.
- [13] Chen, Q., Kum Ja, M., Li, Y., Chua, K.J.; *"Energy, exergy and economic analysis of a hybrid spray-assisted low-temperature desalination/thermal vapor compression system,"* in Energy, **2019**, vol 166, pp 871-885

- [14] Alsehli, M., Alzahrani, M., and Choi, J.K.; "A novel design for solar integrated multi-effect distillation driven by sensible heat and alternate storage tanks," in *Desalination*, **2019**, vol 468.
- [15] El-Ghonemy, A.M.K, "Performance test of a sea water multi-stage flash distillation plant: Case study," in *Alexandria Engineering Journal*, **2018**, vol 57, pp 2401-2413
- [16] McGrath, M.; "Concerns over increase in toxic brine from desalination plants," in *BBC News*, **14 January 2019**.
- [17] Najafi, F. T., "Environmental impact cost analysis of Multi-stage flash, Multi-effect distillation, Mechanical Vapor Compression, and Reverse Osmosis Medium-Size Desalination Facilities," in *ASEE's 123<sup>rd</sup> Annual Conference and Exposition*, **2016**.
- [18] Kaplan, R., Mamrosh, D., Salih, H. H., and Dastgheib, S. A., "Assessment of desalination technologies for treatment of a highly saline brine from a potential CO<sub>2</sub> storage site," in *Desalination*, **2017**, vol 404, pp. 87-101.
- [19] Driesner, T., "The system H<sub>2</sub>O-NaCl. Part II: Correlations for molar volume, enthalpy, and isobaric heat capacity from 0 to 1000°C, 1-5000 bar, and 0 to 1 XNaCl," in *Geochimica et Cosmochimica Acta*, **2007**, vol 71, pp 4902-4919.
- [20] Savage, P. "Organic Chemical Reactions in Supercritical Water." American Chemical Society. **1999**. v. 99, pp 603-621.
- [21] Oldridge, N., "Phase Diagram of Water," Sourced from: <http://chemistnate.com/phase-diagrams.html>, accessed September 2019.
- [22] López, D. E., & Trembly, J. P., "Desalination of hypersaline brines with joule-heating and chemical pre-treatment: Conceptual design and economics," in *Desalination*, 207, vol. 415, pp. 49–57

## **Chapter 3: Previous Solubility Work**

### **3.1 Introduction:**

Substantial work has been performed in the determination of inorganic salt solubility in water over a wide temperature and pressure range. The volume of solubility data becomes sparse in the near-critical and supercritical region of water compared to lower temperatures and pressures. Several research groups have paved the way to fill in the gaps in these higher temperature and pressure ranges. Experimental work as well as numerical model formulation has been produced in an effort to gain an understanding of the unique behavior of supercritical water. A few select works are described in detail below as they pertain to the work to be performed in this thesis.

### **3.2 Bischoff and Pitzer NaCl Solubility Work**

Widely considered the premier researchers in NaCl solubility in the supercritical region of water, Dr. James Bischoff and Dr. Kenneth Pitzer produced numerous papers (along with others) determining the solubility of NaCl in water as a function of temperature, pressure, and concentration. Bischoff and Pitzer utilized solubility data from their own work as well as work from numerous other researchers in order to develop phase relationships for solubility.

### 3.2.1 Background

The solubility work performed by Bischoff and Pitzer focus primarily on the binary H<sub>2</sub>O-NaCl system, specifically with concentrations comparable with seawater (3.2 wt% NaCl). Bischoff and Pitzer's work served primarily to fill in the gaps from datasets formulated by other researchers [1,2,3,4,5]. This work aims to understand the phenomena occurring in deep sea geothermal systems, more specifically the water-subsurface magma chamber interactions and mixing.

The aim of this work doesn't initially sound applicable to supercritical water desalination, however, once we drill down into the thermodynamics of the deep sea geothermal system further, the applicability becomes remarkably clear. Deep sea geothermal systems experience remarkably high pressures (ranging from 200-600 bar) and temperatures (300-800 °C) just like supercritical water desalination systems. Thus, any work that provides insight into the behavior of the system at those conditions is extremely valuable to engineers looking to design effective supercritical water desalination systems.

### 3.2.2 Methods

Bischoff and Pitzer compiled the results of solubility tests performed on H<sub>2</sub>O-NaCl systems in order to establish a more-complete understanding of NaCl solubility at high temperatures and pressures. When gaps in collective datasets were identified, more experimental work was performed [4,6,7,8]. In order to fill in gaps in solubility data the apparatus seen in **Figure 3.1** was utilized.

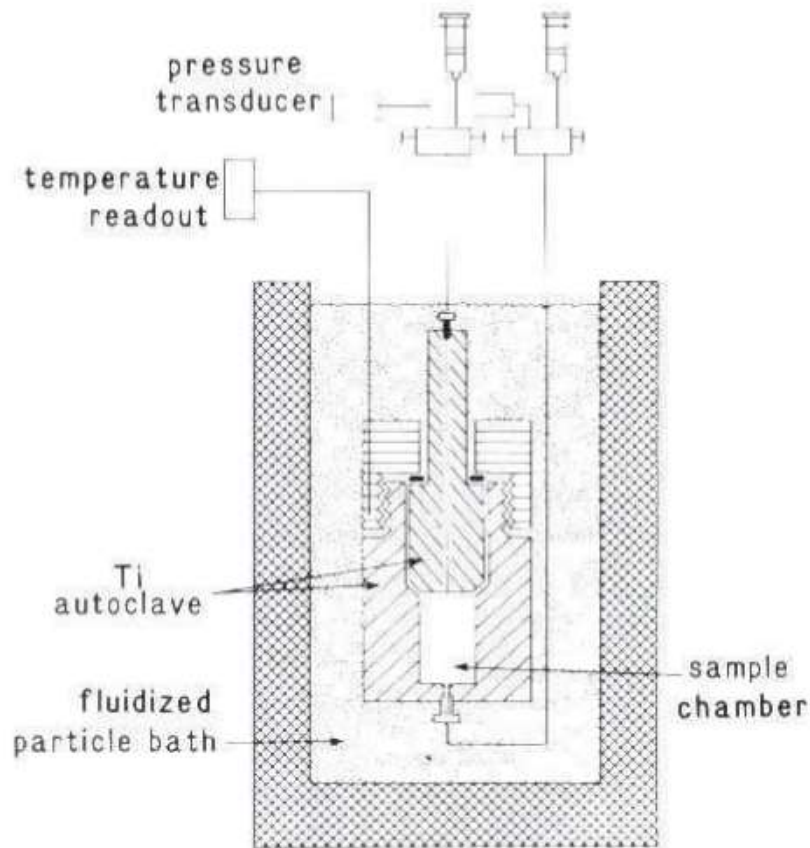


**Figure 3.1:** Experimental apparatus utilized to determine solubility and critical point of  $\text{H}_2\text{O}-\text{NaCl}$  solution [9]

A set amount of solution was loaded into the sample chamber and the system was brought to the determined test pressure. The system was then heated up and small amounts of sample were removed from the top and bottom of the process vessel in order to maintain the desired test pressure. The removed sample was analyzed for salt concentration and saved to maintain a mass balance at the conclusion of the test.

As samples were removed from the system, the two-phase boundary could be determined by the existence of different  $\text{NaCl}$  concentrations in the top and bottom sample. As temperature for each isobar was increased further, the two-phase boundary line could be traced all the way to the composition's critical point. The critical

temperature for each isobar was determined when the top and bottom sample contained the same NaCl concentration.

### 3.2.3 Results

The results of the Bischoff and Pitzer tests and formulations have yielded key datasets for NaCl solubility at varying temperatures and pressures. When plotted, the physical behavior of NaCl-H<sub>2</sub>O systems can be more-easily understood at temperatures and pressures nearing/exceeding the solution's critical point. **Figure 3.2** represents a P-T-x diagram for a 3.2% NaCl solution plotted at different isobars in the sub-critical and supercritical region.

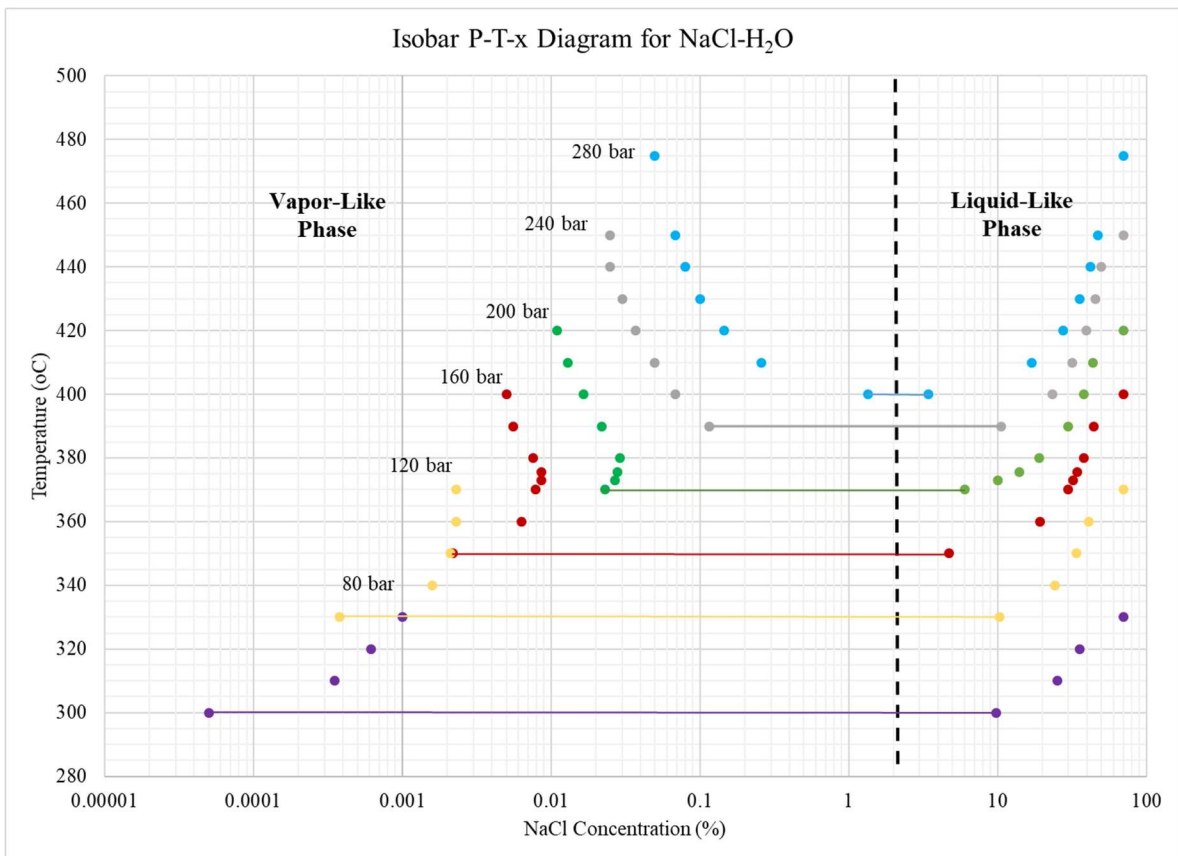


**Figure 3.2:** Isobar P-T-x diagram for a 3.2 wt% NaCl-H<sub>2</sub>O solution [10]

As seen above in **Figure 3.2**, the concentration of NaCl in the vapor-like phase and the liquid-like phase varies significantly as pressure and temperature are varied. For instance, at 240 bar and 420 °C, there is an equilibrium state present in which the vapor-like phase has a 0.037 wt% NaCl concentration and the liquid-like phase at the same conditions has a 39.5 wt% NaCl concentration.

Once able to understand this representation of the data, we can determine process conditions for future supercritical desalination systems based on the desired product stream concentrations. In order to further understand phase behavior, it is useful to represent data in other ways, thus teasing out interesting trends that are not otherwise readily apparent. **Figure 3.3** represents P-T-x results for a 3.2 wt% NaCl solution in the subcritical region plotted as isotherms.



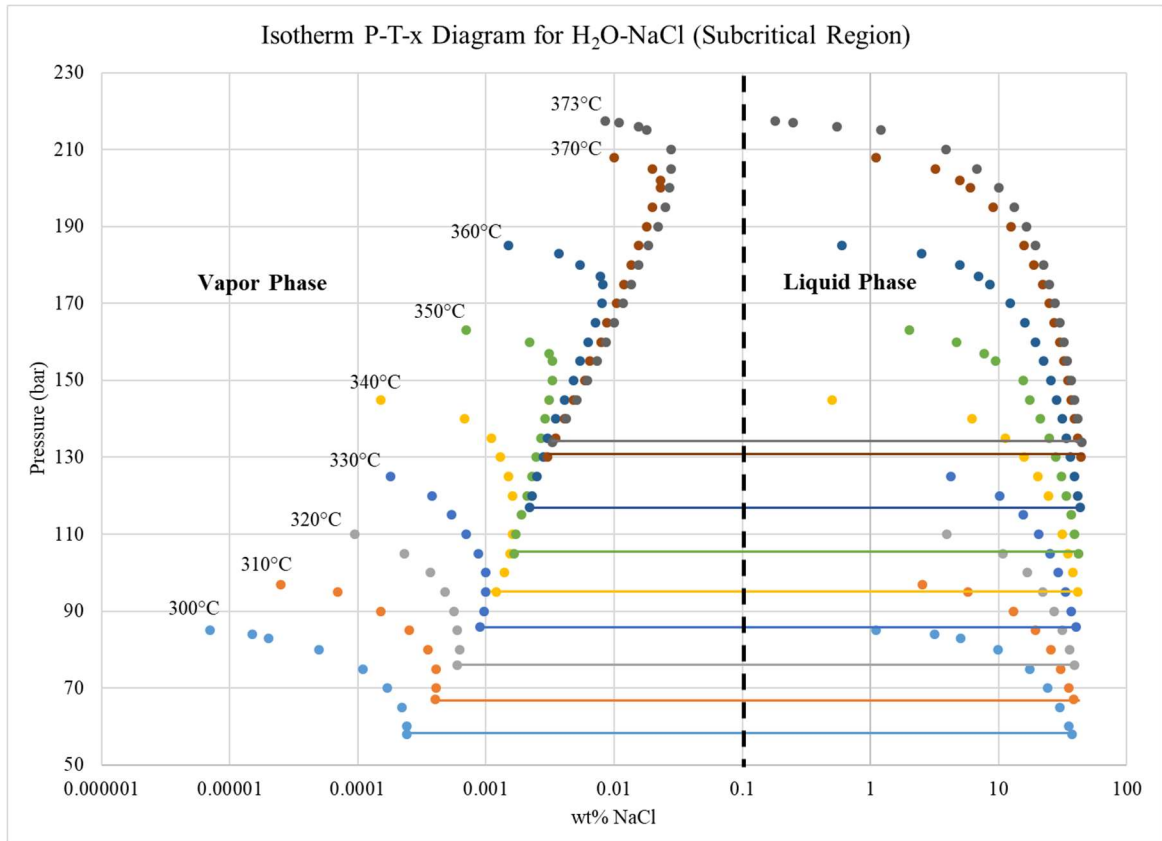


**Figure 3.3:** P-T-x diagram for a 3.2 wt% NaCl-H<sub>2</sub>O solution in the subcritical region [10]

It is evident in **Figure 3.3** that the equilibrium splits for the wt% NaCl in each phase begin to converge as pressure is increased towards the critical point for the solution. The equilibrium split for wt% NaCl in each phase at lower temperatures is wider than at higher pressures and temperatures. Operating at these conditions would make a system more akin to a high temperature multi-effect distillation system producing a clean vapor stream and a high-concentrate liquid stream. For instance, at 300 °C and 85 bar the concentration of NaCl in the vapor phase and liquid phase is  $7.0 \times 10^{-6}$  wt% and 1.1 wt% respectively.

The gap between concentration of NaCl in each phase begins to close as isotherms increase in temperature and pressure. This is evident when looking at the 373

°C isotherm at pressures above 210 bar. At 373 °C and 217.5 bar, the concentration of NaCl in the vapor phase and liquid phase is 0.0085 wt% and 0.18 wt% respectively. This trend towards convergence becomes reality upon reaching the supercritical region as can be seen in **Figure 3.4**.

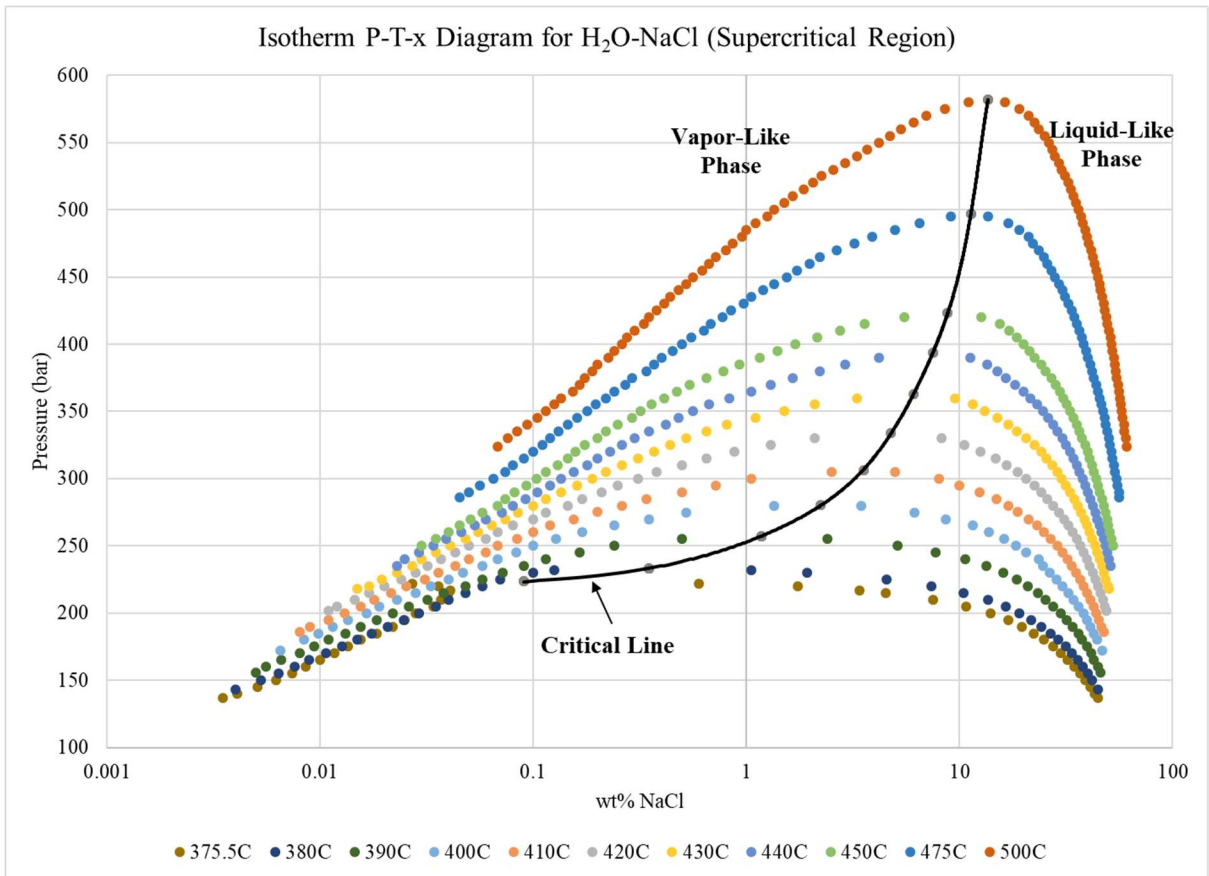


**Figure 3.4:** P-T-x diagram for a 3.2 wt% NaCl-H<sub>2</sub>O solution in the supercritical region [10]

The separation of equilibrium compositions between phases converges down to zero as a single supercritical composition is reached as denoted by the critical line in **Figure 3.4**. The left side of this critical line represents a vapor-like phase while the right side of this critical line represents a liquid-like phase. Each set of process conditions (temperature and pressure) create a two-phase system that has equilibrium compositions of NaCl in each phase. For instance, at 400 °C and 250 bar the vapor-like phase and

liquid-like phase have NaCl concentrations of 0.1 wt% and 18.35 wt% respectively.

However, along this same 400 °C isotherm at 280.7 bar, the two-phase system collapses into a single supercritical phase and the resulting concentration is 2.22 wt%.

### 3.2.4 Discussion

The work performed by Bischoff and Pitzer provides wonderful insight into the solubility of a NaCl-H<sub>2</sub>O system in the near-critical and supercritical regions. The work performed not only allows geochemists to gain an understanding of deep sea hydrothermal phenomena occurring at elevated pressures and temperatures but also creates a benchmark for researchers attempting to solve the growing water crisis as well.

The P-T-x diagrams for H<sub>2</sub>O-NaCl systems as seen in **Figures 3.2-4** allow engineers to determine the process conditions for desalination systems depending on the desired output stream compositions. Though this work yielded valuable results that are widely used and cited today, questions still remain regarding the interpretation of their results as well as the applicability to produced water streams.

If the starting stream composition was 3.2 wt% NaCl in water, it would make sense for the closed system critical composition to also be 3.2 wt% NaCl unless there is a solid phase of salt also present or clean vapor has left the system. However, as **Figure 3.4** shows, the critical composition at different isotherms increases with temperature and pressure, well beyond the starting 3.2 wt% NaCl. The only way for this to be possible is for mass to exit the system (primarily clean water vapor) and not be accounted for at the critical compositions. The experimental set-up for these tests noted that indeed the data acquired was not for a closed system as samples were continuously removed and

analyzed and thus a shifting critical composition was made possible. Removing samples from the system for analysis represent a necessity in composition determination at these extreme conditions despite their imposed effects on the results.

Bischoff and Pitzer noted that this shifting critical composition seen in the data likely results from the intrinsic difficulty in determining composition at the critical point as mentioned earlier. This uncertainty is compounded by extrapolation of composition data near the critical point which itself is noted to be not precise. The near-critical and critical region is the greatest source of uncertainty in Bischoff and Pitzer's work.

The uncertainty in the data around the critical point must be taken into account when using this data for desalination process design. Also, Bischoff and Pitzer's work primarily focused on simulated seawater with a NaCl concentration of 3.2 wt% (approximately 32,000 mg/L) whereas produced water compositions are far more complex with TDS levels around 200,000-300,000 mg/L. Further, the uncertainty in the near-critical and critical region shows the importance of critically applying any data, regardless of how lauded, to current and future work to create a more complete picture of what is occurring at these conditions. Simply applying the results from this work without looking elsewhere to fill in any gaps, build consensus, and identify key divergences will result in new work with the same shortfalls.

### **3.3 Driesner NaCl-H<sub>2</sub>O Empirical Property Model**

In order to develop a functioning supercritical water desalination system, it is imperative that the fluid properties are well understood at the specified process conditions. Salt solubility is usually what comes to mind as being the most important

property to understand for a fluid, however it is equally important that the density, enthalpy, and isobaric heat capacity for the system is well understood. For instance, in order to accurately predict the true residence time of a fluid in a reactor, the density of the solution at those conditions must be understood in order to ascertain the true volume of the solution. With an accurate density known for a solution at various conditions, a system can be designed properly to achieve optimal residence times in key unit operations.

The isobaric heat capacity of a solution is an important property to understand as it dictates how much a solution will resist temperature change when heat is applied. Engineers must know this value for a solution if they are to properly design their heating elements for their system in order to achieve the desired temperature conditions in their system. Enthalpy goes hand-in-hand with isobaric specific heat capacity as it informs the engineers of the energy requirements for achieving specific process conditions. An accurate model that can divulge this information about a system will lead to drastically reduced costs in system design and lead to more effective process designs.

Work performed by Driesner aims to build a more accurate model for H<sub>2</sub>O-NaCl binary systems for temperatures ranging from 0-1000°C, pressures ranging from 0-5000 bar, and compositions ranging from 0-1 X<sub>NaCl</sub> (mole fraction NaCl) [11]. Driesner evaluated current “cutting edge” models and identified key areas in need of improvement for accurate system modeling and utilized experimental data compiled by numerous validated research groups (Bischoff and Pitzer, Knight and Bodnar, among others) in order to construct a more accurate model which best represents system behavior within these process conditions. Driesner’s work produced two companion papers with the first

formulating correlations for phase relationships with varying temperatures, pressures, and compositions ( $X_{\text{NaCl}}$ ) [11]. The second paper formulated correlations for molar volume, enthalpy, and isobaric heat capacity of the modeled binary solution [12].

### 3.3.1 Background

Numerical techniques being employed to model deep sea hydrothermal systems continue to improve, however, many still lack the accuracy needed for confident representation of these systems. A large reason many of these models lack accuracy is the unrealistic assumptions that are made when deriving them. Driesner points out that many studies have utilized extremely simplified fluid properties that don't yield realistic results.

An example of an unreasonable approximation utilized for model production is the "Boussinesq approximation". This approximation was employed by many studies which assumes density variances in all terms not associated with the gravity term are neglected [11]. This assumption drastically simplifies fluid property behavior which reduces accuracy for model outputs. In addition to this approximation, constant fluid properties were applied including viscosity, heat capacity, and thermal expansivity which also drastically reduces model accuracy [11]. Some newer studies utilized more reasonable properties for pure water however it is noted that the properties of  $\text{H}_2\text{O}$ - $\text{NaCl}$  solutions are substantially different than pure water, thus resulting in still unrealistic model outputs [11, 13]. Driesner works to improve the accuracy of model outputs by first utilizing a more applicable P-T-x curve for the system conditions being considered, as seen in **Figure 3.5**.

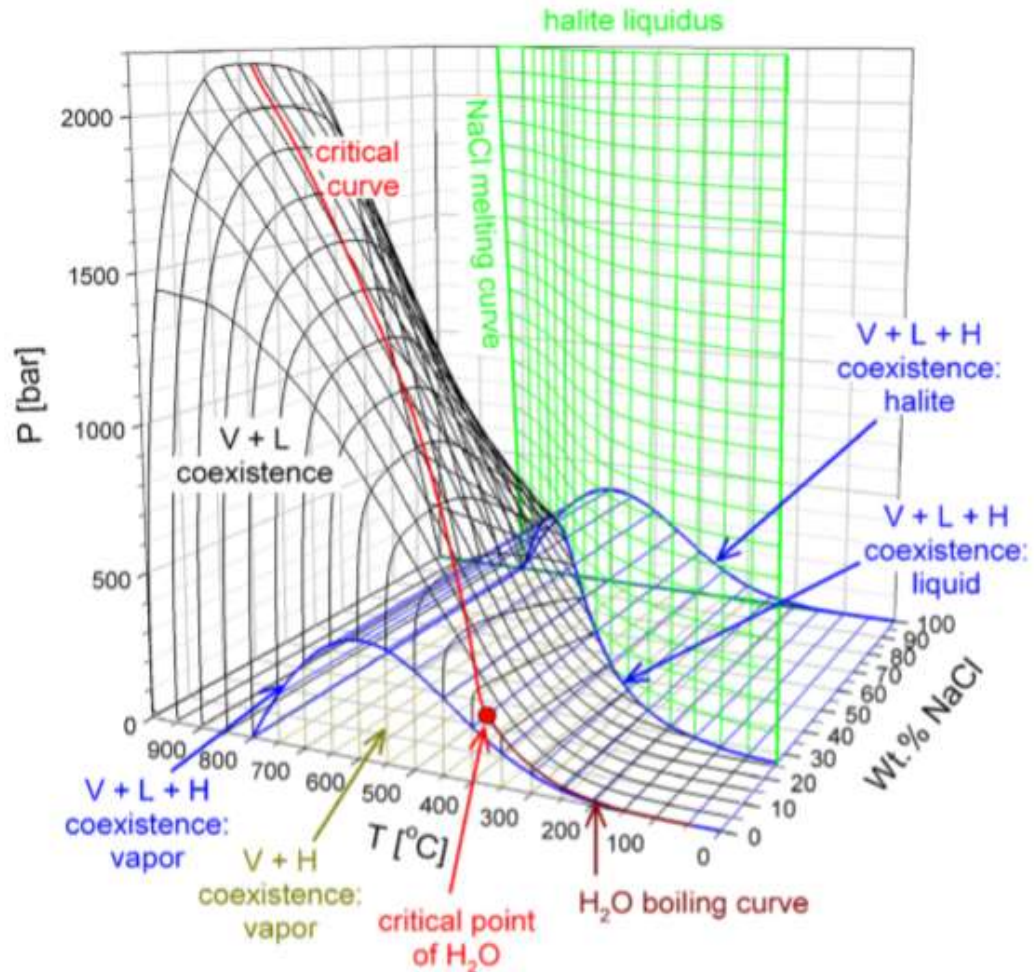


**Figure 3.5:** T-P-x phase diagram of H<sub>2</sub>O-NaCl [11]

The phase diagram seen in **Figure 3.5** allows for the visualization of the different phases present as pressure, temperature, and concentration of NaCl are varied. The critical curve, as denoted by the red line in **Figure 3.5**, marks the point at each set of process conditions (pressure, temperature) where the V+L coexistence ends and a single fluid phase begins, thus a single wt% NaCl exists. Above these conditions all phases collapse into a single phase fluid that cannot be defined by either solely “liquid” or “vapor” characteristics. This critical curve should look familiar as it is constructed using the same data from the P-T-x diagrams formed by Bischoff and Pitzer [10].

Using available data previously compiled by researchers such as Bischoff and Pitzer, previous model formulations such as those constructed by Pitzer and Pabalan, and a strong physical understanding of the phase behavior at these conditions like that seen in **Figure 3.5**, Driesner formulated a more accurate numerical model for a H<sub>2</sub>O-NaCl system at temperatures ranging from 0-1000°C, 0-5000 bar, and compositions ranging from 0-1 X<sub>NaCl</sub>.

### 3.3.2 Methods

Driesner created his model by looking at both a pure H<sub>2</sub>O system and a pure NaCl system separately and then combining these using known experimental values. A few select derivations will be discussed in this work in the interest of brevity.<sup>1</sup>

Driesner began formulating his system model by looking at a pure H<sub>2</sub>O system. Vast amounts of data are available from the International Association for the Properties of Water and Steam (IAPWS/IAPS) and are widely accepted by the scientific community. The data from the IAPS-84 has been modified and able to be implemented into a computer code (C-code library “PROST4.1”) and thus was used as the data set for this model formulation [14, 15]. The IAPS-84 data is not the most recently available data as the IAPWS-95 is also available. However, the IAPWS-95 data did not have a usable C-code library implementation in place thus the older data set was utilized. The differences between the two data sets were deemed insignificant in the resulting model correlations.

---

<sup>1</sup> The complete model formulation can be found in the referenced papers [Driesner and Heinrich 2007, Driesner 2007]



The behavior of a pure NaCl system was determined using the available data from previous studies. The melting curve regression utilized can be seen below in equation 3.1 and is shown to have agreement with the data produced in previous work [16,17].

$$T_{hm} = T_{triple,NaCl} + a(P - P_{triple,NaCl}) \quad (3.1) [11]$$

Where:

- $hm$  = halite melting
- $a$  = derived parameter given in **Table 3.1**

The sublimation curve of NaCl was determined using data available in the widely available JANAF tables. The halite vapor pressure can be determined using the regression found in equation 3.2.

$$\log_{10} P_{NaCl,halite} = \log_{10} P_{triple,NaCl} + b_{subl} \left( \frac{1}{T_{triple,NaCl}+273.15} - \frac{1}{T+273.15} \right) (3.2) [11]$$

Where:

- $b_{subl}$  = is a derived parameter given in **Table 3.1**

The boiling curve for NaCl is important as it is utilized above the triple point of NaCl as the stable curve. The boiling curve for NaCl was determined using the regression seen in equation 3.3.

$$\log_{10} P_{NaCl,liquid} = \log_{10} P_{triple,NaCl} + b_{boil} \left( \frac{1}{T_{triple,NaCl}+273.15} - \frac{1}{T+273.15} \right) (3.3) [11]$$

Where:

- $b_{boil}$  = is a derived parameter given in **Table 3.1**

**Table 3.1:** Derived parameters for the melting curve, sublimation curve, and boiling curve of NaCl [11]

Correlation	Parameter	Value
Halite Melting Temperature ( $T_{hm}$ )	a	$2.47260 \times 10^{-2}$
Halite Vapor Pressure ( $P_{NaCl,halite}$ )	$b_{subl}$	$1.18061 \times 10^4$
Liquid Vapor Pressure ( $P_{NaCl,liquid}$ )	$b_{boil}$	$0.941812 \times 10^4$

The determination of the critical curve is the one of the largest challenges in the formulation of this model. The critical curve is dependent on temperature, pressure and composition ( $X_{NaCl}$ ) and experimental data in the region comes with uncertainty. Much of the data obtained in early supercritical water solubility work lacks complete information on how results were obtained. Later work such as that produced by Bischoff and Pitzer acknowledges the uncertainty caused by the extrapolation of empirically observed relationships of vapor and liquid phases in the region. Thus, a unique approach was taken in order to minimize uncertainties in previous work.

The determination of accurate critical pressures was accomplished by using three different formulations for different temperature ranges, and then stitching the results together to develop a continuous critical curve. The three critical pressure formulations and their applicable temperature ranges can be found in equations 3.4-6.

For temperatures below  $T_{crit}^{H_2O}$ :

$$P_{crit} = P_{crit}^{H_2O} + \sum_{n=1}^7 c_n (T_{crit}^{H_2O} - T)^{c_{nA}} \quad (3.4) [11]$$

For temperature between  $T_{crit}^{H_2O}$  and 500 °C:

$$P_{crit} = P_{crit}^{H_2O} + \sum_{n=8}^{11} c_n (T - T_{crit}^{H_2O})^{c_{nA}} \quad (3.5) [11]$$

For temperatures above 500 °C:

$$P_{crit} = \sum_{n=12}^{14} c_n (T - 500)^{n-12} \quad (3.6) [11]$$

Where:

- $P_{crit}^{H_2O}$  = critical pressure of H<sub>2</sub>O found in **Table 3.2**
- $c_n$  = derived parameter found in **Table 3.2**

**Table 3.2:** Derived parameters for critical curve [11]

Parameter	Value	Parameter	Value
$P_{crit}^{H_2O}$	2.2054915 x 10 <sup>2</sup>	$c_{1A}$	1
$c_1$	-2.36	$c_{2A}$	1.5
$c_2$	1.28534 x 10 <sup>-1</sup>	$c_{3A}$	2
$c_3$	-2.3707 x 10 <sup>-2</sup>	$c_{4A}$	2.5
$c_4$	3.20089 x 10 <sup>-3</sup>	$c_{5A}$	3
$c_5$	-1.38917 x 10 <sup>-4</sup>	$c_{6A}$	4
$c_6$	1.02789 x 10 <sup>-7</sup>	$c_{7A}$	5
$c_7$	-4.8376 x 10 <sup>-11</sup>	$c_{8A}$	1
$c_8$	2.36	$c_{9A}$	2
$c_9$	-1.31417 x 10 <sup>-2</sup>	$c_{10A}$	2.5
$c_{10}$	2.98491 x 10 <sup>-3</sup>	$c_{11A}$	3
$c_{11}$	-1.30114 x 10 <sup>-4</sup>		
$c_{12}$	Value of $P_{crit}$ at 500 °C		
$c_{13}$	First temperature derivative of equation 2.# at 500 °C		
$c_{14}$	-4.88336 x 10 <sup>-4</sup>		

The development of a regression for the critical composition ( $X_{NaCl}$ ) was accomplished by utilizing two separate formulas for two temperature regions. The

formulas used along with their respective temperature ranges can be seen in equations 3.7 and 3.8.

For temperatures from  $T_{crit}^{H_2O}$  to 600 °C:

$$X_{crit,NaCl} = \sum_{i=1}^7 d_i (T - T_{crit}^{H_2O})^i \quad (3.7) [11]$$

For temperatures from 600 to 1000 °C:

$$X_{crit,NaCl} = \sum_{i=8}^{11} d_i (T - 600 \text{ °C})^{i-8} \quad (3.8) [11]$$

Where:

- $d_i$  = derived parameter found in **Table 3.3**

**Table 3.3:** Derived parameters for critical composition [11]

Parameter	Value	Parameter	Value
$d_1$	$8.00000 \times 10^{-5}$	$d_7$	$-4.89423 \times 10^{-18}$
$d_2$	$1.00000 \times 10^{-5}$	$d_8$	$7.77761 \times 10^{-2}$
$d_3$	$-1.37125 \times 10^{-7}$	$d_9$	$2.7042 \times 10^{-4}$
$d_4$	$9.46822 \times 10^{-10}$	$d_{10}$	$-4.244821 \times 10^{-7}$
$d_5$	$-3.50549 \times 10^{-12}$	$d_{11}$	$2.580872 \times 10^{-10}$
$d_6$	$6.57369 \times 10^{-15}$		

Determination of the volumetric properties of the system were accomplished by first treating the system as either pure H<sub>2</sub>O or NaCl. The pure H<sub>2</sub>O system was solved for using the IAPS-84 equation of state due to reasons mentioned earlier in this section.

Determination of the density for a pure NaCl system was accomplished using equations 3.9-3.10.

$$\rho_{hali} = \rho_{halit}^0 + lP \quad (3.9) [12]$$

Where:

- $\rho_{halite}^0 = l_0 + l_1T + l_2T^2$
- $l = l_3 + l_4e^{T/l_5}$ 
  - o  $l_n = \text{derived parameter found in Table 3.4}$

$$\rho_{NaCl,liquid} = \frac{\rho_{NaCl,liquid}^0}{1 - 0.1 \ln(1 + 10P\beta_{NaCl,liquid})} \quad (3.10) [12]$$

Where:

- $\rho_{NaCl,liquid}^0 = \frac{m_0}{m_1 + m_2T + m_3T^2}$
- $\beta_{NaCl,liquid} = m_4 + m_5T$ 
  - o  $m_n = \text{derived parameter found in Table 3.4}$

**Table 3.4:** Derived parameters for halite and liquid NaCl densities [12]

Parameter	Value	Parameter	Value
$l_0$	$2.1704 \times 10^3$	$m_0$	58443
$l_1$	$-2.4599 \times 10^{-1}$	$m_1$	23.772
$l_2$	$-9.5797 \times 10^{-5}$	$m_2$	0.018639
$l_3$	$5.727 \times 10^{-3}$	$m_3$	$-1.9687 \times 10^{-6}$
$l_4$	$2.715 \times 10^{-3}$	$m_4$	$-1.5259 \times 10^{-5}$
$l_5$	733.4	$m_5$	$5.5058 \times 10^{-8}$

Using the equations derived for density for both pure H<sub>2</sub>O and NaCl as well as available experimental data, a formulation for density of a binary H<sub>2</sub>O-NaCl system was determined.<sup>2</sup>

<sup>2</sup> The derivation for the density formulation for a binary H<sub>2</sub>O-NaCl solution can be seen in greater detail in the referenced Driesner 2007 paper.

The enthalpy and isobaric specific heat capacity for a binary H<sub>2</sub>O-NaCl system was determined as seen in equations 3.11-12.

$$h_{solution} = h_{H_2O}(T_h^*, P) \quad (3.11) [12]$$

Where:

- $T_h^* = q_1 + q_2 T$ 
  - $q_1 = q_{10} + q_{11}(1 - X_{NaCl}) + q_{12}(1 - X_{NaCl})^2$
  - $q_2 = q_{20} + q_{21}\sqrt{X_{NaCl}} + q_{22} + q_{23}X_{NaCl}$ 
    - $q_{10,20}$  are eliminated by conditions  $q_1 = 0$  and  $q_2 = 1$  at  $X_{NaCl} = 0$
    - $q_{12,23}$  are eliminated by conditions  $X_{NaCl} = 1$  when:
      - $q_{1,X_{NaCl}=1} = 47.9058 - 9.36994 \times 10^{-3}P + 6.51059 \times 10^{-6}P^2$
      - $q_{2,X_{NaCl}=1} = 0.24102 + 3.45087 \times 10^{-5}P - 4.28356 \times 10^{-9}P^2$
    - $q_{11,21,22}$  are derived values found in **Table 3.5**

Isobaric specific heat capacity can be determined by taking the derivative of the temperature formulae seen above as seen in equation 3.11, yielding equation 3.12.

$$c_p(T, P, X_{NaCl}) = q_2 c_{p,H_2O}(T_h^*, P) \quad (3.12) [12]$$

The isobaric heat capacity for the halite is determined using another regression fitted using experimental data.<sup>3</sup>

**Table 3.5:** Derived parameters for determination of enthalpy and isobaric heat capacity [12]

Parameter	Value
$q_{11}$	$-32.1724 + 0.062155 P$
$q_{21}$	$-1.69513 - 4.52781 \times 10^{-4} P - 6.04279 \times 10^{-8} P^2$
$q_{22}$	$0.0612567 + 1.88082 \times 10^{-5} P$

<sup>3</sup> The derivation for the isobaric heat capacity of a halite can be seen in greater detail in the referenced Driesner 2007 paper.

The developed formulae determining the properties of a binary H<sub>2</sub>O-NaCl solution was tested against experimental data as well as older models for validation. The resulting comparisons for various properties between the model and experimental data/older models can be found in the next section.

### 3.3.3 Results

The results of employing the model created by Driesner were compared to experimental data as well as models created by previous research groups in an effort to validate the model and improve accuracy. The model produced a NaCl vapor pressure curve and was compared to JANAF data as well as four other research groups experimental data. The results of this comparison can be seen in **Figure 3.6**.

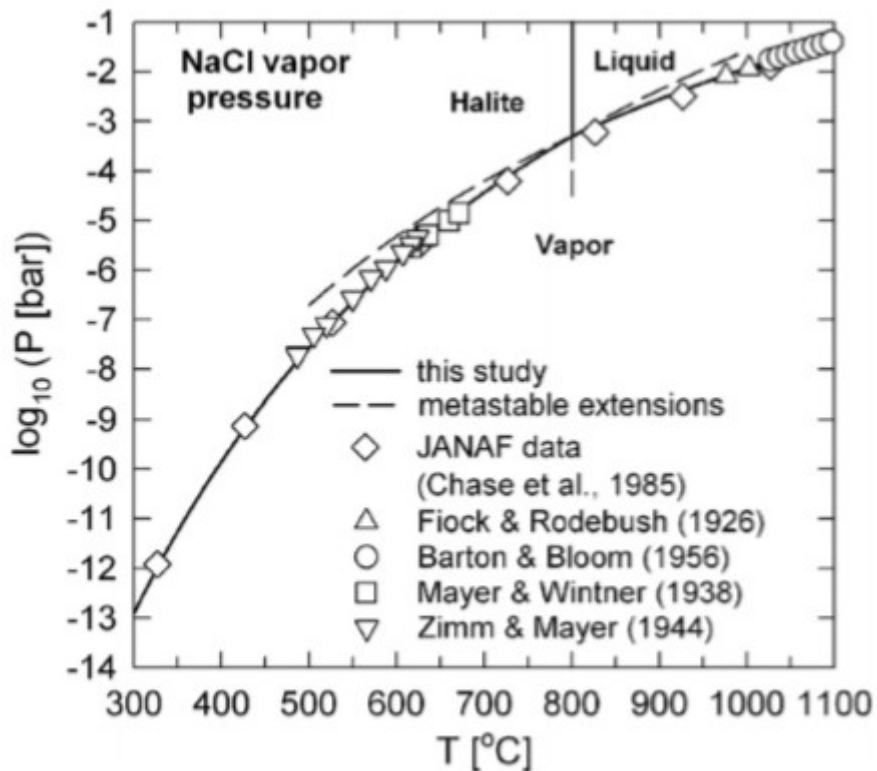


**Figure 3.6:** Comparison of Driesner model output for NaCl vapor pressure vs other experimental work [11]

It is readily apparent when viewing **Figure 3.6** that the derived expression for NaCl vapor pressure closely follows experimental data. The model shows excellent agreement across a large temperature range with multiple datasets thus engendering strong confidence in the model's accuracy. The halite melting curve predicted by the model was compared to multiple other researchers' work and can be seen in **Figure 3.7**.

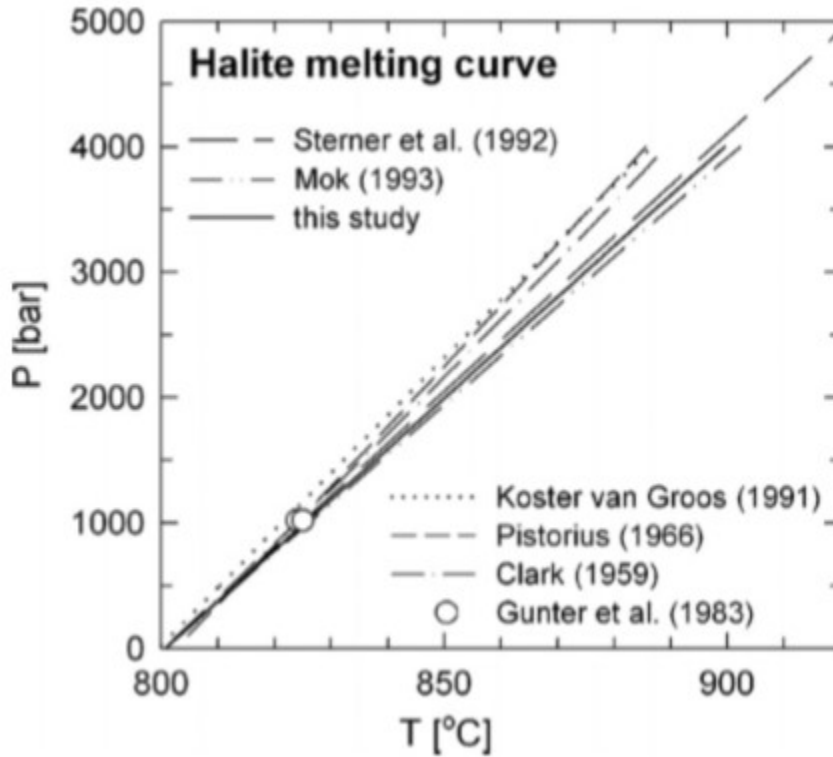


**Figure 3.7:** Comparison of the Driesner simulation output for the halite melting curve vs other studies [11]

The halite melting curve produced by the model shows agreement with work produced by Sterner et al. as well as Mok [17,18]. The model deviated from work produced by Koster van Groos, Pistorius, and Clark as temperature was increased beyond the data available from Gunter et al [16,19,20,21]. The model predicted critical pressure of the H<sub>2</sub>O-NaCl system as temperature was increased can be seen in **Figure 3.8**.



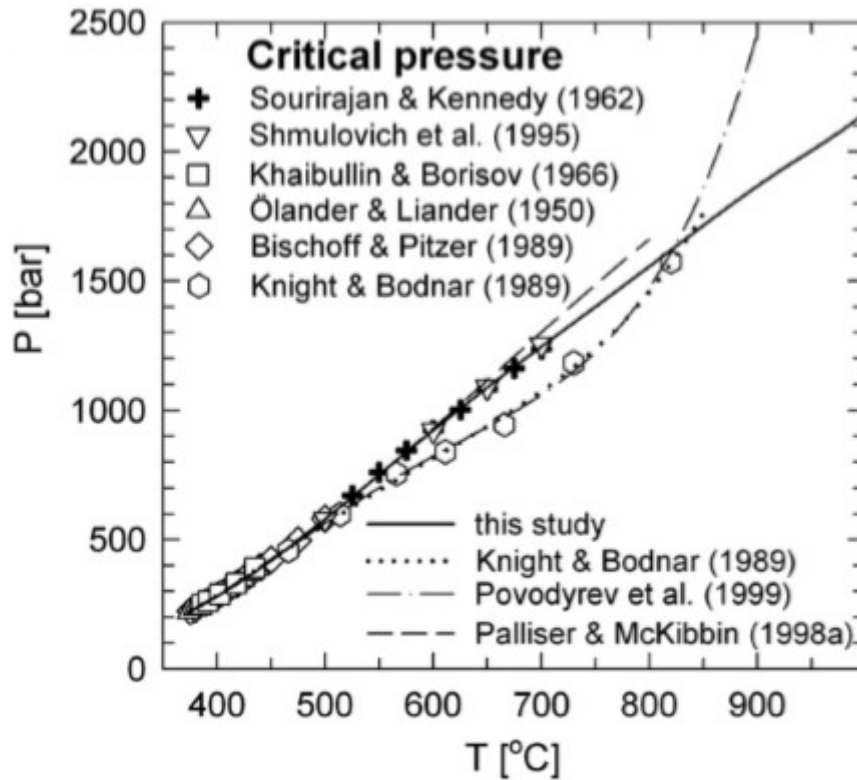


**Figure 3.8:** Comparison of model prediction of critical pressure with other models and experimental data [11]

The model prediction of critical pressure closely follows data produced by Bischoff and Pitzer, Sourirajan and Kennedy, Khaibullin and Borisov, Shmulovich et al., and Ölander and Liander [5,10,22,23,24]. The model deviates from data produced by Knight and Bodnar and thus the models produced which utilized the data from Knight and Bodnar (Knight and Bodnar, Povodyrev et al.) [25,26]. The disagreement in data produced by Knight and Bodnar with the other studies used in comparison led to the exclusion of that dataset from the model formulation.

The critical composition of the H<sub>2</sub>O-NaCl solution was predicted using the derived model and compared to experimental data as well as other produced models. This comparison can be seen in **Figure 3.9**.

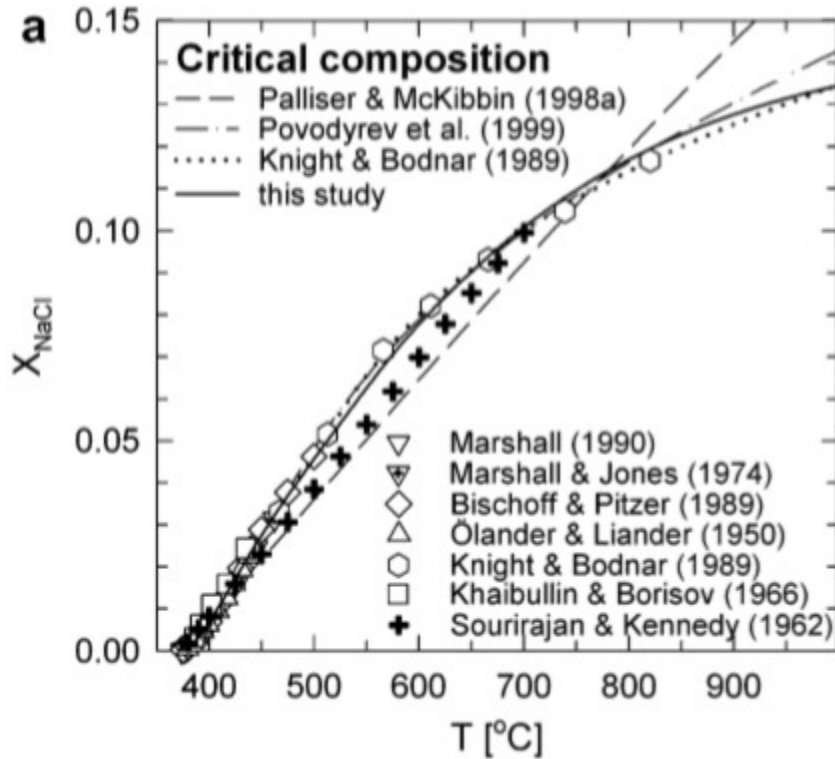


**Figure 3.9:** Comparison of model prediction of critical composition with other models as well as experimental data [11]

The critical composition ( $X_{\text{NaCl}}$ ) predicted by the model formulated by Driesner shows strong agreement with experimental data as well as the Povodyrev et al. and Knight and Bodnar models. The Knight and Bodnar data was particularly useful in this comparison, as opposed to the critical pressure comparison, as it was experimentally observed rather than produced via extrapolation; thus good agreement with the Driesner model improves the confidence in model accuracy.

The density predictions produced by the Driesner model were compared to multiple data sets and plotted as isotherms as a function of pressure. These predictions and their subsequent comparison to experimental data can be seen in **Figure 3.10**.

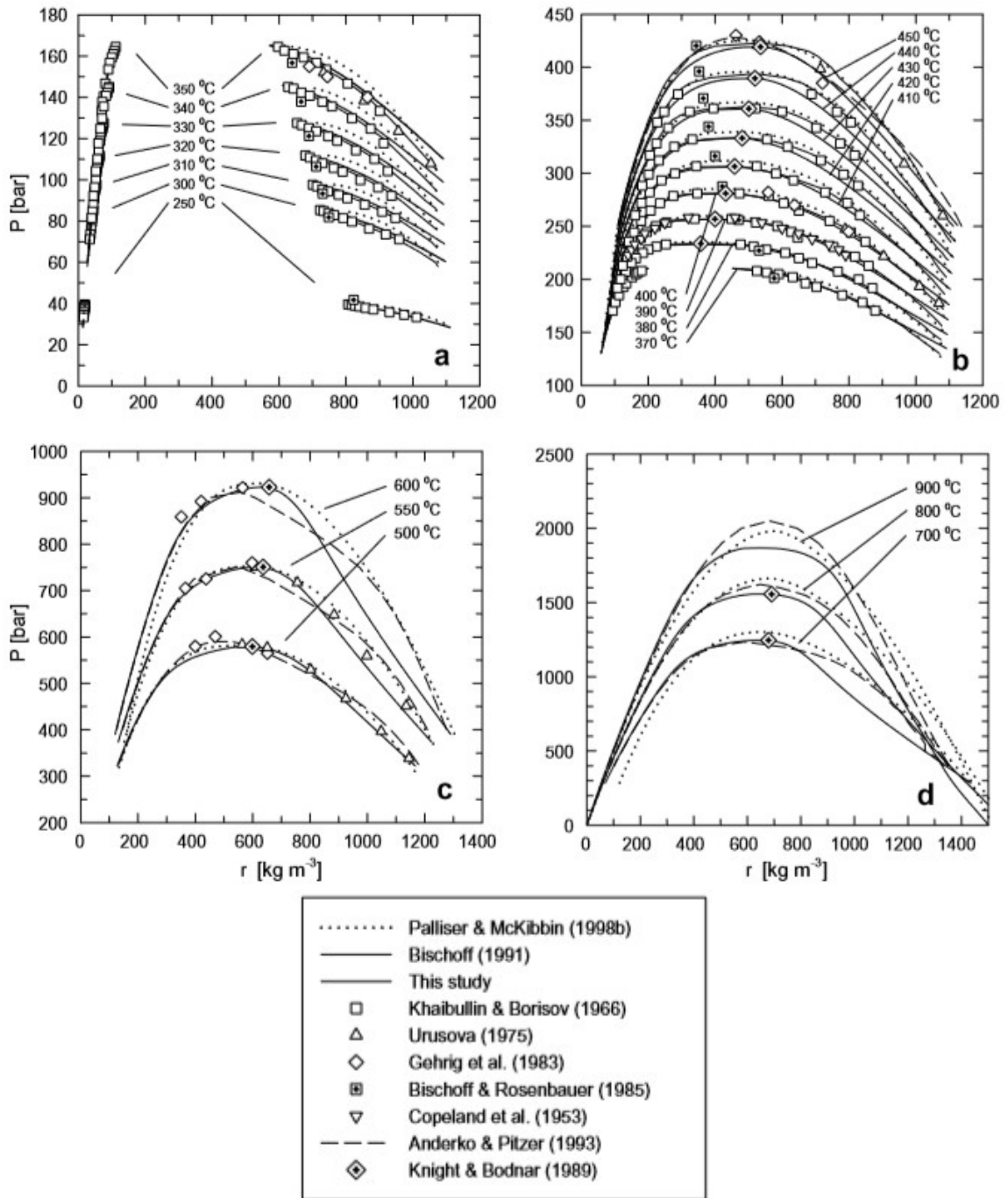


**Figure 3.10:** Comparison of model-predicted density to experimental data with a) subcritical isotherms (250-350 °C), b) supercritical isotherms (370-450 °C), c) 500-600 °C isotherms, and d) 700-900 °C isotherms [12]

The predicted density of the H<sub>2</sub>O-NaCl system produced by the Driesner model shows strong agreement with available experimental data. Part A of **Figure 3.10**

represents the sub-critical isotherms and thus shows the existence of a two-phase system and the resulting two density profiles for each isotherm. The large amount of data available at these conditions allowed for a more accurate formulation for density to be produced thus there is strong agreement between the model predicted density and the experimental data.

Parts B, C, and D of **Figure 3.10** show the supercritical isotherms and the resulting density profiles as functions of pressure. Again, the large amount of data available allowed for a more accurate model formulation of density and thus there is good agreement between the available data and the model predicted density.

The predicted isobaric heat capacity of the H<sub>2</sub>O-NaCl system produced by the Driesner model was compared to data produced by Bischoff and Rosenbauer for a composition comparable to seawater as a function of temperature. This comparison can be seen in **Figure 3.11**.

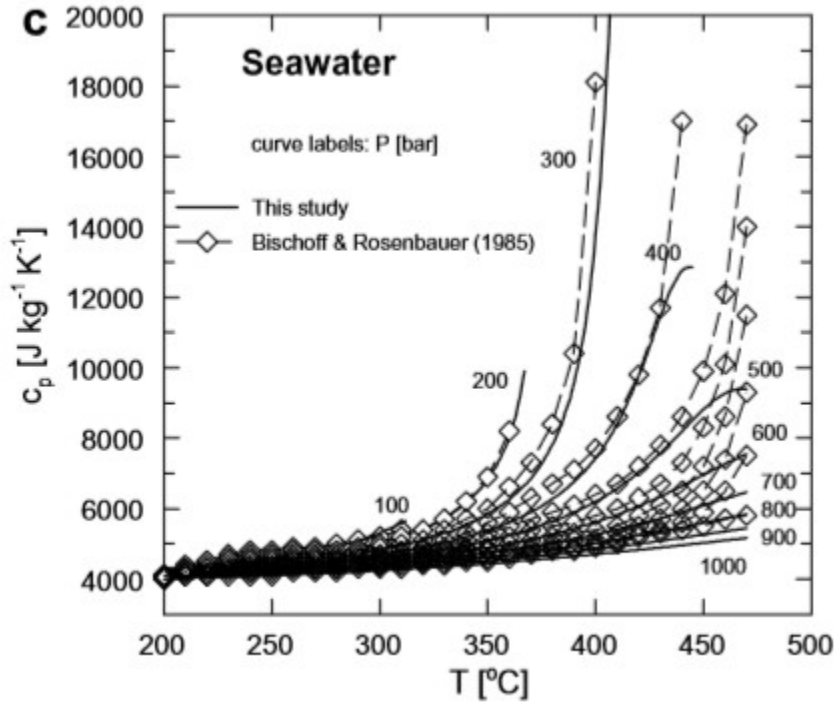


**Figure 3.11:** Comparison of predicted isobaric heat capacity produced by Driesner model vs experimental data [12]

**Figure 3.11** shows strong agreement between the predicted isobaric specific heat capacity of a H<sub>2</sub>O-NaCl system as a function of temperature with experimental data. Isobars ranging from 100 bar to 1000 bar all show minimal deviation between the predicted value and experimental value of isobaric specific heat capacity. This agreement strengthens the confidence in the model's ability to accurately predict system behavior over a wide range of temperatures and pressures, especially with regards to its thermal properties.

Driesner noted in his comparison of isobaric specific heat capacity that the model began to deviate from experimental data at high temperatures, high salinities and moderate pressures. This deviation is likely due to the experimental data at these conditions reflecting heats of dilution which represent variations in enthalpy as functions

of composition; thus the conversion to specific enthalpy and in turn isobaric specific heat capacity is more difficult.

The now-validated property correlations produced by Driesner were implemented into a computer program called “SoWat” [12]. This interactive program is updated as new datasets become available and the correlations are updated along with it.

### **3.3.4 Discussion**

The model produced by Driesner was meticulously formulated utilizing a fundamental physical understanding of the different phases present over a wide temperature, pressure, and composition range along with vast amounts of experimental data and previously derived models. The model improved on previously derived models by utilizing less simplistic fluid property models as well as smaller range integrations.

When formulating property correlations over phase boundaries Driesner split the formulation into multiple steps to account for the drastic property changes across the boundary rather than integrating across the boundary which would yield substantial error. This process was more tedious however it paid dividends when the results were compared to experimental data and showed strong agreement across the board for all properties modeled. The model is not perfect and some areas of the model did yield uncertainty in predicted property values.

Enthalpy and isobaric specific heat capacity were found to yield some uncertainty at high temperatures, high salinities ( $X_{\text{NaCl}} \rightarrow 1$ ), and moderate pressures. This uncertainty arose from the lack of experimental data at these conditions which the formulation was based on. Though these uncertainties exist, they were deemed to have

little effect on the accuracy of specific enthalpy calculations as the data set they were derived from was based on accurate volumetric properties.

The Driesner model produced accurate predictions of key solution properties over a wide range of temperatures, pressures, and compositions ( $X_{\text{NaCl}}$ ). Utilizing datasets produced by multiple research groups, accurate fluid properties, and multi-staged formulations across phase boundaries yielded a model with high fidelity. The availability of this model in a computer program format will allow for easy application to this present work.

### 3.4 Leusbrock Dissertation

Extensive laboratory work has been performed by Ingo Leusbrock at the University of Groningen exploring the solubility of various inorganic salts in the near-supercritical as well as supercritical region. This work explored the solubility behavior of NaCl, NaNO<sub>3</sub>, KCl, KNO<sub>3</sub>, LiCl, LiNO<sub>3</sub>, MgCl<sub>2</sub>, CaCl<sub>2</sub>, Na<sub>2</sub>HPO<sub>4</sub>, NaH<sub>2</sub>PO<sub>4</sub>, and MgSO<sub>4</sub> at temperatures ranging from 380°C (subcritical) to 420°C (supercritical) and pressures of 180 bar (subcritical) to 235 bar (supercritical). Several of these inorganic salts are of special interest to this work as they are found in considerable concentrations in produced water sourced from the Bakken formation in North Dakota.

#### 3.4.1 Background

The properties of water vary considerably from phase to phase. These differences in key properties are exhibited in **Table 3.6**.

**Table 3.6:** Properties of water in the liquid, vapor, and supercritical state [27]

Property	Liquid	Supercritical	Vapor
Density (kg/m <sup>3</sup> )	998	125.1	0.46
Dynamic Viscosity ((N s)/m <sup>2</sup> )	1 x 10 <sup>-3</sup>	2.9 x 10 <sup>-5</sup>	1.6 x 10 <sup>-5</sup>
Thermal conductivity (W/mK)	0.598	0.102	0.033

As can be seen in **Table 3.6**, density drops substantially for pure water from approximately  $998 \text{ kg/m}^3$  in the liquid phase to approximately  $125 \text{ kg/m}^3$  in the supercritical phase. This drop in density follows the same trend as experienced with the dielectric constant for water. These trends can both be seen in **Figure 3.12**.

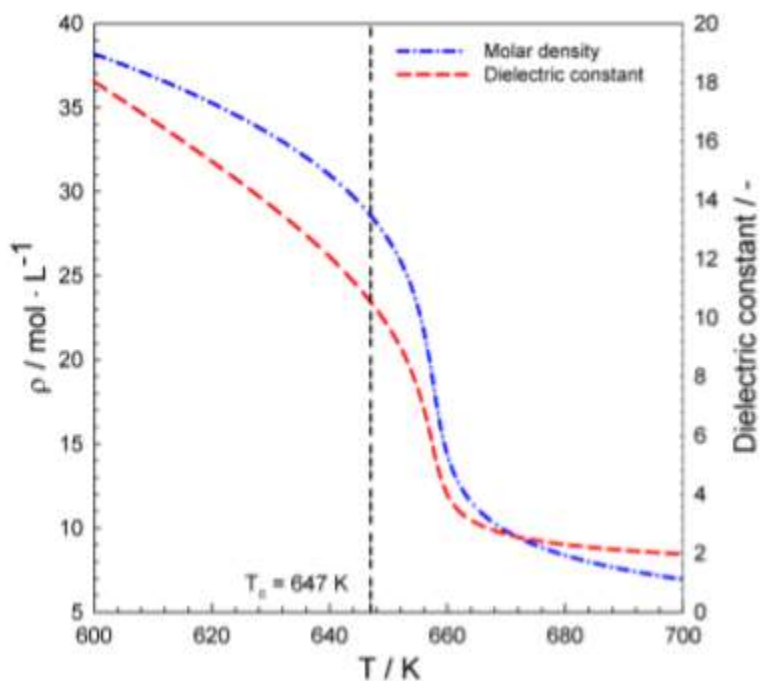


**Figure 3.12:** Density and dielectric constant of water as a function of temperature at 250 bar [28]

As can be seen in **Figure 3.12**, density and the dielectric constant for water follow a similar trend as temperature is increased from 600-700 K ( $326.9 \text{ }^\circ\text{C}$  –  $426.9 \text{ }^\circ\text{C}$ ). The dielectric constant is a good measurement indicating the polarity of water. As this number decreases, water behaves less polar. This trend would then lead us to the assumption that the solubility of polar compounds would also decrease in a similar manner. This is indeed the case as seen in **Figure 3.13**.



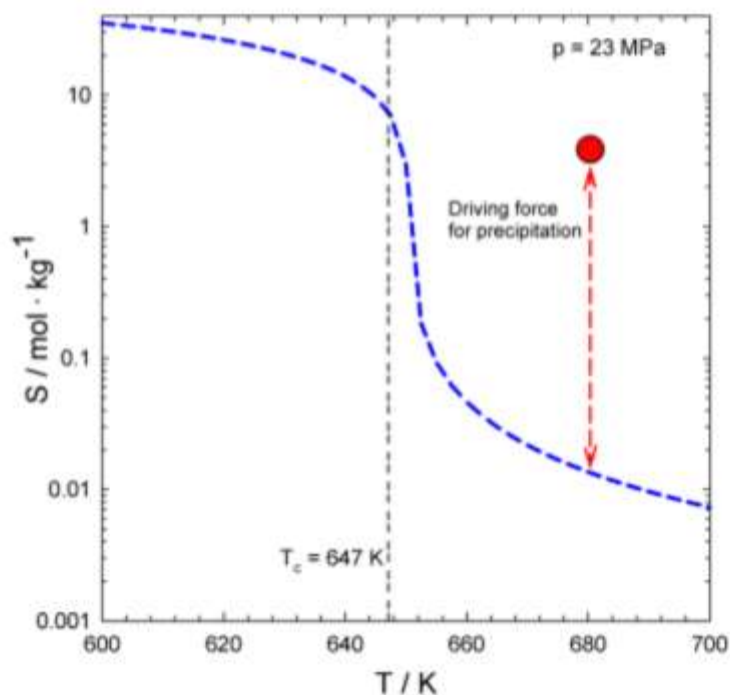


**Figure 3.13:** Solubility of NaCl as a function of temperature at 230 bar. [29]

The solubility of NaCl as a function of temperature from 326.9 °C – 426.9°C at 230 bar as seen in **Figure 3.13** follows nearly an identical trend as seen in **Figure 3.12** with the density as well as dielectric constant of pure water. The similarities of these trends allows researchers to estimate with a reasonable amount of certainty the solubility behavior of NaCl solutions at these conditions when the density of the solution is known at the same conditions. In order to build on this understanding, an empirical and semi-empirical approach by Leusbrock was performed. The empirical approach however would be deemed to be incapable of providing a good representation of experimental data thus it will not be discussed further here.

Leusbrock utilized a semi-empirical method to determine the solubility of various salts based on system conditions such as temperature, pressure, and density. A solubility curve of NaCl as a function of density was constructed and can be seen in **Figure 3.14**.

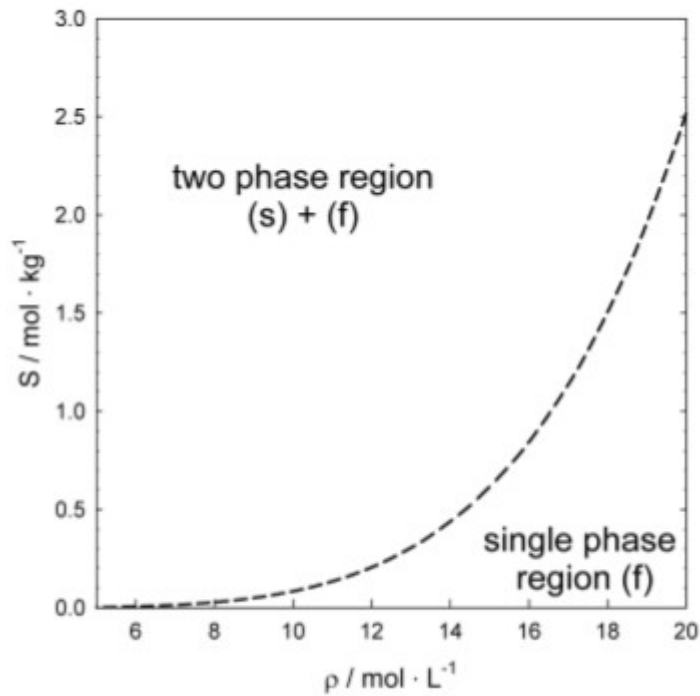
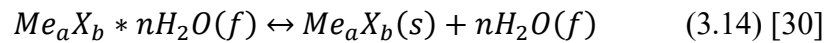
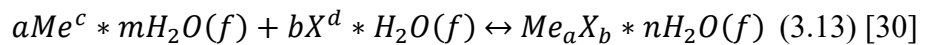


**Figure 3.14:** Solubility of NaCl as a function of density [30]

The region above the solubility curve represents a two phase system of solid NaCl (s) and supercritical water (f). The region below the solubility curve represents a single phase system with dissolved NaCl in supercritical water. The solubility line represents an equilibrium between the two regions. Leusbrock determined that this equilibrium could be represented as shown in equations 3.13 and 3.14.



Where:

- $Me$  = salt cation
- $X$  = salt anion
  - o  $a, b$  = number of ions in salt molecule

- $c, d = \text{valency of ions}$
- $m, n = \text{number of water molecules}$

Using equations 2.13 and 2.14, an equilibrium constant could be determined as seen in equation 2.15.

$$K_s = \frac{\alpha_{Me_aX_b \cdot nH_2O(f)}}{\alpha_{Me_aX_b(s)} \times \alpha_{nH_2O(f)}} \quad (3.15) [30]$$

Where:

- $\alpha = \text{activity coefficient of each species on a molality basis}$

Leusbrock simplified this equation substantially by assuming unity for the activity coefficient of solid salts, neglecting the interaction of solvated salt complexes as well as the water molecules themselves, and assuming the solution was ideal. The Arrhenius approach for representing the equilibrium constant was utilized, and after systematic derivation, the concentration of salts was represented using equation 3.16.

$$\ln(c_{MeX}) = A' - \frac{B'}{T} + C' \ln(T) + D' \ln(\rho) \quad (3.16)^4 [30]$$

Where:

- $c_{MeX} = \text{concentration of salt}$
- $A', B', C', \text{ and } D' = \text{fitting parameters}$
- $T = \text{temperature}$
- $\rho = \text{density}$

In order to validate the semi-empirical approach produced above, an experimental set-up was produced and tested for various salts.

---

<sup>4</sup> This derivation can be seen in greater detail in the referenced Leusbrock 2011 paper.

### 3.4.2 Methods

The validation of the semi-empirical formulations derived above were validated using the experimental set up scheme seen in **Figure 3.15** as well as previous work performed by other researchers [31,32,33,34,35,36,37].

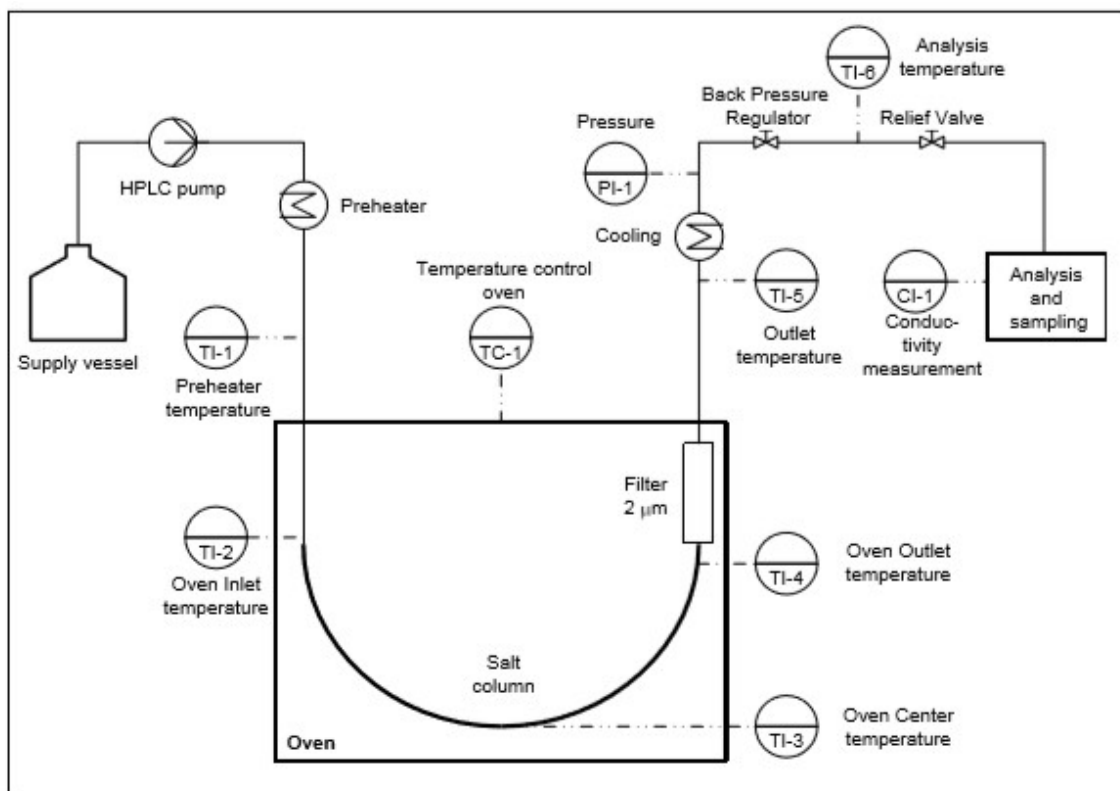


**Figure 3.15:** Experimental process scheme for salt solubility determination [30]

The experimental system was constructed using Hastelloy tubing designed to handle pressures up to 250 bar and temperatures as high as 450 °C. Flow rates for the brine solution ranged between 1-10 mL/min. Inline conductivity measurements provided real-time concentration analysis for the system. More accurate post-mortem ion analysis was performed using an ICP-AES (for cations) and IC (for anions).

### 3.4.3 Results

The derived semi-empirical method (equation 3.16) was found to provide good representation of salt solubility when compared to experimental work performed by Leusbrock as well as multiple other research groups as seen in **Figure 3.16**.

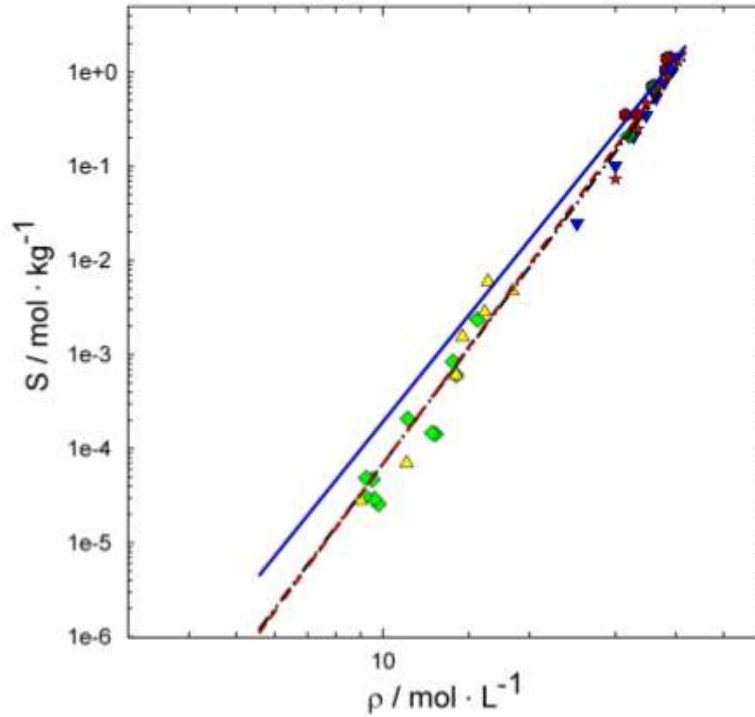


**Figure 3.16:** Solubility of  $\text{Na}_2\text{SO}_4$  as a function of density. The dashed line represents the semi-empirical method represented with equation (3.16). The solid line represents the less accurate empirical method [30].

The semi-empirical method was applied to laboratory data for  $\text{NaCl}$  and  $\text{NaNO}_3$  producing the fitting parameters found in **Table 3.7**.

**Table 3.7:** Fitting parameters for equation 3.16 for various salts [30]

Salt	A'/-	B'/-	C'/-	D'/-
NaCl	-59.93	-2514	6.23	4.01
NaNO <sub>3</sub>	-18.04	-61	1.13	3.06

The results of experimental testing using the process set up seen in **Figure 3.16** were plotted as a function of molar density (mol/L). The results of a few selected salts

are shown in this paper based on their relevance to this work.<sup>5</sup> The solubility of NaNO<sub>3</sub> can be seen in **Figure 3.17**.

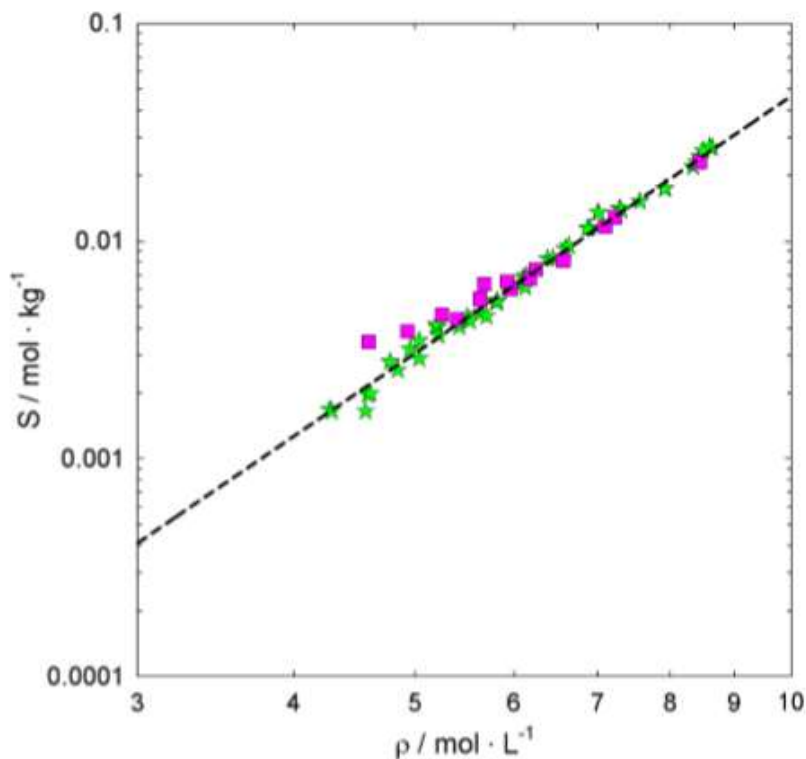


**Figure 3.17:** Solubility of NaNO<sub>3</sub> as a function of density. \* represent Leusbrock experimental data, squares represent Dell-Orco et al. data, and the dashed line represents the semi-empirical model results [30,38]

The solubility of NaNO<sub>3</sub> data produced by Leusbrock appears to show good agreement with previous experimental work produced as well as the semi-empirical formulation produced by Leusbrock. The ability of the semi-empirical formulation to accurately reflect the solubility of NaNO<sub>3</sub> is important in building confidence in the model's applicability to other salts. The results of the solubility tests for NaCl as a function of density can be seen in **Figure 3.18**.

<sup>5</sup> The complete set of results for Leusbrock's experimental work can be found in the referenced Leusbrock 2011 paper.

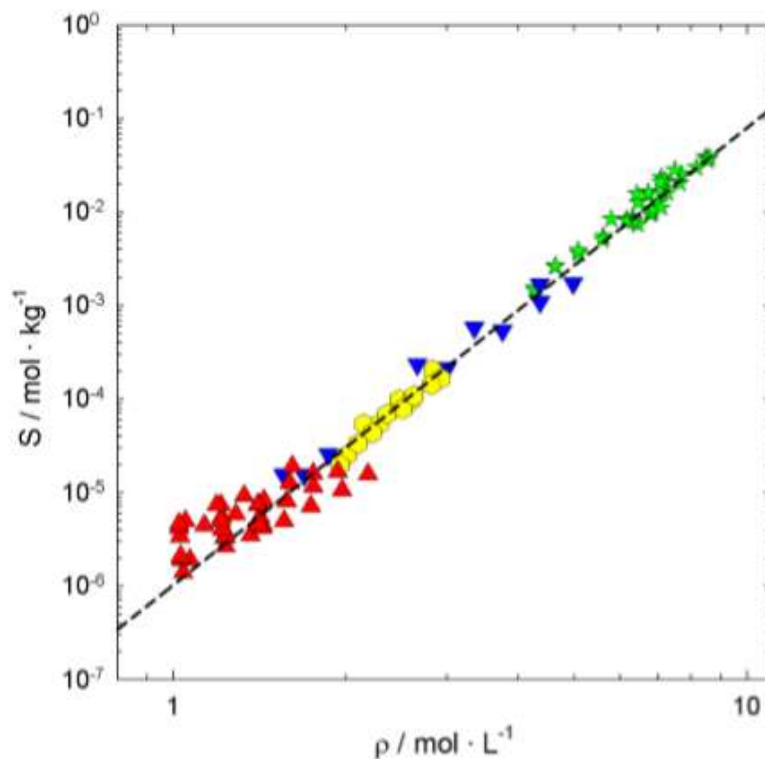


**Figure 3.18:** Solubility of NaCl as a function of density. \* represent Leusbrock experimental results, triangles represent Galobardes et al. data, delta represents Armellini et al. data, hexagons represent Higashi et al. data, and the dashed line represents the semi-empirical model results [30,39,40]

The solubility data for NaCl produced by Leusbrock shows strong agreement with previous experimental work along with the semi-empirical model. Again the agreement of the model with experimental data builds more confidence in the model's ability to be applied to other salts and yield accurate results. The solubility of KCl as a function of density can be seen in **Figure 3.19**.

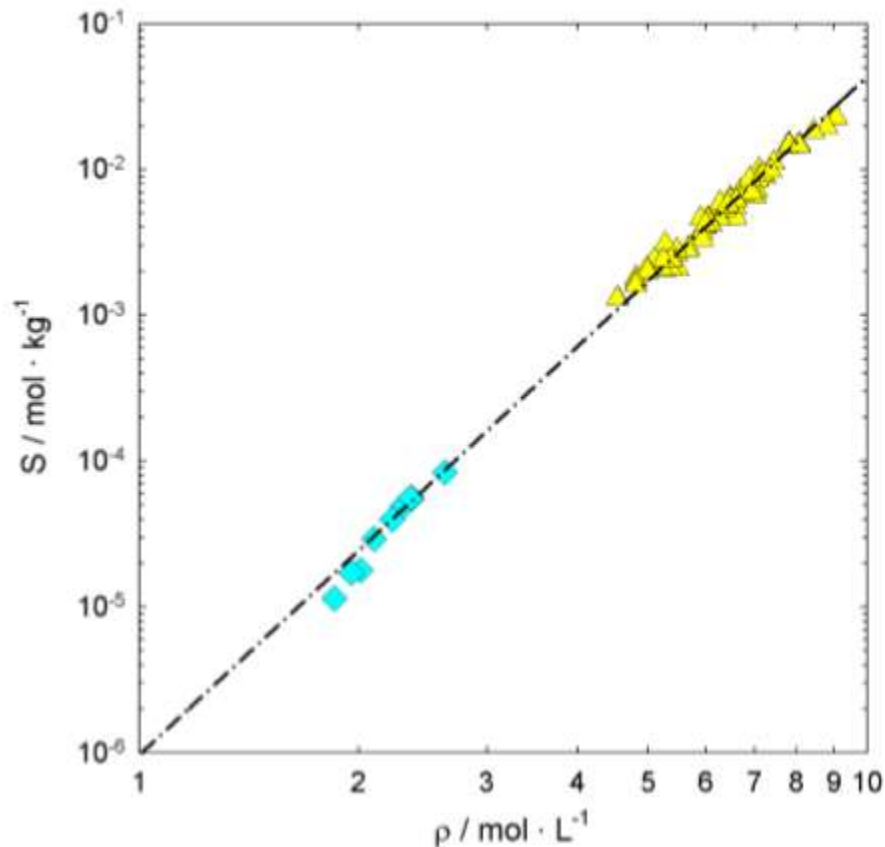


**Figure 3.19:** Solubility of KCl as a function of density. Triangles represent Leusbrock experimental results, diamonds represent Higashi et al. data, and the dashed line represents the semi-empirical model results [30,40]

The solubility data for KCl produced by Leusbrock shows strong agreement with previous experimental work along with the semi-empirical model. Leusbrock's work helped fill in current experimental gaps at higher densities of solvent (lower temperatures) which allows for a greater understanding of KCl's solubility in H<sub>2</sub>O over a wide range of conditions. Again the agreement of the model with experimental data builds more confidence in the model's ability to be applied to other salts and yield accurate results.



### 3.4.4 Discussion

The work performed by Leusbrock provides valuable insight into an accurate semi-empirical method for determining the solubility of various salts in the supercritical region. This method has been validated using work performed by other research groups as well as laboratory results from Leusbrock himself.

It is important to note that the semi-empirical approach developed by Leusbrock is only valid across the small temperature range he produced data at. Extrapolating beyond this temperature range leads to erroneous predictions in salt solubilities. It is because of this key caveat with the semi-empirical approach that this wasn't employed as a model to evaluate and compare later in chapter four of this thesis.

The potential shortfalls of applying the work performed by Leusbrock to this work are the very small concentrations of salt brines tested (i.e. approximately 3,000 mg/L NaCl). Produced water has concentrations of NaCl nearly 30x the concentrations being tested by Leusbrock. This revelation must be kept in mind when applying his results to this work.

### 3.5 References

- [1] Pitzer, K. S., and Pabalan, R.T., "*Thermodynamics of NaCl in steam,*" in *Geochimica et Cosmo-chimica*, **1986**, vol 50, pp. 1445-1454.
- [2] Pitzer, K. S., and Li, Y.-g, "*Critical phenomena and thermodynamics of dilute aqueous sodium chloride to 823K,*" in *Proceedings of the National Academy of Sciences*, **1984**, vol 81, pp. 1268-1271.
- [3] Pitzer, K. S., Peiper, J. C., and Busey, R. H., "*Thermodynamic properties of aqueous sodium chloride solutions,*" in *Journal of Physical Chemistry Reference Data*, **1984**, vol 13, pp. 1-102.
- [4] Pitzer, K. S., Bischoff, J. L., and Rosebauer, R. J., "*Critical behavior of dilute NaCl in H<sub>2</sub>O*" in *Chemical Physics Letters*, **1987**, vol 134, pp. 60-63.
- [5] Sourirajan, S., and Kennedy, G. C., "*The system NaCl-H<sub>2</sub>O at elevated temperatures and pressures,*" in *American Journal of Science*, **1962**, vol 260, pp. 115-242.

- [6] Bischoff, J. L., Rosenbauer, R. J., and Pitzer, K. S., “*The system NaCl-H<sub>2</sub>O: relations of vapor-liquid near the critical temperature of water and of vapor-liquid=halite from 300° to 500 °C,*” in *Geochimica et Cosmochimica Acta*, **1986**, vol 50, pp. 1437-1444.
- [7] Rosenbauer, R., and Bischoff, J. L., “*Pressure-composition relations for coexisting gases and liquids and the critical points in the system NaCl-H<sub>2</sub>O at 450, 475, and 500 °C,*” in *Geochimica et Cosmochimica Acta*, **1987**, vol 51, pp. 2349-2354.
- [8] Rosenbauer, R., and Bischoff, J. L., “*Liquid-vapor relations in the critical region of the system NaCl-H<sub>2</sub>O 380° to 415° C: a refined determination of the critical point and the two-phase boundary of seawater,*” in *Geochimica et Cosmochimica Acta*, **1988**, vol 53, pp. 2121-2126.
- [9] Bischoff, J. L., and Rosenbauer, R. J., “*The critical point and two-phase boundary of seawater, 200-500°C,*” in *Earth and Planetary Science Letters*, **1984**, vol 68, pp. 172-180.
- [10] Bischoff, J. and Pitzer, K., “*Liquid-vapor relations for the system NaCl-H<sub>2</sub>O: summary of the P-T-x surface from 300° and 500°C,*” in *American Journal of Science*, **1989**, vol 289, 217-248.
- [11] Driesner, T. and Heinrich, C., “*The system H<sub>2</sub>O-NaCl. Part I: Correlation formulae for phase relations in temperature-pressure-composition space from 0 to 1000°C, 0 to 5000 bar, and 0 to 1 X<sub>NaCl</sub>,*” in *Geochimica et Cosmochimica Acta*, **2007**, vol 71, pp 4880-4901.
- [12] Driesner, T., “*The system H<sub>2</sub>O-NaCl. Part II: Correlations for molar volume, enthalpy, and isobaric heat capacity from 0 to 1000°C, 1-5000 bar, and 0 to 1 X<sub>NaCl</sub>,*” in *Geochimica et Cosmochimica Acta*, **2007**, vol 71, pp 4902-4919.
- [13] Hayba, D. O., and Ingebritsen, S. E., “*Multiphase groundwater flow near cooling plutons,*” in *J. Geophys. Res. So. Ea.*, **1997**, vol 102, pp. 12235-12252.
- [14] Bauer, O., and Engel, O., “*PROST-PROPERTIES of Water and Steam. C Computer Program,*” in Technische Universität Hamburg-Harburg, Department of Applied Thermodynamics, **1998**.
- [15] Haar, L., Gallagher, J. S., and Kell, G. S., “*NBS/NRC Steam Tables,*” from Taylor and Francis, London, **1984**, pp 320.
- [16] Gunter, W. D., Chou, I.-M., and Girsberger, S., “*Phase relations in the system NaCl-KCl-H<sub>2</sub>O. II. Differential thermal analysis of the halite liquidus in the NaCl-H<sub>2</sub>O binary above 450 °C,*” in *Geochimica et Cosmochimica Acta*, **1983**, vol 47, pp. 863-873.
- [17] Mok, U., “*Volumetric determinations in the systems NaCl-H<sub>2</sub>O and KCl-H<sub>2</sub>O to 450 MPa and 900 °C,*” at ETH Zurich, **1993**.
- [18] Sterner, S. M., Chou, I.-M., Downs, R. T., and Pitzer, K. S., “*Phase relations in the system NaCl-KCl-H<sub>2</sub>O. V. Thermodynamic PTX analysis of solid-liquid equilibria at high temperatures and pressures,*” in *Geochimica et Cosmochimica Acta*, **1992**, vol 56, pp. 2295-2309.
- [19] Koster van Groos, A. F., “*Differential thermal analysis of the liquidus relations in the system NaCl-H<sub>2</sub>O to 6kbar,*” in *Geochimica et Cosmochimica Acta*, **1991**, vol 55, pp. 2811-2817.

- [20] Pistorius, C. W. F. T., “*Effect of pressure on the melting points of the sodium halides,*” in *J. Chem. Phys.*, **1966**, vol 45, pp. 3513-3519.
- [21] Clark, S. P., “*The effect of pressure on the melting points of eight alkali halides,*” in *J. Chem. Phys.*, **1959**, vol 31, pp. 1526-1531.
- [22] Shmulovich, K. I., Tkacheko, S. I., and Plyasunova, N. V., “*Phase equilibria in fluid systems at high pressures and temperatures,*” in *Fluids in the Crust*, **1995**, pp. 193-215.
- [23] Khaibullin, I. K., and Borisov, N. M., “*Experimental investigation of the thermal properties of aqueous and vapor solutions of sodium and potassium chlorides at phase equilibrium,*” in *High Temperature*, **1966**, vol 4, pp 518-523.
- [24] Olander, A. and Liander, H., “*The phase diagram of sodium chloride and steam above the critical point,*” in *Acta Chem. Scand.*, **1950**, vol 4, pp. 1437-1445.
- [25] Knight, C. L., and Bodnar, R. J., “*Synthetic fluid inclusions. IX. Critical PVTX properties of NaCl-H<sub>2</sub>O solutions,*” in *Geochimica et Cosmochimica Acta*, **1989**, vol 53, pp. 3-8.
- [26] Povodyrev, A. A., Anisimov, M. A., Sengers, J. V., Marshall, W. L., and Levelt, Sengers, J. M. H., “*Critical locus of aqueous solutions of sodium chloride,*” in *Int. J. Thermophys.*, **1999**, vol 20, pp. 1529.
- [27] W. Wagner, “*The IAPWS formulation 1995 for the thermodynamic properties of ordinary water substance for general and scientific use,*” in *Journal of Physical and Chemical Reference Data*, **1999**, vol 31, pp 387.
- [28] “*International Association for the Properties of Water and Steam, Release on the static dielectric constant of ordinary water substance for temperatures from 238 K to 873 K and pressures up to 1000 MPa,*” from IAPWS, Erlangen, Germany
- [29] I. Leusbrock, S. Metz, G. Rexwinkel, G. F. Versteeg, “*Quantitative approaches for the description of solubilities of inorganic compounds in near-critical and supercritical water,*” in *The Journal of Supercritical Fluids*, **2008**, vol 47, pp 117-127.
- [30] I. Leusbrock, “*Removal of inorganic compounds via supercritical water: fundamentals and applications,*” from Groningen: Rijksuniversiteit Groningen, **2011**.
- [31] M. S. Khan, S. N. Rogak, “*Solubility of Na<sub>2</sub>SO<sub>4</sub>, Na<sub>2</sub>CO<sub>3</sub> and their mixture in supercritical water,*” in *The Journal of Supercritical Fluids*, **2004**, vol 30, pp 359.
- [32] S. N. Rogak, P. Teshima, “*Deposition of sodium sulfate in a heated flow of supercritical water,*” in *AIChE Journal*, **1999**, vol 45, pp 240.
- [33] F. J. Armellini, J. W. Tester, “*Solubility of sodium chloride and sulfate in sub- and supercritical water vapor from 450-550°C and 100-250 bar,*” in *Fluid Phase Equilibria*, **1993**, vol 84, pp 123.
- [34] M. Ravich, F. Borovaya, “*Phase equilibria in the sodium sulphate-water system at high temperatures and pressures,*” in *Russian Journal of Inorganic chemistry*, **1964**, vol 9, pp 520–532.
- [35] M. M. DiPippo, K. Sako, J. W. Tester, “*Ternary phase equilibria for the sodium chloride-sodium sulfate-water system at 200 and 250 bar up to 400 deg.C.,*” in *Fluid Phase Equilibria*, **1999**, vol 157, pp 229

- [36] D. Shvedov, P. Tremaine, “*The solubility for aqueous sodium sulphate and the reduction of sulphate by magnetite under near-critical conditions,*” in Proceedings of the 4th International Symposium on Hydrothermal Reactions, **1997**.
- [37] M. Hodes, P. Griffith, K. A. Smith, W. S. Hurst, W. J. Bowers, K. Sako, “*Salt solubility and deposition in high temperature and pressure aqueous solutions,*” in American Institute of Chemical Engineers Journal, **2004**, vol 50, pp 2038 – 2049.
- [38] Dell’Orco, P., Eaton, H., Reynolds, T., and Buelow, S., “*The solubility of 1:1 nitrate electrolytes in supercritical water,*” in The Journal of Supercritical Fluids, **1995**, vol 3, pp. 217.
- [39] Galobardes, J. F., Vanhare, D. R., and Rogers, L. B., “*Solubility of sodium-chloride in dry steam,*” in Journal of Chemical and Engineering Data, **1981**, vol 4, pp. 363-366.
- [40] Higashi et al., “*Measurement and correlation for solubilities of alkali metal chlorides in water vapor at high temperature and pressure,*” in Fluid Phase Equilibria, **2005**, vol 547, pp. 228-229.

## Chapter 4: Comparison of Concentration Models

### 4.1 Introduction

With the strong foundation for solubility work presented earlier in this work, a few different concentration programs were employed to test their validity against previous models and experimental work. Ultimately the goal of this work is to find the best program for modeling concentration of complex solutions such as produced water. Laboratory testing is expensive, time consuming, and tedious. Thus employing a model which can produce concentration data with reasonable accuracy can help engineers design desalination technologies for these complex solutions with the speed of relevance.

Modeling a binary H<sub>2</sub>O-NaCl system is far simpler than attempting to model a multi-component system such as produced water. Fortunately, when a solution's primary constituent is NaCl, concentration for the system as a whole can be modeled as a H<sub>2</sub>O-NaCl brine with accuracy [1]. Produced water's primary constituent is NaCl by far with the next closest constituent (in the samples we have tested) being CaCl<sub>2</sub>. With the general composition of a produced water sample known and the Trembly and Ogden assumption applied, we can compare various models for accuracy with regards to produced water concentration. The Trembly and Ogden assumption serves as the linchpin in our modeling efforts which allows us to employ the available H<sub>2</sub>O-NaCl system models for comparison and evaluation for ability to model produced water concentration.

## 4.2 HSC Equilibrium Modeling

The modeling program HSC Chemistry was utilized as a means to determine the concentration of a pure H<sub>2</sub>O-NaCl solution as a function of pressure and temperature. The results of this simulation would then be compared to other modeling efforts as well as experimental data to determine the validity of the program. After generating a predicted concentration curve for a binary H<sub>2</sub>O-NaCl solution that was used to compare with other models and experimental data, a produced water sample was modeled to determine concentration as a function of temperature and pressure as well.

### 4.2.1 Theory

HSC Chemistry solves concentration problems utilizing “Gibbs energy minimization” and delivers equilibrium concentration compositions for each set of prescribed temperature and pressure conditions. The Gibbs function for the system can be given by equation 4.1.

$$nG(n_i, s, T, P) = \sum n_i \Delta G_{fi}^0 + \sum n_i RT \ln(P) + \sum n_i RT \ln(y_i) + \sum n_i RT \ln(\varphi_i) \quad (4.1) [2]$$

Where:

- $nG$  = total Gibbs free energy of the system
- $n_i$  = number of moles of species  $i$
- $y_i$  = mole fraction of species  $i$
- $\Delta G_{fi}^0$  = standard Gibbs free energy of formation for species  $i$
- $\varphi_i$  = fugacity coefficient of species  $i$  in mixture

The goal of this program is to find the  $n_i, s$  which minimize  $nG$  at each set of process conditions, thus delivering species compositions in each phase at each set of process conditions. This program is based on equilibrium compositions, thus insinuating

that there is an infinite amount of time for species to reach equilibrium. In other words, the kinetics of this system are treated as being infinitely fast, thus the system isn't constrained by mass transfer rates.

#### **4.2.2 Methods**

A 10 wt% NaCl-H<sub>2</sub>O solution was used as the input solution to be modeled by HSC. The solution was simulated over the process conditions of 25-450 °C. In order to determine the pressure to model the solution at, the assumption was made that pressure differences at these conditions (200-240 bar) would yield insignificant concentration differences thus a single isobar could be used for simulations.

In order to test this theory, the pressure was varied over these conditions to evaluate the importance of pressure at these conditions compared to temperature. The results of the simulations were plotted against each other to determine the pressure dependence on concentration. From this comparison, a single isobar was chosen as the simulation pressure to be used for comparison with other models. The resulting simulation results were then used for comparison with other models as well as experimental data to determine the most accurate model.

In order to simulate a produced water solution across the desired temperature range to determine concentration of common ions present in produced water, a 50 L sample was sourced from a well site in the Bakken formation in western North Dakota. This sample was analyzed using ICP-MS and IC by Standard Laboratories in Illinois to determine the complete ion composition. The composition of this solution was used as the simulation input for HSC in order to model the concentration of different ions at 240

bar as temperature was increased from 25 °C – 450 °C. The produced water composition input used in the HSC simulation is found in **Table 4.1**.

**Table 4.1:** Produced water ion composition used as HSC solution composition input.

Constituents	Concentration (mg/L)	MW (g/mol)	mol/L	% mol
Ca <sup>+2</sup>	22400	40.08	0.559	0.010
Mg <sup>+2</sup>	1430	24.31	0.059	0.001
Na <sup>+</sup>	89500	22.99	3.893	0.070
K <sup>+</sup>	7400	39.10	0.189	0.003
Li <sup>+</sup>	60	6.94	0.009	0.000
Ba <sup>+2</sup>	33	137.33	0.000	0.000
Fe <sup>+2</sup>	152	55.85	0.003	0.000
Mn <sup>+2</sup>	18	54.94	0.000	0.000
Sr <sup>+2</sup>	1540	87.62	0.018	0.000
Pb <sup>+2</sup>	1	207.20	0.000	0.000
Cl <sup>-</sup>	189800	35.45	5.354	0.096
Br <sup>-</sup>	816	79.90	0.010	0.000
SO <sub>4</sub> <sup>-2</sup>	197	96.06	0.002	0.000
F <sup>-</sup>	33	19.00	0.002	0.000
HCO <sub>3</sub> <sup>-</sup>	61	61.02	0.001	0.000
NO <sub>3</sub> <sup>-</sup>	64	62.00	0.001	0.000
H <sub>2</sub> O (L)	NA	18.02	55.500	1.000

### 4.2.3 Results

Upon completion of each simulation, the predicted concentration results were recorded into Microsoft Excel to be plotted for evaluation. The raw data from each model can be found in Appendix A. The first simulations completed were for a 10 wt% NaCl-H<sub>2</sub>O solution over the temperature range of 25-450°C under the isobaric conditions of 200 bar, 220 bar, and 240 bar. The pressure dependence of concentration at these conditions was evaluated by comparing the predicted concentrations for each isobar simulation. This comparison is seen in **Figure 4.1**.



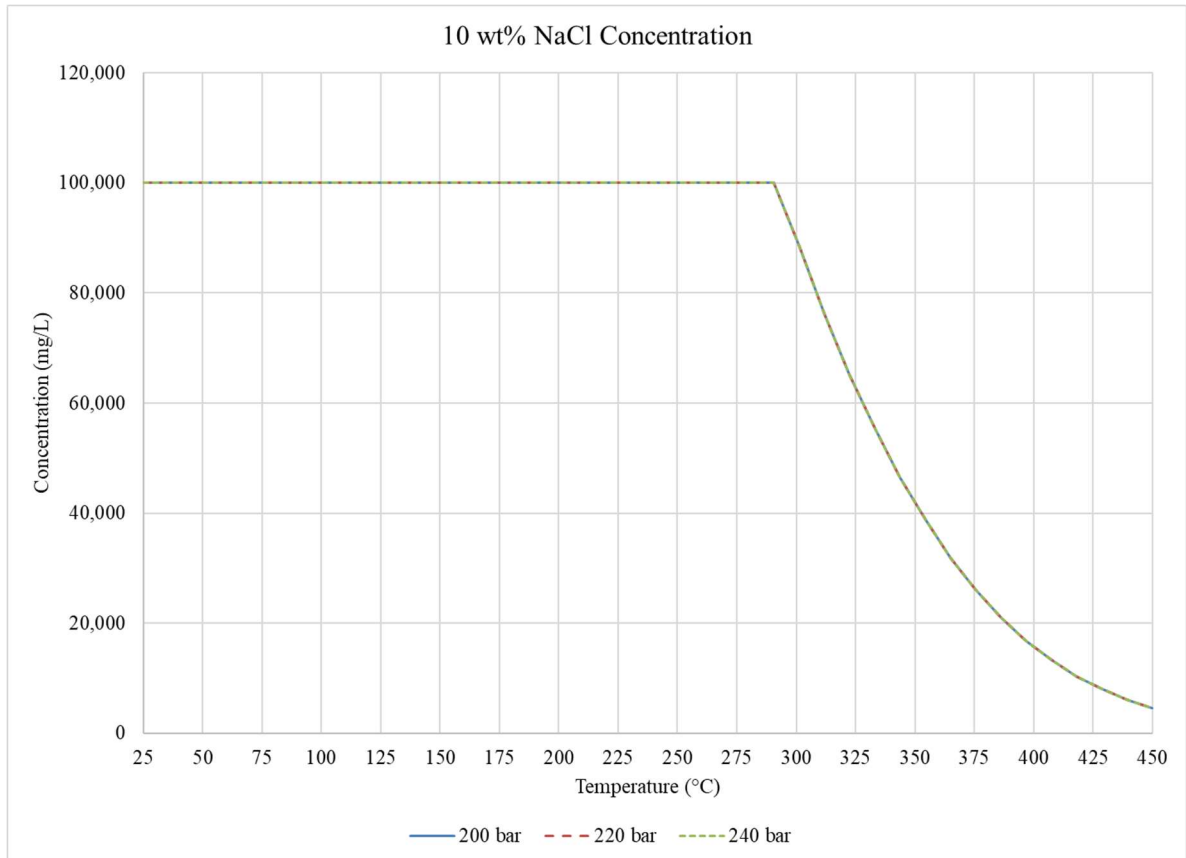


**Figure 4.1:** Predicted concentration of a 10 wt% NaCl-H<sub>2</sub>O solution over the temperature range of 25-450 °C.

All three isobars' (200, 220, and 240 bar) predicted concentration data sets are plotted against each other as seen in **Figure 4.1**. It is evident that at these conditions, the pressure difference between 200-240 bar is not a factor in predicting the concentration of NaCl. The lack of pressure dependence between 200-240 bar allows future simulations to take place at one isobar as the simulation results will be the same regardless. Thus, when simulating the sample of produced water sourced from the Bakken, 240 bar was the only isobar simulated across the 25-450 °C temperature range. The results of this simulation can be seen in **Figure 4.2**.

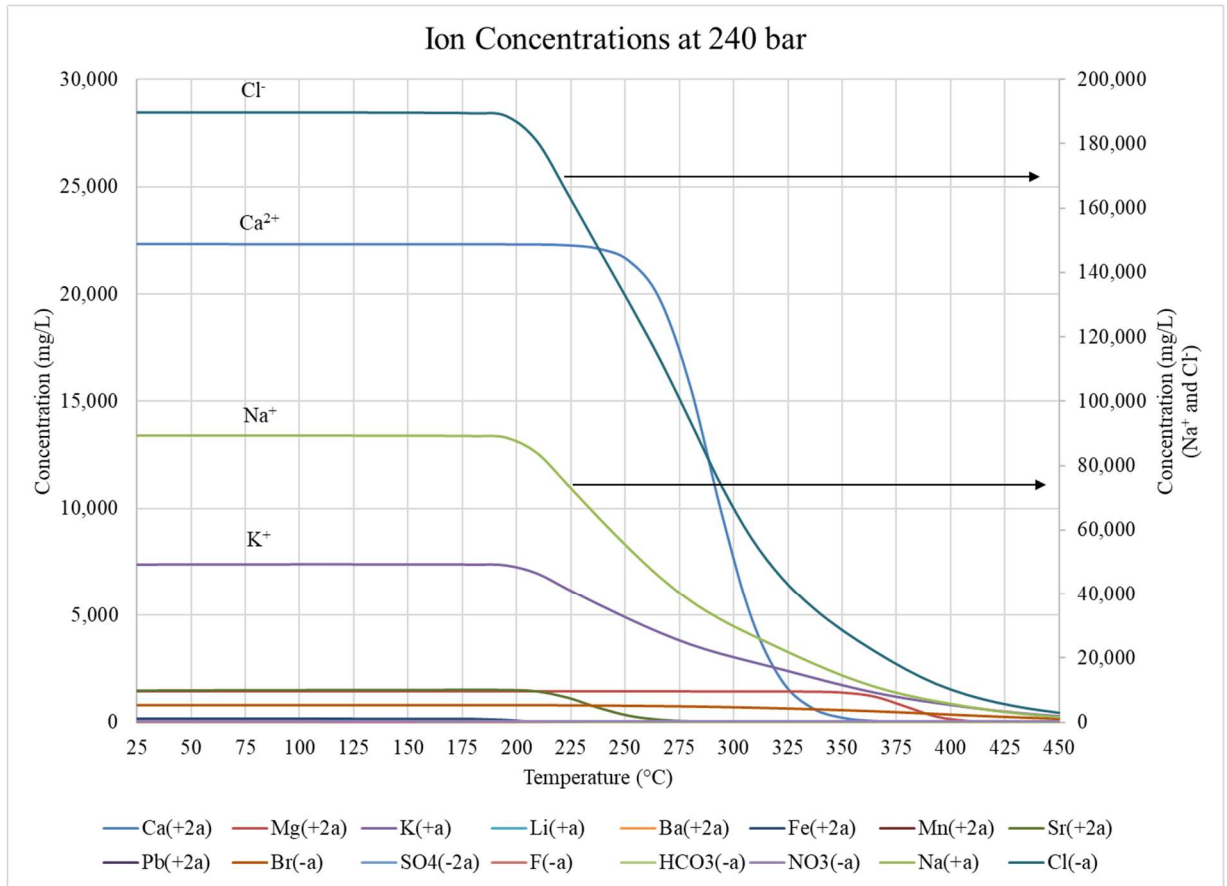


**Figure 4.2:** HSC simulation output for produced water ion concentration at 240 bar.

The predicted ion concentration for the sample of produced water seen in **Figure 4.2** shows no desalination occurring until approximately 200 °C. The chloride, sodium, and potassium ions all begin precipitating out of solution at approximately 200 °C while the calcium ion begins to precipitate around 250 °C. A closer look at the less prevalent ions in solution reveals similar desalination trends, albeit at different temperatures, as seen in **Figure 4.3**.

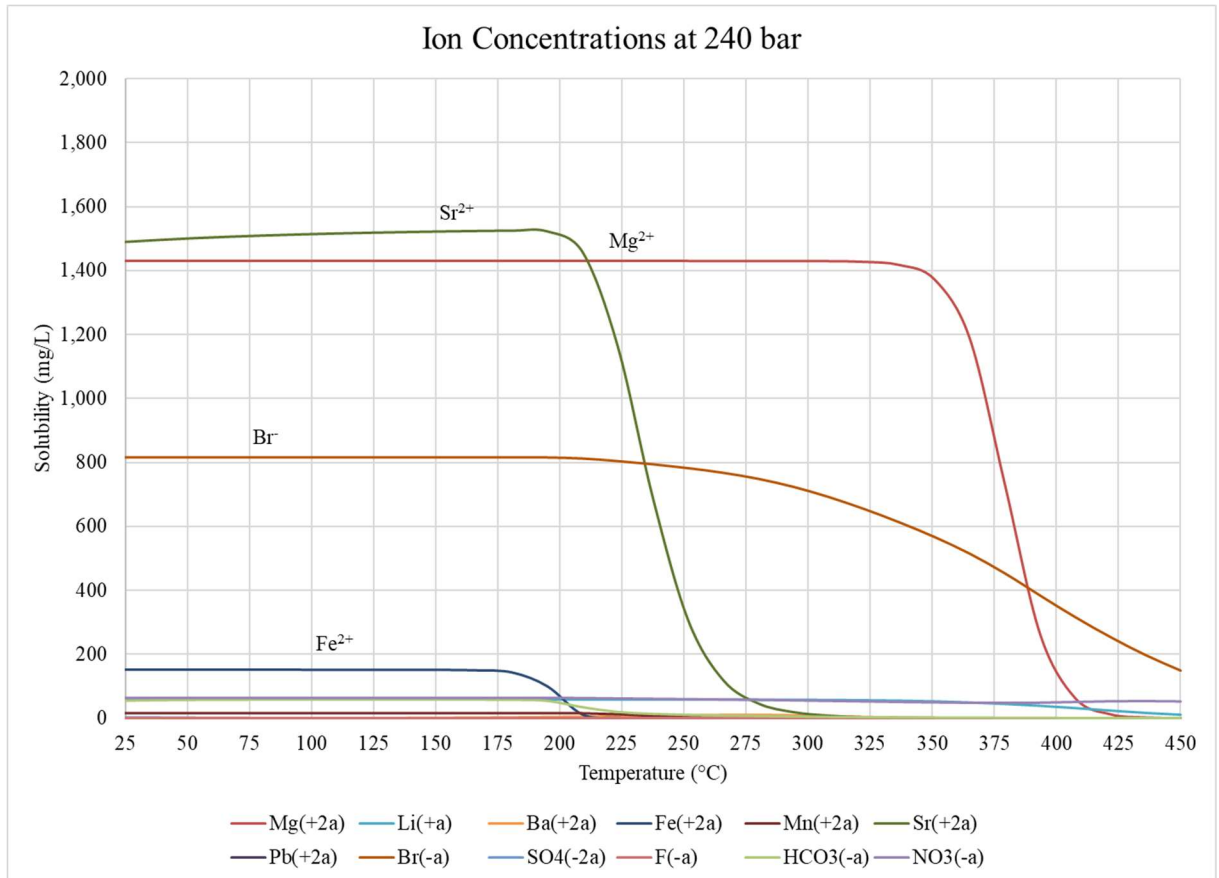


**Figure 4.3:** HSC-predicted ion concentrations for less prevalent ions in produced water.

**Figure 4.3** shows a rapid desalination of  $\text{Sr}^{2+}$  occurring at 200 °C until approximately 300 °C. Magnesium follows a similar trend as strontium from 350-425 °C. Bromide exhibits a gradual desalination starting at approximately 225 °C and precipitating nearly 80% of its dissolved composition upon reaching 450 °C.

It is important to pay special attention to the scale used for each concentration chart as the less prevalent ions are in solution below 2,000 mg/L whereas sodium, calcium and chloride are all well above 10,000 mg/L. Though the less prevalent ions are in significantly lower concentrations than the more prevalent ions, their presence can still cause problems with scaling as they precipitate out of solution.

#### **4.2.4 Discussion**

The results of the predicted concentrations for both a pure NaCl-H<sub>2</sub>O solution as well as produced water exhibit trends that are of concern regarding their accuracy. There is no discernable change in concentration behavior across phase boundaries as would be expected around the critical point of the solution. Literature shows that salt solubility decreases rapidly across the critical line of the solution however this isn't reflected in the HSC-produced results [3].

One explanation for the lack of concentration behavior change around the critical point of water is a lack of available data in this region which forces the program to extrapolate results. As was discussed throughout the literature review in Chapter 3 of this thesis, extrapolation in this region yields inaccurate results, especially across phase boundaries. This very issue is something the Driesner model aimed to eliminate by segmenting phase boundaries into multiple formulas to better represent solubility behavior across them.

Further evaluation of the HSC concentration results vs other models will better explain discrepancies and shortfalls in the model predictions.

#### **4.3 PHREEQC Species Distribution Modeling**

The geochemical modeling program PHREEQC was utilized as a prediction mechanism for the concentration of inorganic salts in produced water. In order to evaluate the validity of the PHREEQC program, a binary NaCl-H<sub>2</sub>O solution was modeled at 240 bar across a wide temperature range (25-450 °C) and its results were compared to other models as well as experimental data.

Commonly employed in hydrogeochemical environments, such as those experienced in the oil and gas industry, PHREEQC offers a wide range of applications from concentration determination to mass transport problems. A common use of PHREEQC is evaluation of potential scale formation across process conditions, a common concern in the drilling and operation of well sites. Employment of this program to predict the concentration of various ions which constitute produced water could be of great value to engineers designing desalination technologies if this model proves to be valid.

#### **4.3.1 Theory**

PHREEQC (pH-REdox-Equilibrium-C code) is a computer program that simulates chemical reactions as well as species transport in water, industrial, and experimental processes. PHREEQC determines concentration of species in different phases to achieve equilibrium as a function of specified reversible/irreversible geochemical reactions [4]. A numerical model was developed to achieve the equilibrium composition across phases utilizing available data sets.<sup>6</sup>

The distribution of species and their concentrations across phases is determined using a combination of ion-association and Pitzer/SIT (specific ion interaction theory) equations which account for the solutions non-idealities. These equations utilize parameters from experimentally-derived datasets for species across a large range of temperatures and pressures. In order to achieve equilibrium throughout phases, PHREEQC alters the concentration of species in each phase until the equilibrium criteria

---

<sup>6</sup> The complete numerical model is available in the referenced PHREEQC manual (2013).

is met. This is how concentration is determined as temperature is varied across the desired range.

#### 4.3.2 Methods

Taking advantage of the “Trembly and Ogden assumption”<sup>7</sup>, a 10 wt% NaCl-H<sub>2</sub>O brine was chosen as the solution for initial simulation. The solution was modeled across the temperature range 25-450 °C and held constant at 240 bar throughout the simulation. The pressure was held constant throughout the simulation as the assumption was made (and supported by the HSC results) that the variance in pressure from 200-240 bar would yield insignificant concentration changes. The simulation results were then used for comparison with other models as well as experimental data to determine the most accurate model at these high temperatures and pressures.

Once the 10 wt% NaCl-H<sub>2</sub>O brine was modeled across the desired temperature range at 240 bar and a PHREEQC-predicted concentration curve was produced for comparison with other models, a produced water sample was modeled across the temperature range 25-450 °C and 240 bar. In order to simulate a produced water solution across the desired temperature range to determine concentration of common ions present in produced water, a sample of produced water was acquired.

A sample of produced water from the Bakken formation in western North Dakota was analyzed using ICP-MS and IC by Standard Laboratories in Illinois to determine the complete ion composition. The composition of this solution was used as the simulation input for PHREEQC in order to model the concentration of different ions at 240 bar as

---

<sup>7</sup> This assumption states that a multicomponent brine can be accurately represented as a binary NaCl-H<sub>2</sub>O solution as long as the primary constituent of the brine is NaCl.

temperature was varied from 25 °C – 450 °C. The input composition for this simulation can be found in **Table 4.1**.

### 4.3.3 Results

The simulation results produced by PHREEQC for both a 10 wt% NaCl-H<sub>2</sub>O solution and a sample of produced water across the temperature range 25-450 °C and 240 bar were plotted for evaluation. The raw results from both simulations can be found in Appendix A. The results from the 10 wt% NaCl-H<sub>2</sub>O solution simulation can be seen in **Figure 4.4**.<sup>8</sup>

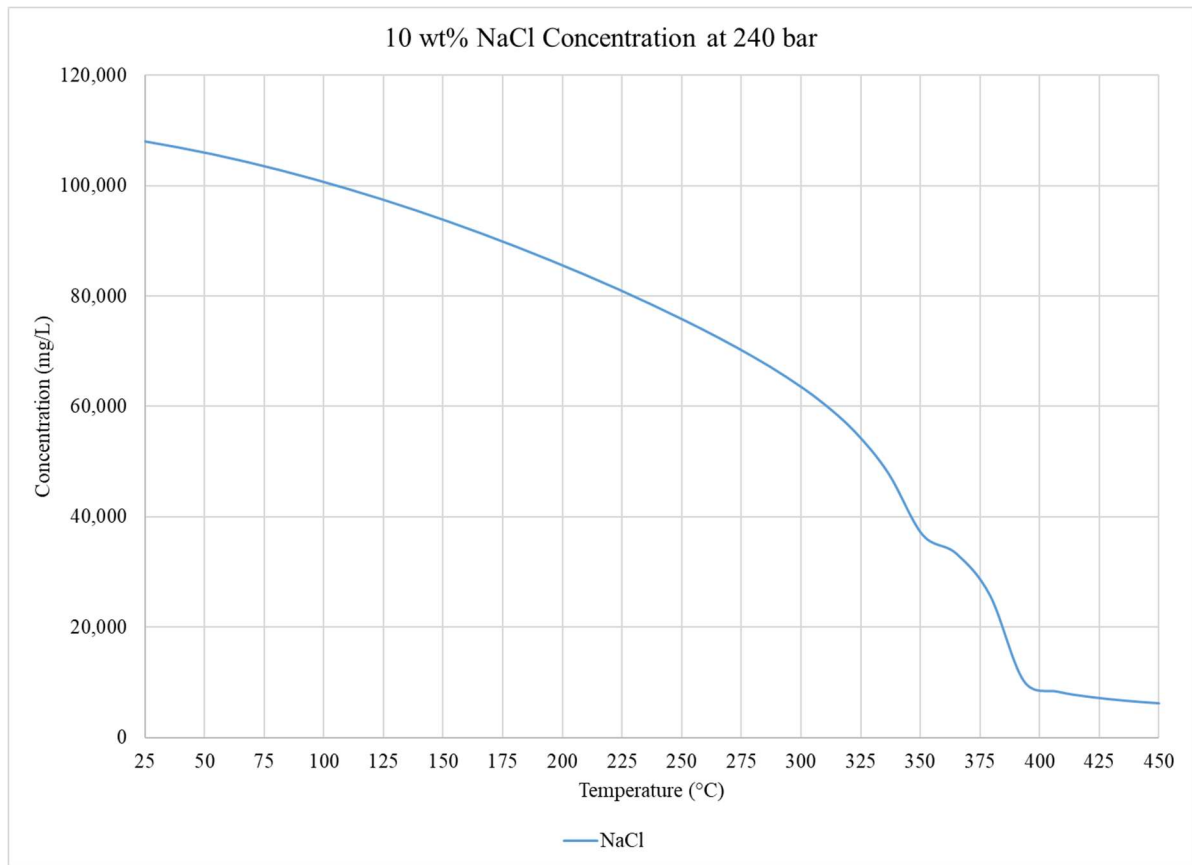


**Figure 4.4:** PHREEQC-predicted NaCl concentration at 240 bar.

<sup>8</sup> The solution modeled was an approximately 14 wt% solution and the simulated concentrations were adjusted by a factor of 0.78 to achieve the same initial concentration as used in the other models (HSC, AspenPlus, and SoWat) for comparison.

The PHREEQC-predicted NaCl concentration curve seen in **Figure 4.4** shows a gradual desalination trend which increases as the solution approaches the critical temperature for the solution (approximately 385 °C). The concentration of NaCl decreases by approximately 70% from its starting concentration once the solution temperature is brought to 365 °C. This desalination results in an approximately 1.5% concentration decrease per 10 °C solution temperature increase from 25-300 °C. Of course it is readily apparent that this desalination is not linear, especially as temperature exceeds 300 °C thus this 1.5% concentration decrease per 10 °C “rule” should not be applied past 300 °C.

The rapid desalination that occurs across the critical phase boundary is drastic as the concentration of NaCl decreases by approximately 20% from the initial concentration (approximately 100,000 mg/L) in that region (365-394 °C) alone. A small “pause” in desalination can be seen at approximately 350-360 °C. This is likely due to the model extrapolating between datasets for NaCl as there is no underlying physical explanation otherwise. The desalination behavior that is exhibited by a NaCl-H<sub>2</sub>O solution is also evident in the simulation of a sample of produced water as seen in **Figure 4.5**.



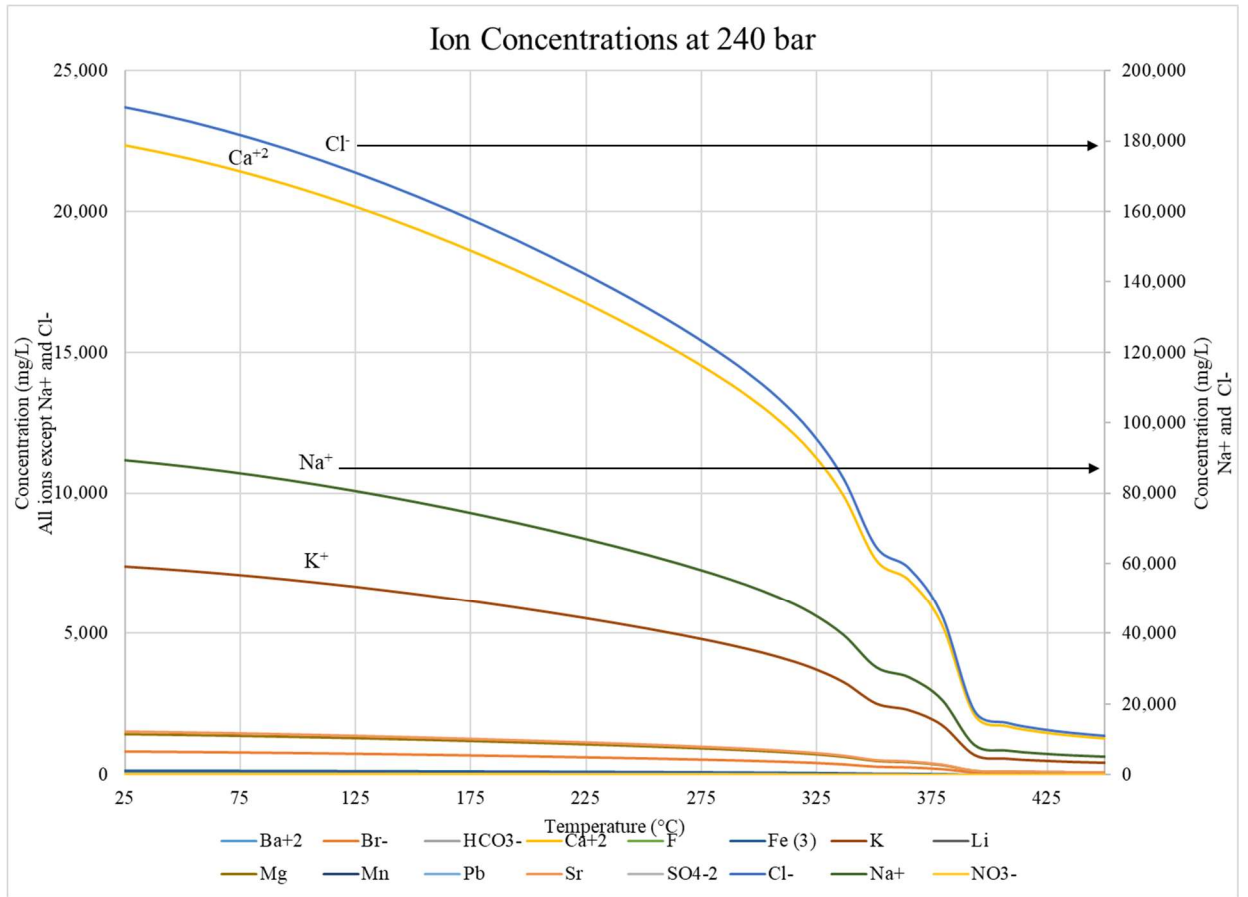


**Figure 4.5:** PHREEQC simulation output for produced water ion concentration at 240 bar

It can be seen in **Figure 4.5** that PHREEQC predicts all ions experience reduced concentration as temperature is increased. As temperature nears the critical point of this solution (approximately 390 °C) the concentration of Cl<sup>-</sup>, Ca<sup>+2</sup>, Na<sup>+</sup>, and K<sup>+</sup> decreases rapidly as literature suggests will occur.

The gradual decrease in concentration for chloride, calcium, sodium, and potassium in the subcritical region (up to 365 °C) results in approximately 70% desalination from their initial concentrations. This desalination occurs across an approximately 350 °C temperature change. The desalination that occurs across the

critical boundary of the solution is much more drastic considering the small temperature window the desalination occurs through.

Nearly 91% of the chloride, calcium, sodium, and potassium ions have precipitated out of solution once the solution passes its critical boundary (393.33 °C). This means that approximately 20% of the chloride, calcium, sodium, and potassium drop out of solution across a 28 °C temperature change. Similar behavior can be seen to exist for the less prevalent ions in solution as well.

As was seen in the NaCl-H<sub>2</sub>O simulation results in **Figure 4.4**, is a small “pause” in desalination which occurs from approximately 350-360 °C for calcium, chloride, sodium, and potassium that can be seen in **Figure 4.5** which does not have a behavioral explanation, thus it is likely a result of the model extrapolating between known datasets. The lack of available data across small temperature increments for multiple ions, especially near the critical point, leads to unexpected trends that don't match conventional wisdom.

#### **4.3.4 Discussion**

Upon evaluation of the PHREEQC-predicted concentrations of both a 10 wt% NaCl-H<sub>2</sub>O solution and a sample of produced water across a large temperature range at 240 bar, the model predicted a concentration decrease as temperature was increased. The gradual decrease experienced in concentration for all ions increased as important phase boundaries were reached. The model appeared to take the critical phase boundary into account when predicting concentration as there was a drastic decrease in concentration near/across the critical point of the solution as seen in both **Figures 4.4** and **4.5** which

agrees with literature [3]. This concentration decrease coincides with a decrease in solution density, as literature would suggest.

A drawback of this model is the “pause” in desalination which occurs at 350-360 °C for all ions with no physical explanation beyond model error. This likely is due to inconsistencies between datasets which the model draws from for important species-specific parameters. The model draws primarily from a *pitzer.dat* dataset for its aqueous model which provides reasonable results across a wide range of conditions however the model is limited in its species data as well as around the critical point. The lack of data around the critical point manifests itself in unrealistic concentration results such as the one experienced at 350-360 °C.

Notwithstanding the small section of unrealistic results experienced over a small 10 °C temperature range just below the critical temperature of water, the PHREEQC model appears to deliver reasonable concentration predictions across a wide temperature range at 240 bar. This is due to the part-empirical nature of the model which derives values for key equilibrium determinations from validated datasets across a wide range of conditions and species. This model will be further evaluated against other models to determine which model is the most valid across these process conditions.

#### **4.4 AspenPlus Electrolyte Modeling**

The simulation program AspenPlus was utilized to predict the concentration behavior of a NaCl-H<sub>2</sub>O solution as well as a sample produced water solution.

Commonly employed by process engineers for a wide variety of simulations, AspenPlus is used for anything from process separation schemes to reactor design to process

economics. Employing AspenPlus to accurately predict the concentration of multi-component process streams such as produced water would be of great value to engineers as AspenPlus has many other applications which could be utilized for other design projects.

#### 4.4.1 Theory

The electrolyte simulation module in AspenPlus has the ability to model multi-component process streams across a wide range of conditions and determine the concentration of the species in those streams. The electrolyte simulation module uses the ELENRTL property method in order to determine species concentrations at different process conditions.

The ELECNRTL property method is a robust property method based on correlations derived from experimental data which functions within the “Activity Coefficient Model” in AspenPlus. The ELECNRTL method is more robust than the Pitzer property method as it is able to handle multi-component streams with high concentrations with more accuracy [5].

The Activity Coefficient Model in AspenPlus uses ELECNRTL for the property method and the Redlich-Kwong equation of state for the vapor phase. The activity coefficient model considers an ideal solution in which mole fraction for species is directly proportional to fugacity of that component. This can be seen in equation 4.2.

$$f_i^l = x_i f_i^{*,l} \quad (4.2) [5]$$

Where:

- $x_i = \text{species mole fraction}$
- $f_i^{*,l} = \text{liquid component fugacity}$

This equation assumes an ideal solution, i.e. one where dissolved species are identical in size, character, and are randomly distributed. The solutions we are modeling are not ideal and thus this must be accounted for in our approach. This non-ideality is accounted for using an activity coefficient as seen in equation 4.3.

$$f_i^l = x_i \gamma_i f_i^{*,l} \quad (4.3) [5]$$

Where:

- $\gamma_i = \text{activity coefficient for species } i$

An ideal solution is one where  $\gamma_i = 1$ , aka “unity”. The more a solution deviates from unity the more non-ideal the solution is. Using this approach, the vapor liquid equilibrium for a solution is modeled using equation 4.4.

$$\varphi_i^v \gamma_i p = x_i \gamma_i f_i^{*,l} \quad (4.4) [5]$$

Where:

- $\varphi_i^v = \text{vapor phase fugacity coefficient (from Redlich – Kwong EOS)}$
- $p = \text{pressure}$

Using equations 4.2-4 and the necessary species parameters available from AspenPlus’s database, the concentration for various species in solution at different process conditions can be determined.<sup>9</sup> This approach does have a few shortfalls however.

This model is able to accurately predict vapor phase properties up to medium pressures. This pressure range is subjective and may be cause for inaccuracy as the system pressures being utilized for these simulations are at 240 bar which may be

---

<sup>9</sup> The complete model equations utilized can be seen in greater detail in the referenced Aspen Manual (2006).

considered well above “medium pressure”. The datasets that AspenPlus utilizes are incomplete and lack important species parameters at high temperatures and pressures which will manifest in inaccurate results at these extreme conditions.

#### **4.4.2 Methods**

Once again taking advantage of the “Trembly and Ogden assumption”, a 10 wt% NaCl-H<sub>2</sub>O brine was chosen as the solution for initial simulation. The solution was modeled across the temperature range 25-450 °C and held constant at 240 bar throughout the simulation. The pressure was held constant throughout the simulation as the assumption was made (and supported by the HSC results) that the variance in pressure from 200-240 bar would yield insignificant concentration changes. The simulation results were then used for comparison with other models as well as experimental data to determine the most accurate model at these high temperatures and pressures.

Once the 10 wt% NaCl-H<sub>2</sub>O brine was modeled across the desired temperature range at 240 bar and an AspenPlus-predicted concentration curve was produced for comparison with other models, a produced water sample was modeled across the temperature range 25-450 °C and 240 bar. In order to simulate a produced water solution across the desired temperature range to determine concentration of common ions present in produced water, a sample of produced water from the Bakken formation in western North Dakota was acquired.

This sample was analyzed using ICP-MS and IC by Standard Laboratories in Illinois to determine the complete ion composition. The composition of this solution was used as the simulation input for AspenPlus in order to model the concentration of different ions at 240 bar as temperature was varied from 25 °C – 450 °C. The input

composition for this simulation can be found in **Table 4.1**. The raw data produced by these simulations can be found in Appendix A.

#### 4.4.3 Results

The results of the AspenPlus concentration simulations were logged into Microsoft excel and plotted for evaluation. The predicted concentration results of the 10 wt% NaCl-H<sub>2</sub>O solution can be seen in **Figure 4.6**.

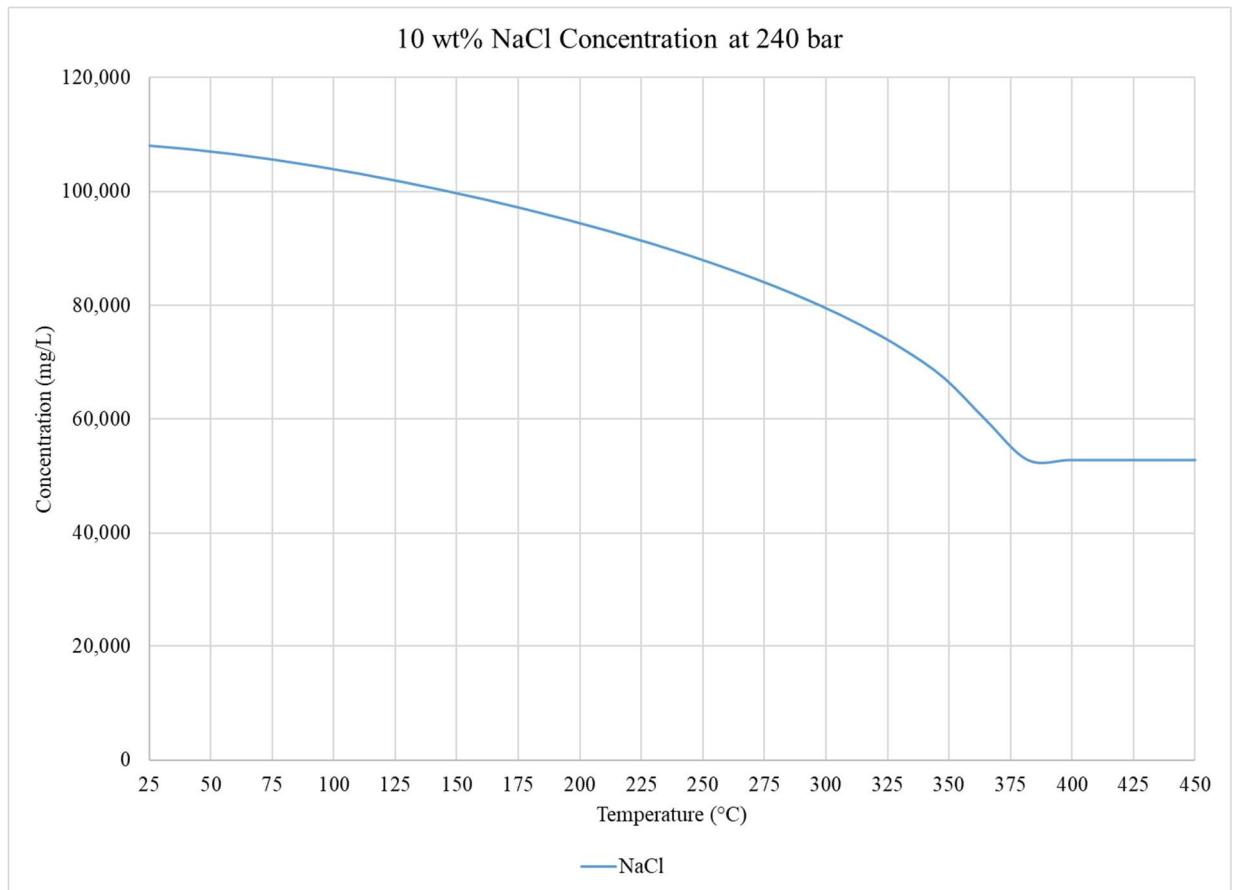


**Figure 4.6:** AspenPlus generated NaCl concentration as a function of temperature.

As seen in **Figure 4.6**, the predicted concentration of NaCl gradually decreases as temperature is increased from 25-375 °C. Across that temperature range, the predicted concentration decreases approximately 45% from the initial concentration. As the critical

point is reached for the solution, approximately 385 °C, the predicted concentration becomes stagnant at the last calculated concentration, approximately 50,000 mg/L.

The stagnation trend for concentration seen at these conditions is clearly a break from what is expected based on literature and experimental results [3,6]. The expected concentration trend as the solution crosses the critical boundary is a rapid decrease in concentration towards zero. This however, is not the case for this simulation.

This stagnant trend is likely caused by a lack of data in this region which the model uses to determine its predicted results and thus the model breaks down and is unable to accurately extrapolate further. Thus, the last known value which the model calculates with confidence is chosen for the rest of the simulation conditions which it doesn't have data for. The same behavior can be seen for a produced water sample simulation as seen in **Figure 4.7**.



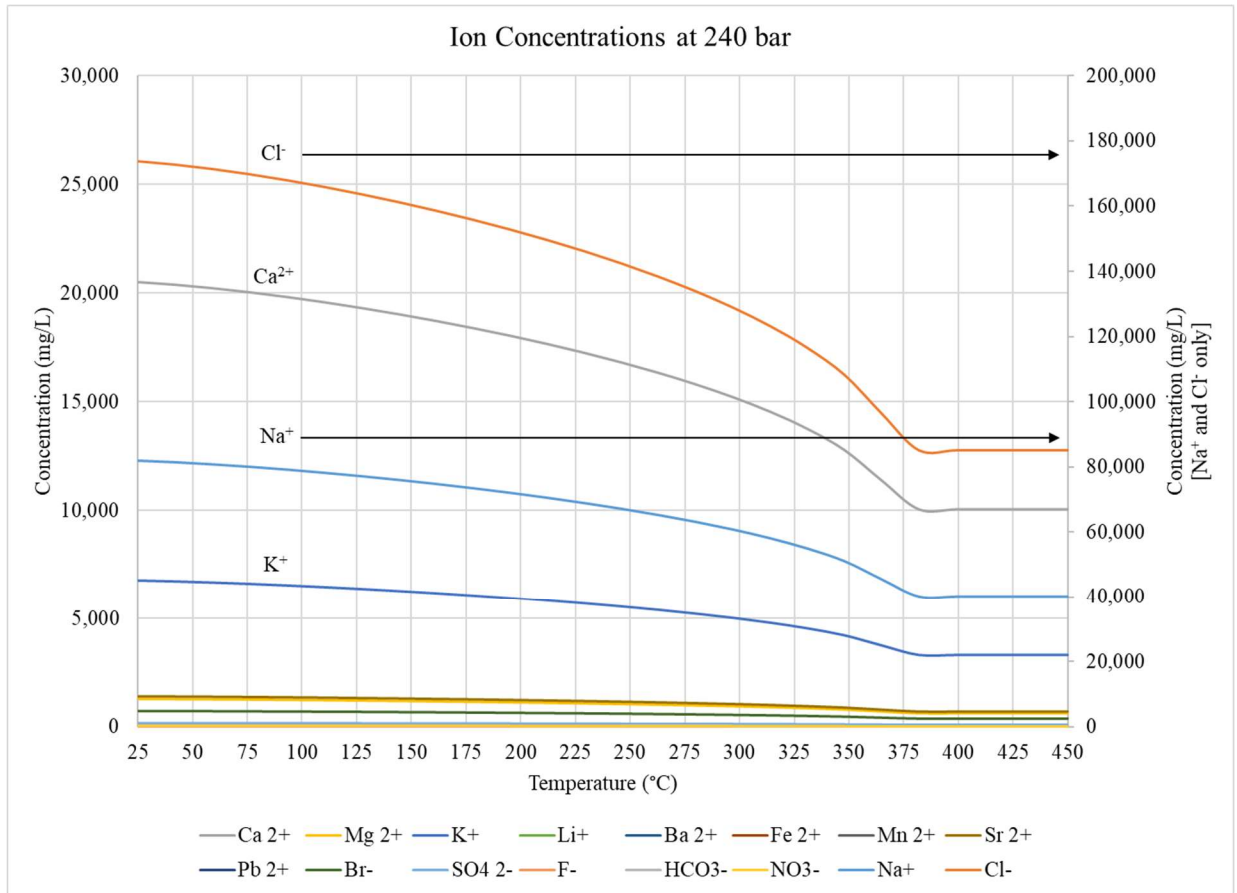


**Figure 4.7:** AspenPlus generated ion concentration for a sample of produced water as a function of temperature

The AspenPlus-predicted concentration of high-prevalence ions in produced water can be seen in **Figure 4.7**. As seen with the 10 wt% NaCl-H<sub>2</sub>O simulation across the same process conditions, the concentration for all ions gradually decreases, as temperature is increased in the system. The concentration for all ions begins to decrease at a higher rate as the temperature in the system nears the critical point of the solution. As the critical point of the solution is reached, approximately 385 °C, the concentration trend becomes stagnant and remains that way through the remainder of the simulation.

As was the case for the 10 wt% NaCl-H<sub>2</sub>O solution simulation, the model no longer has the necessary data to produce concentration results thus the model breaks down and uses its last known calculated value as a result for the remainder of the

simulation. When a closer look is taken at the less prevalent ions present in produced water, this same trend is experienced. This can be seen in **Figure 4.8**.

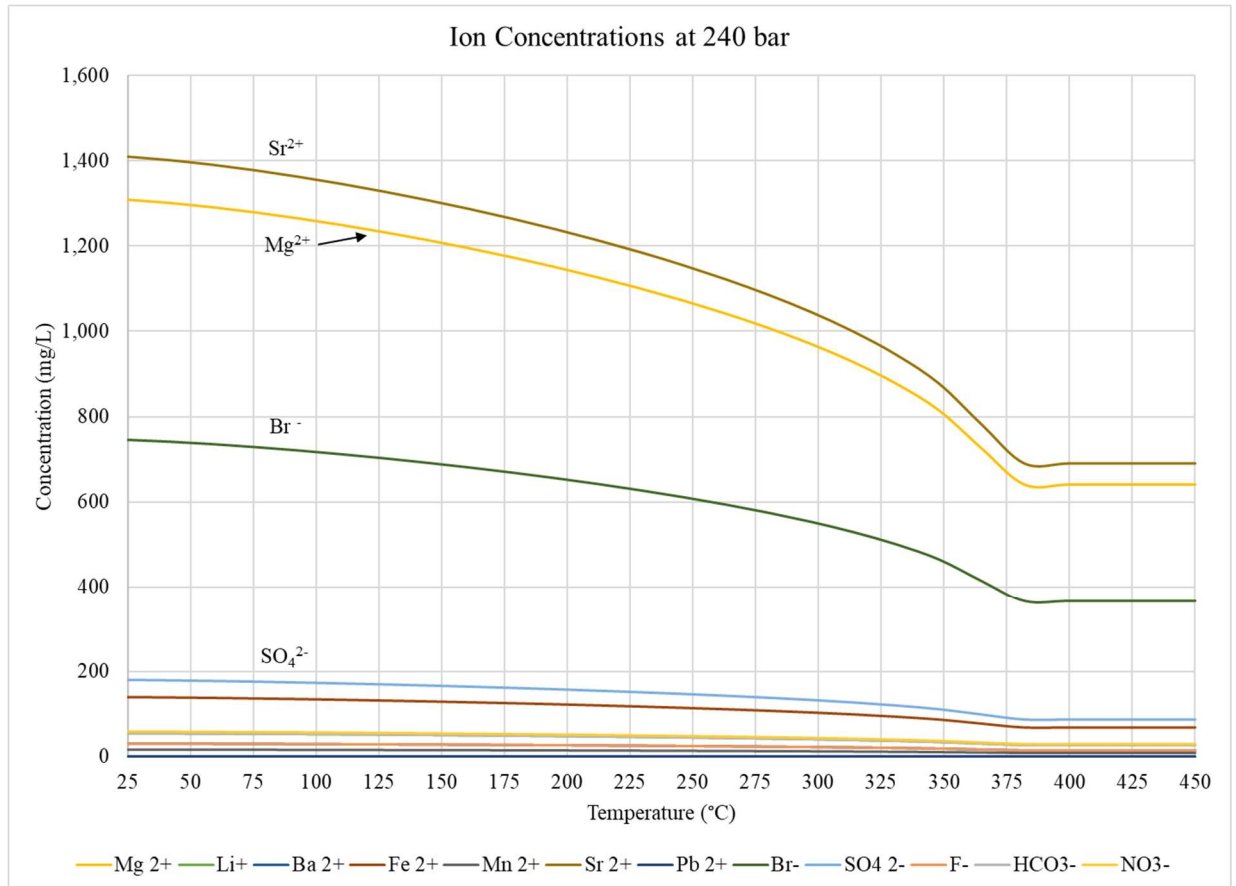


**Figure 4.8:** AspenPlus generated ion concentrations (less prevalent ions) for a sample of produced water as a function of temperature at 240 bar.

The less prevalent ions present in produced water exhibit nearly identical concentration behavior as the more prevalent ions ( $\text{Ca}^{2+}$ ,  $\text{Na}^+$ ,  $\text{Cl}^-$ ,  $\text{K}^+$ ) do. It is important to pay special attention to the quantity that these ions are in solution as they are all well below 2,000 mg/L whereas others being examined in this work ( $\text{Ca}^{2+}$ ,  $\text{Na}^+$ ,  $\text{Cl}^-$ ,  $\text{K}^+$ ) are well above 10,000 mg/L in concentration. However, though these species are present in much smaller quantities than others such as  $\text{Na}^+$  and  $\text{Cl}^-$ , their concentrations are still of high importance to oil and gas companies. These less prevalent ions, strontium and barium especially, can form thick coats of scale which is detrimental to process piping.

Thus, understanding their concentration behavior throughout these process conditions is vital so effective treatment options can be utilized to ensure their removal. However, once again the AspenPlus model's lack of data to use for these species at these conditions proves to be detrimental to the model's ability to accurately predict ion concentration across the critical boundary.

#### **4.4.4 Discussion**

The predicted concentrations of dissolved ions in both the 10 wt% NaCl-H<sub>2</sub>O solution and the produced water sample are reasonable until the near-critical region of water. The predicted concentration of NaCl in the 10 wt% solution decreased with temperature at an increasing rate upon reaching the near-critical point of the solution. This trend coincided with density decreases experienced by the process fluid.

Once at the near-critical point of the solution, the model no longer was able to produce results for concentration as the datasets being utilized for concentration calculations did not have data at these conditions. The lack of available species parameters at these conditions forced the model to use the last-known value for concentration as its generated result from the near-critical point through the remainder of the simulation (450 °C). This yielded unreasonable and inaccurate concentration results from approximately 365-450 °C.

The inability of the AspenPlus model to predict concentrations of dissolved ions past the critical point of the solution is a substantial problem when trying to develop desalination technologies which operate at high temperatures and pressures. This modeling program is not applicable at these conditions and thus cannot be utilized for process design if the conditions are near/above the process solution's critical point.

Though the model cannot predict concentrations near/above the solution's critical point, the model did produce reasonable concentration results from 25-365 °C. This is despite being at pressures commonly considered to be above "medium range" which is surprising as the underlying vapor phase property equations are considered to be no longer accurate [5]. Though these results appear reasonable, they may not be as accurate as other models. The accuracy of these results will be further evaluated once compared to other model simulations of the same 10 wt% NaCl-H<sub>2</sub>O solution.

Despite the reasonable concentration results produced by the AspenPlus model from 25-365 °C, the model proved to be unable to predict species concentrations beyond 365 °C. Even if the model is able to produce accurate results at lower temperatures, it is unable to operate as a stand-alone model if being utilized to predict ion concentrations for a supercritical water desalination system.

#### **4.5 SoWat Empirical NaCl-H<sub>2</sub>O Property Model**

The empirically-derived NaCl-H<sub>2</sub>O solution property program SoWat was employed as a tool to simulate the concentration of a 10 wt% NaCl-H<sub>2</sub>O solution from 25-450 °C at 240 bar. The program was developed using the empirical model developed by Thomas Driesner and written in C-code which operates on the DOS system [7,8]. The ability to employ this model to accurately predict produced water concentrations along with other solution properties (density, specific heat, enthalpy) would be an excellent resource for engineers working to develop a supercritical desalination technology.

##### **4.5.1 Theory**

The program SoWat utilizes the empirically-derived Driesner model which simulates a binary NaCl-H<sub>2</sub>O solution across a large temperature, pressure, and

composition range.<sup>10</sup> The model was produced to be valid from 0-1000 °C, 1-5000 bar, and compositions from 0-1  $X_{\text{NaCl}}$ . The large temperature, pressure, and composition range which this model was developed to be valid across makes it an excellent candidate to be utilized in produced water concentration simulation as well as other important solution properties, assuming the Trembly and Ogden assumption is employed and valid.

#### 4.5.2 Methods

The Trembly and Ogden assumption is critical in employing this modeling program towards produced water concentration simulation. Without making this assumption, this model would not be applicable as it is derived for only a binary NaCl-H<sub>2</sub>O solution. However, employing this assumption allows this model to be utilized in produced water concentration simulation as produced water's primary constituent is NaCl (by far).<sup>11</sup>

A 10 wt% solution was modeled across the temperature range 25-450 °C and held constant at 240 bar throughout the simulation. The pressure was held constant throughout the simulation as the assumption was made (and supported by the HSC results) that the variance in pressure from 200-240 bar would yield insignificant concentration changes. The simulation results were then used for comparison with other models as well as experimental data to determine the most accurate model at these high temperatures and pressures. This model served as a benchmark for concentration comparison with the other models as it was validated for simulation of a binary NaCl-

---

<sup>10</sup> The model theory is discussed in full in the referenced Driesner papers "Part I and II (2007)" as well as in Chapter 3 of this thesis.

<sup>11</sup> This is verified by the multiple produced water samples which have been sourced from the Bakken Formation in western North Dakota by this writer and analyzed by Standard Laboratories in Illinois.

H<sub>2</sub>O solution at these process conditions. A detailed comparison of experimental data to the SoWat model derived by Driesner can be found in section 3.3 of this thesis. This section shows the ability of this model to accurately predict salt concentration over a wide range of process conditions, including those being used in this work.

The simulation yielded the amount of phases present at each set of process conditions (temperature, pressure, and initial solution NaCl concentration) as well as the density, molar volume, heat capacity, and composition ( $X_{\text{NaCl}}$ ) for each phase present. The results of the simulation were then tabulated into Microsoft Excel and plotted for evaluation. The raw data from these simulations can be found in Appendix A.

#### **4.5.3 Results**

The SoWat predicted solution property results for a 10 wt% NaCl-H<sub>2</sub>O solution was reduced in Microsoft Excel and plotted for evaluation. The SoWat-predicted concentration for this solution can be seen in **Figure 4.9**.

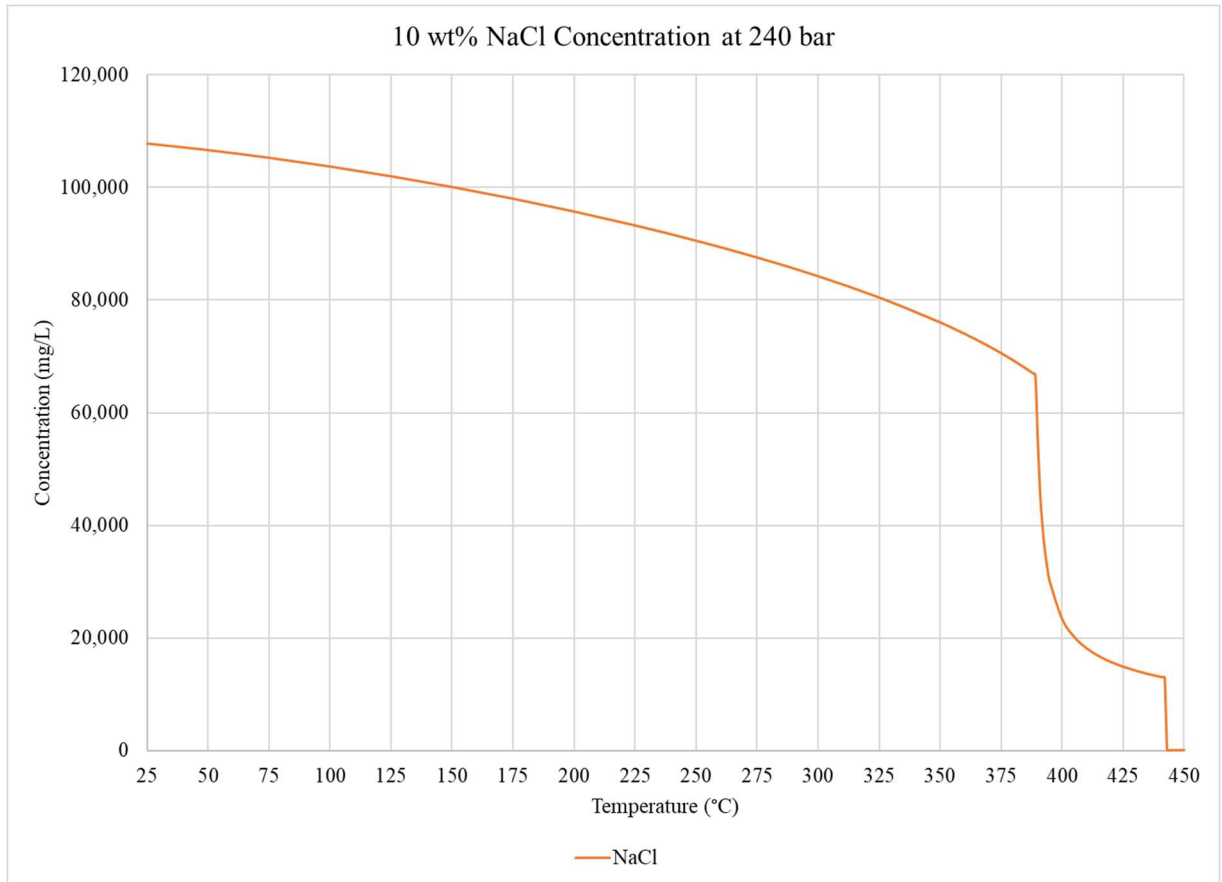


**Figure 4.9:** Driesner model-predicted NaCl concentration at 240 bar

It can be seen in **Figure 4.9** that concentration decreases gradually as temperature is increased until approximately 390 °C, where the critical point of the solution is determined to be. Once this temperature is surpassed, the concentration of NaCl decreases drastically. The concentration of NaCl decreases approximately 38% across the temperature range 25-389 °C from the initial concentration. Across the temperature range 389-400 °C, NaCl concentration decreases approximately 40% from the initial solution concentration alone.

This rapid decrease in concentration coincides with the phase change experienced at the critical point of the solution. This predicted concentration behavior shows strong

agreement with what is expected based on literature [3,6,7,8]. Another rapid decrease in NaCl concentration can be seen at approximately 440 °C.

The rapid decrease in NaCl concentration at approximately 440 °C results in a roughly 10% decrease from the initial solution concentration. This behavior is the result of another predicted phase change. The predicted concentration along with the predicted phase changes can be seen in **Figure 4.10**.

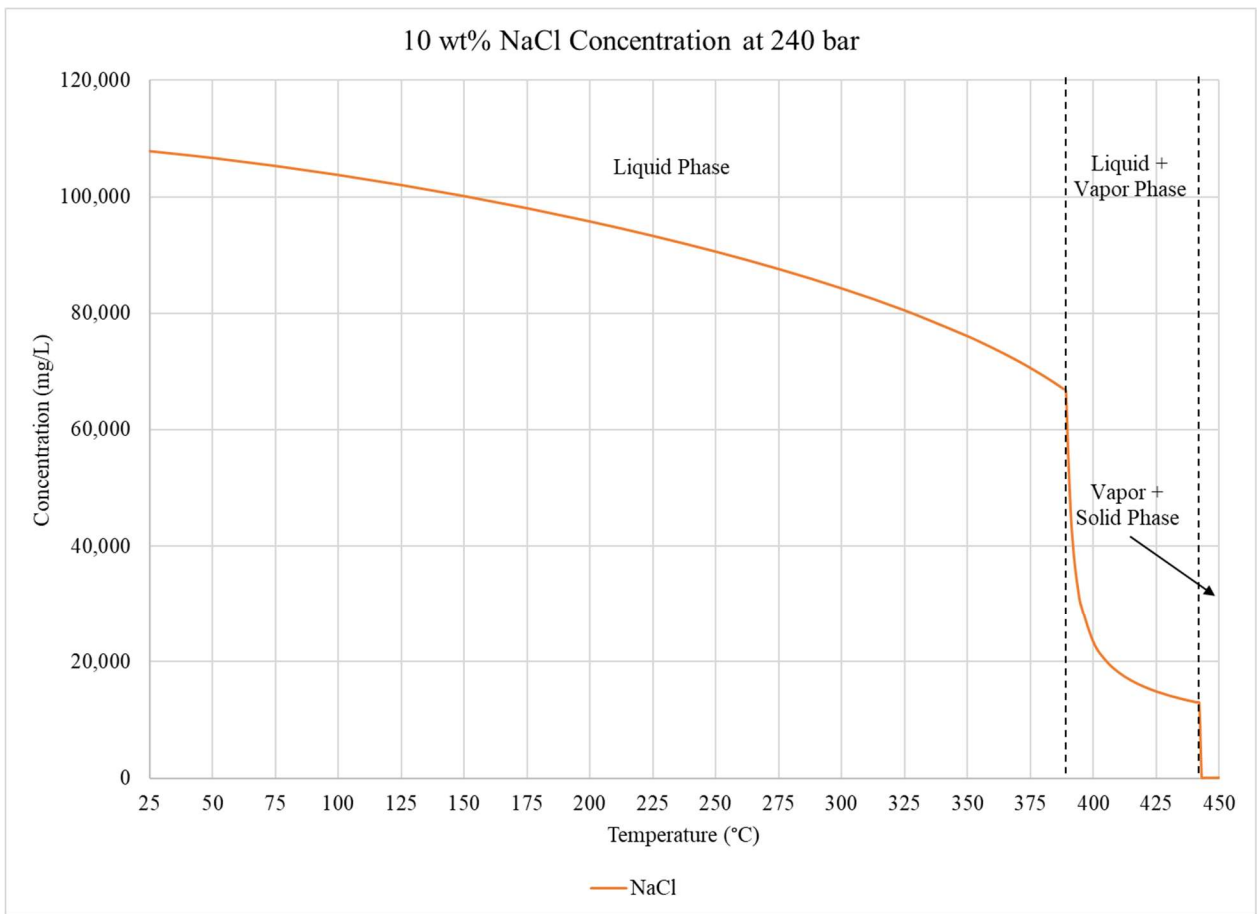


**Figure 4.10:** Driesner model predicted concentration with phases present

The predicted phases present as seen in **Figure 4.10** coincide with key concentration behavior changes. The concentration of NaCl decreases gradually as temperature is increased throughout the liquid phase. Once the model predicted a two-phase system at approximately 390 °C the concentration of NaCl decreased drastically.



NaCl concentration decreased drastically once more as the model predicted a new two-phase system to be in existence, a vapor and a solid phase.

One of the key differences between this model and others being evaluated is the solution properties that the model predicts along with concentration. These solution properties are important to consider when developing an effective desalination system. The SoWat-predicted solution density curve as a function of temperature was constructed using a mass-weighted average of the densities for each present phase. This density curve can be seen in **Figure 4.11**.

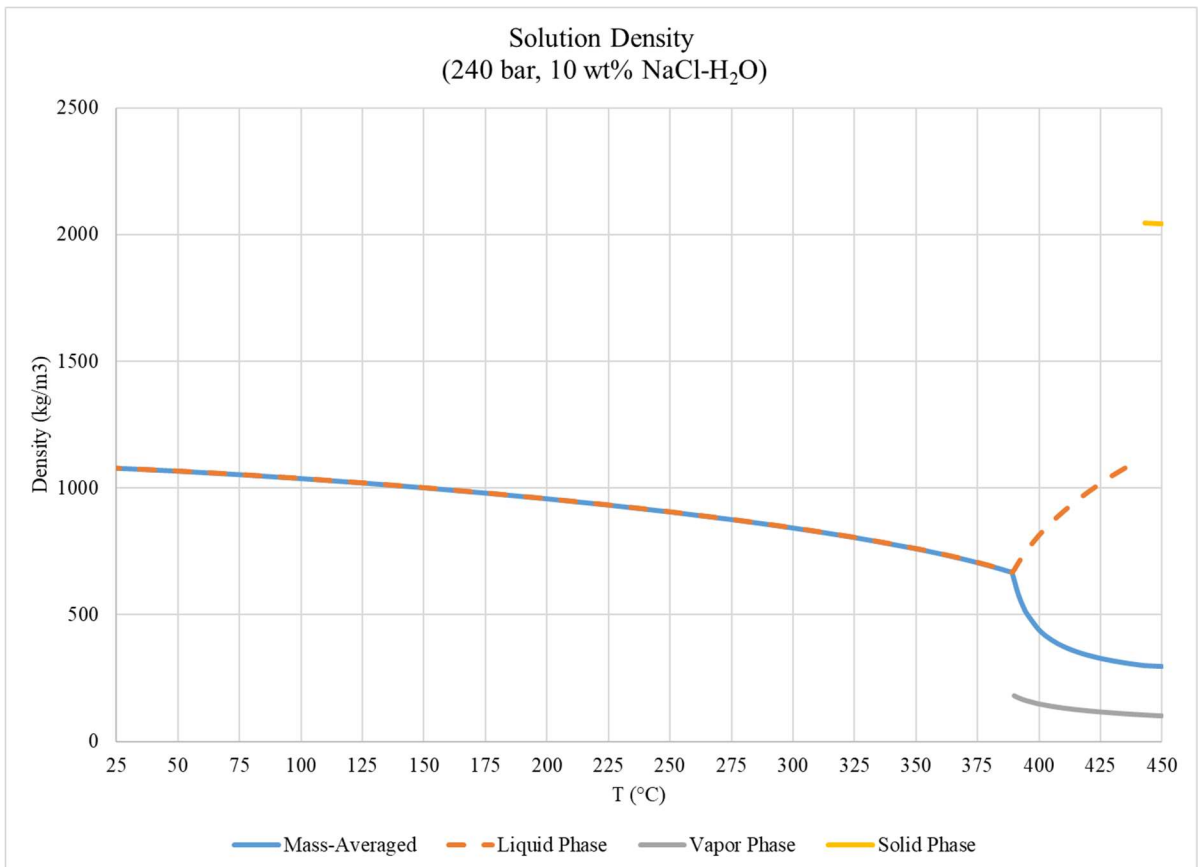


**Figure 4.11:** Driesner model-predicted solution mass averaged density as a function of temperature as well as each phase's predicted density

The Driesner model-predicted density seen in **Figure 4.11** follows the expected trend based on literature [3,7,8]. A slight decrease in solution density can be seen from

25-389 °C until the critical phase boundary is reached at 390 °C. Upon reaching this phase boundary, the density of the solution drops rapidly to approximately 300 kg/m<sup>3</sup>. This decrease in density is substantial compared to the initial starting solution density of 1080 kg/m<sup>3</sup>. The decrease in density towards the vapor-like phase trend at these conditions is due to the vapor-like phase being the largest present phase at these conditions. The specific heat of the solution was also calculated and the mass-averaged specific heat as a function of temperature can be seen in **Figure 4.12**.

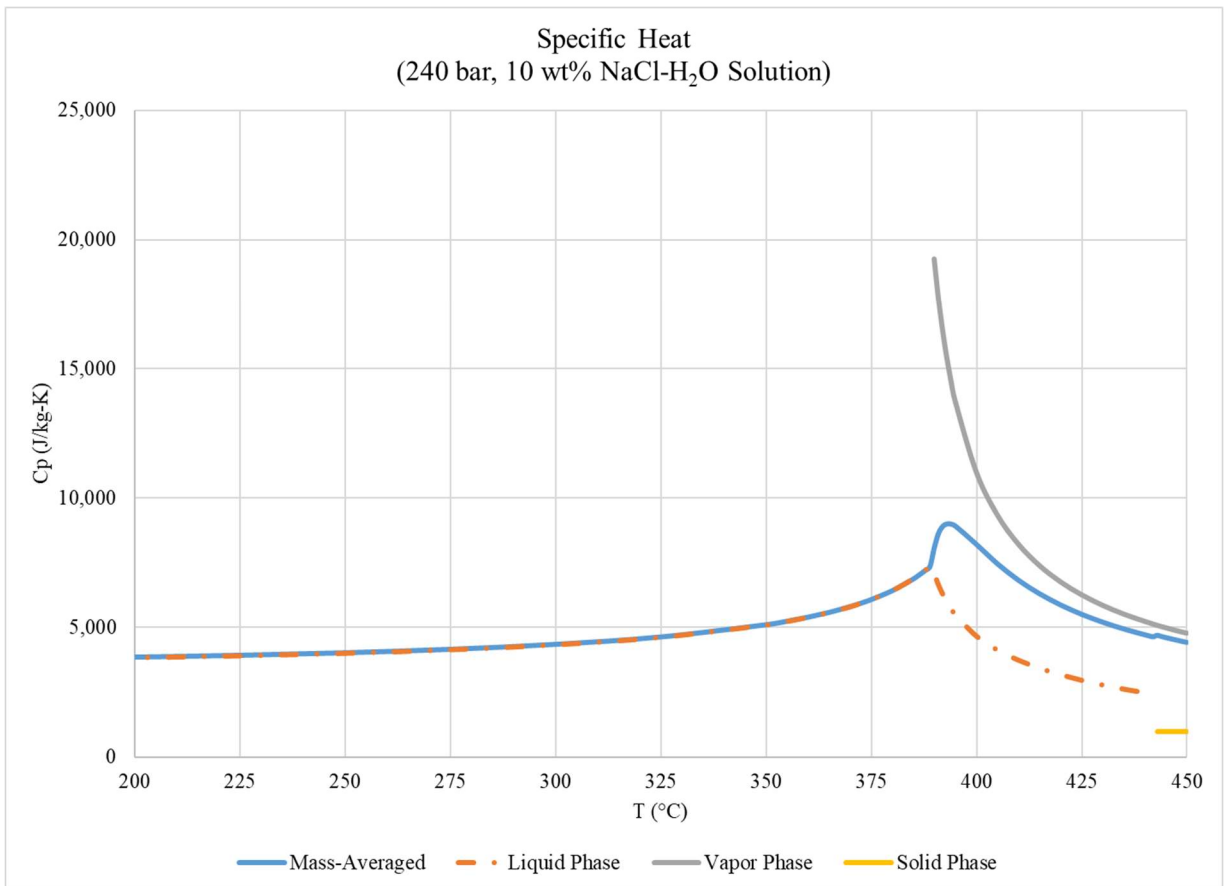


**Figure 4.12:** Driesner model-predicted mass-averaged specific heat as a function of temperature along with each phase's specific heat

The predicted specific heat for the solution as a function of temperature varies significantly across the process temperature range simulated. The most significant change in the predicted solution's specific heat capacity comes as the critical phase is

reached and surpassed at 390 °C. Once this solution reaches 390 °C the specific heat capacity increases to a maximum of 9,000 J/kg-K at 394 °C before decreasing to 4,400 J/kg-K at 450 °C. This trend follows the vapor-like phase trend at these conditions, likely as this phase is the largest present phase at these conditions.

#### **4.5.4 Discussion**

The Driesner model predicts valuable solution properties across the desired process conditions. The model's unique ability to accurately predict which phases are present at each set of process conditions as well as their respective properties (specific heat capacity, density, molar volume, and composition [ $X_{\text{NaCl}}$ ]) increases the value of the model for use by engineers.

The rigorous validation method this model underwent throughout its formulation builds a high confidence level for users that the predicted properties are accurate [7,8]. By utilizing a mass balance for dissolved NaCl, the complete solution phase composition can be determined with relative ease. Once the mass fraction for each phase present in solution is known, total solution properties can be determined on a mass-averaged basis as seen in **Figures 4.9-4.12**.

This model offers great value for engineers as important fluid properties like density as well as heat capacity can be determined with reasonable accuracy. The ability to know the specific heat capacity of a process fluid at desired process conditions allows for improved design characteristics with regards to heat transfer unit operations. The same rationale is applied to density as true residence times in key unit operations are dependent on fluid density.

The only potential drawback of applying this model to produced water simulations is the use of the Trembly and Ogden assumption. This assumption states that multicomponent brines can be accurately modeled as NaCl-H<sub>2</sub>O solutions if the primary constituent in the multicomponent brine is NaCl [1]. The application of this model to multi-component brines such as produced water hinges on the application of the Trembly and Ogden assumption. If this assumption proves to not be as valid as previously thought, this model will not sufficiently predict fluid properties for a multi-component system as it does for a pure NaCl-H<sub>2</sub>O solution.

Assuming the validity of the Trembly and Ogden assumption remains intact, the Driesner model successfully predicts fluid properties such as concentration, specific heat capacity, and density for any solution where the primary dissolved constituent is NaCl. This model accurately predicts behavior across key phase boundaries in the necessary high temperature and pressure process conditions likely to be employed in a supercritical water desalination system, thus its employment in technology design is recommended.

#### **4.6 Comparison of Models**

In an effort to evaluate the accuracy of various concentration prediction models for a hypersalinated brine at high temperatures and pressures, these models were compared against the SoWat predicted curve as well as experimental data. The goal of this comparison is to determine which model, and subsequently which underlying modeling procedure, best provides accurate concentration predictions across the process conditions anticipated in a supercritical water desalination system.

The SoWat predicted concentration curve served as the benchmark for comparison for the 3.2wt% NaCl-H<sub>2</sub>O solution simulations as it was developed

specifically for simulating binary NaCl-H<sub>2</sub>O solutions across these conditions. The SoWat model was empirically-derived and rigorously validated across the desired process conditions, thus building strong confidence in the model's fidelity [7,8]. The other models (HSC, PHREEQC, AspenPlus) have not been validated across these conditions thus a comparison with the SoWat model will provide good insight into their accuracy.

#### **4.6.1 Methods**

A 10 wt% NaCl-H<sub>2</sub>O solution was simulated using the modeling programs HSC, PHREEQC, AspenPlus, and SoWat across the temperature range 25-450 °C and 240bar in order to determine the concentration of NaCl as a function of temperature. These results were scaled accordingly to a starting concentration of 3.2 wt% NaCl to be comparable with experimental data from Bischoff and Pitzer and Leusbrock.<sup>12</sup> The results of each simulation were plotted against the SoWat generated concentration curve as well as experimental data to determine where each model deviates from one another and the data and as a result, determine which model best predicts concentration across the desired temperature range and pressure condition.

The experimental data used for model validation was obtained from Bischoff and Pitzer as well as Leusbrock and is available from 380-450 °C at 240 bar [3,6]. Though this dataset is small, it represents a key region of concern for model accuracy as it encompasses the phase transition near the critical point of the solution.

---

<sup>12</sup> Simulating a 3.2 wt% NaCl-H<sub>2</sub>O solution yielded no difference in concentration with the scaled 10 wt% NaCl-H<sub>2</sub>O solution results as the experienced trend is the same

#### 4.6.2 Results:

The predicted concentration results from each modeling program were plotted as a function of temperature and compared to a set of experimental data produced by Bischoff and Pitzer. The results from these simulations can be seen in **Figure 4.13**.

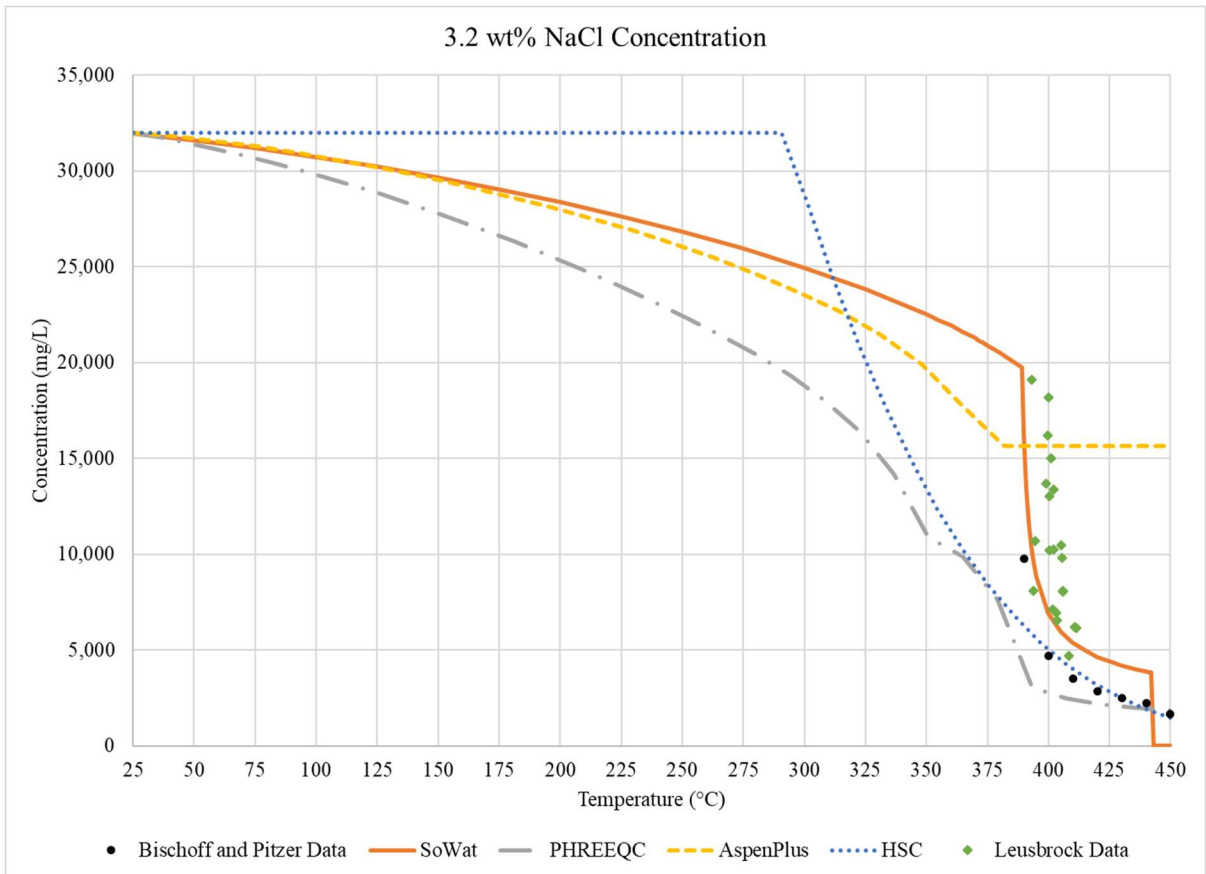


**Figure 4.13:** Predicted concentration of a 3.2 wt% NaCl-H<sub>2</sub>O solution at 240 bar compared with experimental data produced at these same process conditions<sup>13</sup> [6,3]

As can be seen in **Figure 4.13**, there is substantial deviation in predicted concentration between the models being evaluated in this work. All models simulated the same 3.2 wt% NaCl-H<sub>2</sub>O solution across the same process conditions yet yielded substantially different results.

<sup>13</sup> The Leusbrock data was produced at 225-230 bar however remains applicable based on the small temperature variance at these elevated conditions. This data was adjusted to a starting solution concentration of 3.2 wt% NaCl for comparison.

The HSC model deviated from all other evaluated models from 0-300 °C by overestimating NaCl concentration at these conditions compared to the other models. The HSC-predicted concentration curve converges back towards the PHREEQC-predicted concentration curve at 300-450 °C, which underestimates NaCl concentration compared to the SoWat and AspenPlus generated concentration curves at these conditions. The HSC-predicted concentration curve for NaCl shows strong agreement with Bischoff and Pitzer experimental data from 400-450 °C however does not show agreement with the Leusbrock data, underestimating concentration by approximately 14,000 mg/L (~72%).

The SoWat generated NaCl concentration curve follows the AspenPlus generated concentration curve from 25-275 °C. At approximately 275 °C a divergence between the two curves becomes substantial as the AspenPlus concentration curve underestimates concentration compared to the SoWat predictions until approximately 390 °C, when the AspenPlus generated concentration curve becomes unreasonable as it no longer generates new concentration predictions and defaults to the predicted concentration value at 382 °C (15,660 mg/L). The SoWat generated concentration curve shows good agreement with the Leusbrock data as it crosses the critical phase boundary. The SoWat curve continues to show good agreement with the Bischoff and Pitzer experimental data from 390-450 °C, overestimating the concentration by an average of 2,000 mg/L (~39%).

The PHREEQC-predicted concentration curve underestimates NaCl concentration compared to the other models as well as the experimental data throughout the entire temperature range. The greatest divergence from the rest of the models' predicted concentration results occurs from 325-375 °C. The PHREEQC-predicted concentration

shows moderate agreement with the Bischoff and Pitzer data from 400-450 °C, underestimating concentration throughout.

#### **4.6.3 Discussion:**

The comparison of model-predicted NaCl concentration for a 3.2 wt% NaCl-H<sub>2</sub>O solution with each other as well as experimental data yielded clear conclusions regarding the varying accuracies for each model. All models showed substantial deviations for predicted concentration between each other, and a few deviated from selected experimental data as well.

The HSC model, built upon the Gibbs energy minimization theory for equilibrium concentration determination showed good agreement with experimental data from 400-450 °C however it diverged substantially from all other models from approximately 25-350 °C. The divergences from the other models at lower temperatures brings into question the accuracy of this model from the start.

Though the HSC model shows good agreement with the experimental data from 400-450 °C, these predicted values are extrapolations from known species parameters at lower temperatures which makes them inherently less reliable, especially across the phase boundary occurring around 390 °C. The model's agreement with the data may be coincidental as this concentration trend began around 300 °C and showed no regard for the phase boundary change around 390 °C, which disagrees with literature findings substantially. The use of Gibbs energy minimization as a concentration modeling approach depends on the availability of species parameters across all needed temperature and pressure conditions. When these species parameters are not available as needed, the



model extrapolates to predict concentrations, sometimes yielding agreeable results across specific temperature ranges (400-450 °C), however most often not (25-390 °C).

The AspenPlus generated concentration curve showed reasonable agreement with the SoWat model until approximately 275 °C when the concentration decreased at a faster rate than the SoWat-predicted results. Unfortunately, a lack of the necessary species parameters available in the AspenPlus's functional database forced this model to break down at approximately 385 °C and stop producing new concentration values. This lack of data for the model to utilize forces the ELECNRTL-based model to utilize the "last known" concentration value for all process conditions which it doesn't have species parameters available for. This shortfall in the model renders it incapable of predicting produced water concentration at the process conditions of concern.

The PHREEQC-predicted concentration curve underestimates NaCl concentration across the entire temperature range of concern compared to the rest of the evaluated models as well as the selected experimental data. The predicted NaCl concentration curve deviation from the other evaluated models reaches a maximum around 350 °C. The other models' predicted concentration curves converge towards the PHREEQC curve around 400 °C, where the model shows moderate agreement with the experimental data. The consistent underestimation of concentration as the inexplicable trend "pauses" experienced around 360 °C and 400 °C are likely a result of the inconsistencies in datasets used in the model formulation. Though this model shows moderate agreement with experimental data around 400-450 °C, the deviations from the SoWat-derived concentration trend and the inexplicable trend behavior changes at 360 °C and 400 °C reduce the confidence in applying this model to produced water modeling.

The SoWat-predicted NaCl concentration trend serves as the benchmark for simulating a NaCl-H<sub>2</sub>O solution across these conditions as it was designed and validated to do exactly that. The predicted concentration curve shows clear consideration for the phase change occurring at 390 °C as well as another occurring at 444 °C. The model overestimates concentration compared to the Bischoff and Pitzer data available from 390-450 °C however it follows its trend behavior well. This trend agreement comes as no surprise as the Bischoff and Pitzer data served as a deriving dataset for the empirical model formulation which SoWat is based on.

The benefits of applying the SoWat model to produced water simulations go beyond concentration prediction. The SoWat model also predicts phase presence, phase/solution density, molar volume, and specific heat capacity. All of these properties are valuable fluid properties for engineers to know when designing a desalination process which operates at extreme conditions like those evaluated here in this work.

#### **4.7 References**

- [1] Ogden, D. D., and Trembly, J. P., “Desalination of hypersaline brines via Joule-heating: Experimental investigations and comparison of results to existing methods,” in *Desalination*, 2017, vol. 424, pp. 149-158.
- [2] Lwin, Y., Chemical Equilibrium by Gibbs Energy Minimization on Spreadsheets,” in *Int. J. Engng Ed.*, 2000, vol 16, pp. 335-339.
- [3] I. Leusbrock, “Removal of inorganic compounds via supercritical water: fundamentals and applications,” from Groningen: Rijksuniversiteit Groningen, 2011
- [4] Parkhurst, D. L., and Appelo, C. A., J., “Description of Input and Examples for PHREEQC Version 3-A Computer Program for Speciation, Batch-Reaction, One-Dimensional Transport, and Inverse Geochemical Calculations,” from U.S. Geological Survey, U.S. Department of the Interior, 2013.
- [5] “Aspen Physical Property System-Physical Property Methods and Models,” from Aspen Technology, 2006, version number 2006.

- [6] Bischoff, J. and Pitzer, K., "Liquid-vapor relations for the system NaCl-H<sub>2</sub>O: summary of the P-T-x surface from 300° and 500°C," in *American Journal of Science*, 1989, vol 289, 217-248.
- [7] Driesner, T. and Heinrich, C., "The system H<sub>2</sub>O-NaCl. Part I: Correlation formulae for phase relations in temperature-pressure-composition space from 0 to 1000°C, 0 to 5000 bar, and 0 to 1 XNaCl," in *Geochimica et Cosmochimica Acta*, 2007, vol 71, pp 4880-4901.
- [8] Driesner, T., "The system H<sub>2</sub>O-NaCl. Part II: Correlations for molar volume, enthalpy, and isobaric heat capacity from 0 to 1000°C, 1-5000 bar, and 0 to 1 XNaCl," in *Geochimica et Cosmochimica Acta*, 2007, vol 71, pp 4902-4919.

## **Chapter 5: Summary/Future Work**

### **5.1 Summary of work Performed**

Four simulation methods based on different concentration determination methods were evaluated on their ability to accurately predict species concentration, specifically NaCl, across the temperature range 25-450 °C at 240 bar. These models were compared against each other as well as experimental data to determine the most applicable model for produced water simulation. The most applicable model for produced water simulation can then be utilized in supercritical water desalination technological design as a method to efficiently and cost effectively determine necessary system conditions and design.

#### **5.1.1 HSC Equilibrium Modeling**

The evaluation of a concentration model based on Gibbs energy minimization was performed in two steps. First, a 10wt% NaCl-H<sub>2</sub>O solution was simulated across the temperature range 25-450 °C at 200, 220, and 240 bar. The assumption that pressure variance (200-240 bar) at these conditions won't yield significant differences in predicted concentration. The results from the three simulations at different conditions confirmed the assumption made was valid thus all future simulations were completed isobarically at 240 bar (chosen based on concurrent developmental work being performed by colleagues, separate from this work).

Second, once the 10 wt% NaCl-H<sub>2</sub>O solution was simulated across the desired process conditions, a sample of produced water, which was sourced from the Bakken Formation in western North Dakota, was simulated across the same conditions. The validity of the model was assessed based on the 10 wt% NaCl-H<sub>2</sub>O solution simulation results and their performance against other models, primarily the empirically derived SoWat model, as well as a select region of experimental data.

### **5.1.2 PHREEQC Species Distribution Modeling**

The evaluation of a concentration model based on derived equilibrium constants as well as select experimental data was performed in two steps. First, a 10 wt% NaCl-H<sub>2</sub>O solution was simulated across the temperature range 25-450 °C at 240 bar. The solution was modeled isobarically at 240 bar based on the assumption that the small pressure differences at these conditions (200-240 bar) would not yield significant differences in predicted concentration. This assumption was validated by the simulations produced using HSC.

Second, once the 10 wt% NaCl-H<sub>2</sub>O solution was simulated across the desired process conditions, a sample of produced water, which was sourced from the Bakken Formation in western North Dakota, was simulated across the same conditions. The validity of the model was assessed based on the 10 wt% NaCl-H<sub>2</sub>O solution simulation results and their performance against other models, primarily the empirically derived SoWat model, as well as a select region of experimental data.

### **5.1.3 AspenPlus Electrolyte Modeling**

The evaluation of a concentration model based on the ELECNRTL property method was performed in two steps. First, a 10 wt% NaCl-H<sub>2</sub>O solution was simulated across the temperature range 25-450 °C at 240 bar. The solution was modeled isobarically at 240 bar based on the assumption that the small pressure differences at these conditions (200-240 bar) would not yield significant differences in predicted concentration. This assumption was validated by the simulations produced using HSC.

Second, once the 10 wt% NaCl-H<sub>2</sub>O solution was simulated across the desired process conditions, a sample of produced water, which was sourced from the Bakken Formation in western North Dakota, was simulated across the same conditions. The validity of the model was assessed based on the 10 wt% NaCl-H<sub>2</sub>O solution simulation results and their performance against other models, primarily the empirically derived SoWat model, as well as a select region of experimental data.

### **5.1.4 SoWat Empirical NaCl-H<sub>2</sub>O Property Modeling**

The empirically-derived concentration model which supports the program SoWat served as the benchmark for predicted concentration for a 10 wt% NaCl-H<sub>2</sub>O solution across the temperature range 25-450 °C at 240 bar. This program had been rigorously validated across these conditions for a binary NaCl-H<sub>2</sub>O solution, thus this model would inform the accuracy of other models simulating the same solution across the same conditions.

The simulation of a 10 wt% NaCl-H<sub>2</sub>O solution across the temperature range 25-450 °C at 240 bar not only produced predicted concentration data for the process

conditions, but also key fluid properties such as density, specific heat capacity, and which phases are present at each set of process conditions. This model was evaluated primarily on its agreement with a select set of data produced by Bischoff and Pitzer across the temperature range 390-450 °C at 240 bar.

### **5.1.5 Comparison of Models**

The evaluation of each model, and thus their underlying formulations, for their accuracy in determining species concentrations across the temperature range 25-450 °C at 240 bar was accomplished by comparing their predicted results to an empirically-derived model results as well as experimental data. All models simulated a 10 wt% NaCl-H<sub>2</sub>O solution across the same process conditions so they could be properly evaluated against an empirically-derived model produced for binary NaCl-H<sub>2</sub>O simulations.

Because the available experimental data was for a 3.2 wt% NaCl-H<sub>2</sub>O solution, all models were adjusted to have complementary starting solution concentrations. The results of all models were compared to each other, the SoWat model, and the experimental data for evaluation.

## **5.2 Summary of Findings**

The evaluation of the NaCl concentration trends produced by each model found strengths and weaknesses for each model. Once these strengths and weaknesses for each model were evaluated, the applicability to produced water simulation at supercritical conditions was determined for each model.

The HSC model, supported by Gibbs energy minimization, produced a NaCl concentration trend which showed good agreement with experimental data from 400-450

°C at 240 bar. Unfortunately, this model showed substantial deviations from the SoWat predicted concentration curve at lower temperatures. The model was forced to extrapolate key species parameters at higher temperatures which makes the results less reliable for consistent use.

The PHREEQC predicted NaCl concentration trend showed moderate agreement with the experimental data from 400-450 °C at 240 bar. Unfortunately, the model underestimates NaCl concentration compared to the SoWat predicted results as well as experimental data across the entire temperature range of interest. There are a few inexplicable “pauses” in the expected concentration trend that are a result of species parameters inconsistencies between the various databases being used by the model. These weaknesses render the model unreliable in produced water concentration modeling across the process conditions of interest.

The AspenPlus model shows good agreement with the SoWat predicted concentration trend at lower temperatures until deviating around 275 °C, resulting in an underestimation of concentration. The AspenPlus model becomes unusable at approximately 385 °C due to a lack of the necessary species parameters in the AspenPlus database, resulting in a complete breakdown of the model. From 385-400 °C the model predicts a constant NaCl concentration of approximately 15,700 mg/L. This value was chosen as it is the last known calculable value the model could produce with the necessary species parameters available. The breakdown of the model at 385 °C renders the model ineffective at produced water simulation for the purpose of designing a supercritical water desalination system.



The empirically-derived SoWat model serves as the best candidate for simulating produced water streams across the desired process conditions for developing supercritical water desalination systems. The application of this model to produced water streams is contingent on the Trembly and Ogden assumption which states that multi-component streams can be accurately simulated as a binary NaCl-H<sub>2</sub>O stream if the primary constituent is NaCl.

The SoWat model, rigorously validated across the necessary temperature, pressure, and composition range can accurately predict concentration, specific heat capacity, and density for produced water streams. This information can be used confidently by engineers to design effective supercritical water desalination systems swiftly and cost efficiently.

Until other models based on conventional concentration formulations such as Gibbs energy minimization, ELECNRTL property methods, and equilibrium constants have the necessary species parameter data across all process conditions of interest, they will not be adequately prepared to model produced water streams concentration accurately. An empirically-derived method such as the one used by the SoWat program can model key produced water properties such as concentration, specific heat capacity, and density with accuracy when the Trembly and Ogden assumption is applied.

### **5.3 Future Work**

The primary area of focus for future work should be experimental testing that produces concentration data for all species of focus across the temperature range 25-450

°C at 240 bar. Though expensive, time consuming, and tedious, experimental work is the best step forward for improving concentration modeling.

Nearly every model utilized in this study deviated from experimental data as well as the empirically-derived SoWat model due to a lack of available data for the species being evaluated across the desired process conditions. An improved understanding of concentration for various species commonly present in produced water such as ( $\text{Na}^+$ ,  $\text{Cl}^-$ ,  $\text{K}^+$ ,  $\text{Sr}^{2+}$ ,  $\text{Ba}^{2+}$ ,  $\text{Mg}^{2+}$ ,  $\text{SO}_4^{2-}$ , and  $\text{Br}^-$ ) would fill in gaps currently present in species databases which models such as HSC, AspenPlus, and PHREEQC all draw from in order to predict concentration.

A recommended experimental procedure for concentration determination of these species is that which was utilized by Leusbrock and seen in **Figure 5.1** [1].

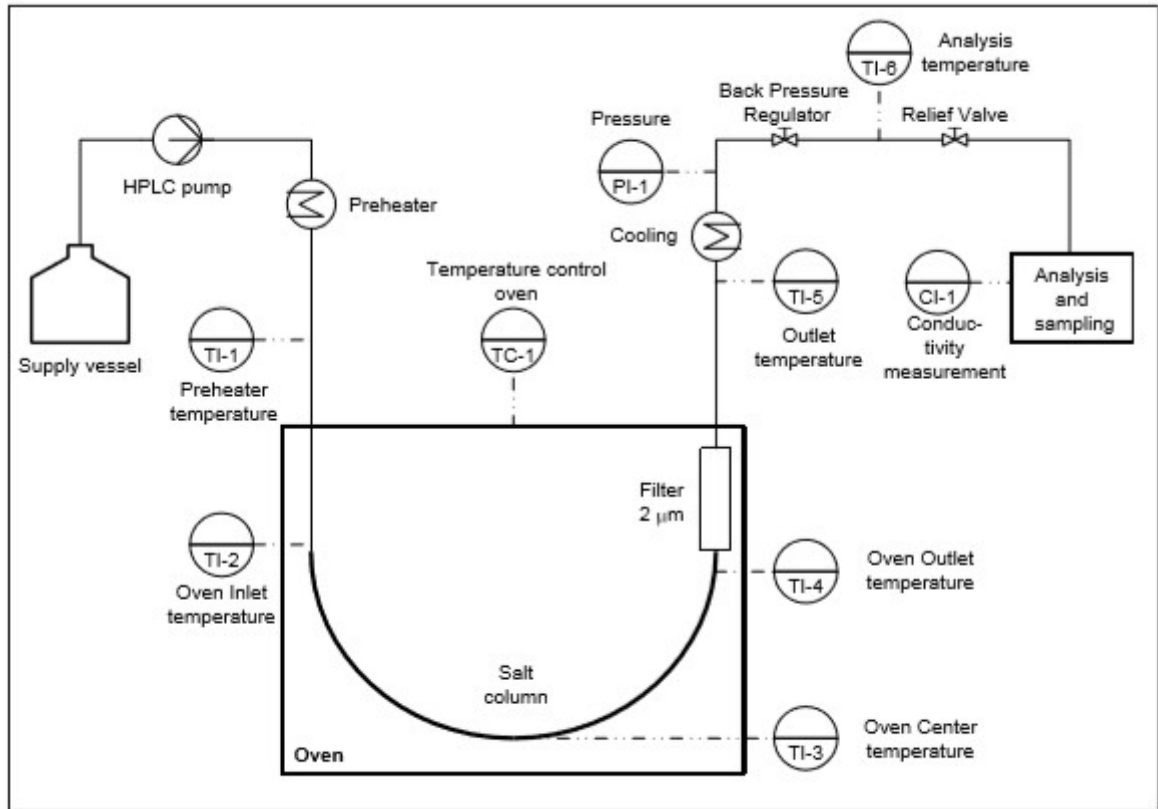


**Figure 5.1:** Experimental apparatus for determination of salt species solubility [1]

The experimental apparatus utilized in Leusbrock's work as seen in **Figure 5.1** produced good results for salt concentrations which agreed with numerous other works.<sup>14</sup> Utilizing an apparatus similar to this will likely produce valuable concentration data which can in turn be utilized by concentration modeling programs to produce valid concentration predictions across a wide range of temperatures and compositions.

Other future work to consider would be a comparison of predicted specific heat capacity as well as density for a sample solution produced by different models. AspenPlus has the ability to predict density as well as specific heat capacity while PHREEQC has the ability to predict solution density. A comparison of these predicted

<sup>14</sup>For more information regarding the results produced using this experimental apparatus see the reference Leusbrock paper (2011) or Section 3.4 of Chapter 3 of this thesis.

properties would provide more insight into the different models' ability to predict solution properties for the purpose of designing a supercritical water desalination system.

#### **5.4 References**

- [1] I. Leusbrock, "*Removal of inorganic compounds via supercritical water: fundamentals and applications,*" from Groningen: Rijksuniversiteit Groningen, **2011**.

# Appendix

## Appendix A: Raw Simulation Data:

**Table A.1: HSC 10 wt% NaCl-H<sub>2</sub>O raw results**

Temperature	200 bar	200 bar	220 bar	220 bar	240 bar	240 bar
°C	Na + (mg/L)	Cl- (mg/L)	Na + (mg/L)	Cl- (mg/L)	Na + (mg/L)	Cl- (mg/L)
25	39339.09865	60665.6399	39339.09865	60665.6399	39339.09865	60665.6399
35.625	39339.09865	60665.6399	39339.09865	60665.6399	39339.09865	60665.6399
46.25	39339.09865	60665.6399	39339.09865	60665.6399	39339.09865	60665.6399
56.875	39339.09865	60665.6399	39339.09865	60665.6399	39339.09865	60665.6399
67.5	39339.09865	60665.6399	39339.09865	60665.6399	39339.09865	60665.6399
78.125	39339.09865	60665.6399	39339.09865	60665.6399	39339.09865	60665.6399
88.75	39339.09865	60665.6399	39339.09865	60665.6399	39339.09865	60665.6399
99.375	39339.09865	60665.6399	39339.09865	60665.6399	39339.09865	60665.6399
110	39339.09865	60665.6399	39339.09865	60665.6399	39339.09865	60665.6399
120.625	39339.09865	60665.6399	39339.09865	60665.6399	39339.09865	60665.6399
131.25	39339.09865	60665.6399	39339.09865	60665.6399	39339.09865	60665.6399
141.875	39339.09865	60665.6399	39339.09865	60665.6399	39339.09865	60665.6399
152.5	39339.09865	60665.6399	39339.09865	60665.6399	39339.09865	60665.6399
163.125	39339.09865	60665.6399	39339.09865	60665.6399	39339.09865	60665.6399
173.75	39339.09865	60665.6399	39339.09865	60665.6399	39339.09865	60665.6399
184.375	39339.09865	60665.6399	39339.09865	60665.6399	39339.09865	60665.6399
195	39339.09865	60665.6399	39339.09865	60665.6399	39339.09865	60665.6399
205.625	39339.09865	60665.6399	39339.09865	60665.6399	39339.09865	60665.6399
216.25	39339.09865	60665.6399	39339.09865	60665.6399	39339.09865	60665.6399
226.875	39339.09865	60665.6399	39339.09865	60665.6399	39339.09865	60665.6399
237.5	39339.09865	60665.6399	39339.09865	60665.6399	39339.09865	60665.6399
248.125	39339.09865	60665.6399	39339.09865	60665.6399	39339.09865	60665.6399
258.75	39339.09865	60665.6399	39339.09865	60665.6399	39339.09865	60665.6399
269.375	39339.09865	60665.6399	39339.09865	60665.6399	39339.09865	60665.6399
280	39339.09865	60665.6399	39339.09865	60665.6399	39339.09865	60665.6399
290.625	39339.09865	60665.6399	39339.09865	60665.6399	39339.09865	60665.6399
301.25	34775.08037	53627.37266	34775.08037	53627.37266	34775.08037	53627.37266
311.875	30007.72983	46275.54252	30007.72983	46275.54252	30007.72983	46275.54252
322.5	25676.84882	39596.80108	25676.84882	39596.80108	25676.84882	39596.80108
333.125	21779.53941	33586.67941	21779.53941	33586.67941	21779.53941	33586.67941
343.75	18306.4833	28230.80757	18306.4833	28230.80757	18306.4833	28230.80757
354.375	15242.56169	23505.87051	15242.56169	23505.87051	15242.56169	23505.87051
365	12567.60991	19380.77188	12567.60991	19380.77188	12567.60991	19380.77188
375.625	10257.27833	15817.96165	10257.27833	15817.96165	10257.27833	15817.96165
386.25	8283.966329	12774.87628	8283.966329	12774.87628	8283.966329	12774.87628
396.875	6617.792583	10205.43519	6617.792583	10205.43519	6617.792583	10205.43519
407.5	5227.563337	8061.533838	5227.563337	8061.533838	5227.563337	8061.533838
418.125	4081.700181	6294.4745	4081.700181	6294.4745	4081.700181	6294.4745
428.75	3149.09151	4856.279328	3149.09151	4856.279328	3149.09151	4856.279328
439.375	2399.836678	3700.837913	2399.836678	3700.837913	2399.836678	3700.837913
450	1805.858952	2784.852543	1805.858952	2784.852543	1805.858952	2784.852543

**Table A.2 HSC produced water simulation raw results**

Temperature, °C	Ca(+2a)	Mg(+2a)	Na(+a)	K(+a)	Li(+a)	Ba(+2a)	Fe(+2a)	Mn(+2a)	Sr(+2a)	Pb(+2a)	Cl(-a)	Br(-a)	SO4(-2a)	F(-a)	HCO3(-a)	NO3(-a)
25.000	22317.151	1429.999	89447.753	7377.909	60.000	0.006	152.000	17.700	1489.249	0.000	189702.424	815.942	2.621	0.081	56.167	63.821
39.167	22313.981	1429.999	89455.089	7385.028	60.000	0.014	152.000	17.700	1495.641	0.000	189719.116	815.960	2.074	0.094	57.836	63.899
53.333	22311.263	1429.999	89458.043	7388.671	60.000	0.030	152.000	17.700	1500.990	0.000	189726.392	815.968	1.467	0.103	58.724	63.935
67.500	22308.958	1429.999	89458.552	7390.715	60.000	0.060	151.999	17.700	1505.517	0.000	189728.687	815.971	0.960	0.107	59.241	63.954
81.667	22307.012	1429.999	89457.269	7391.889	60.000	0.113	151.998	17.700	1509.373	0.000	189727.558	815.973	0.592	0.106	59.559	63.965
95.833	22305.362	1429.999	89454.290	7392.509	60.000	0.202	151.996	17.700	1512.669	0.000	189723.389	815.972	0.347	0.102	59.754	63.971
110.000	22303.948	1429.999	89449.341	7392.714	60.000	0.346	151.988	17.700	1515.496	0.000	189715.853	815.969	0.194	0.094	59.868	63.975
124.167	22302.717	1429.999	89441.702	7392.533	60.000	0.569	151.962	17.700	1517.927	0.000	189703.840	815.965	0.104	0.084	59.918	63.977
138.333	22301.624	1429.999	89429.851	7391.896	60.000	0.902	151.873	17.700	1520.018	0.000	189684.875	815.957	0.052	0.072	59.904	63.978
152.500	22300.627	1429.999	89410.399	7390.558	60.000	1.378	151.536	17.700	1521.808	0.000	189653.276	815.945	0.025	0.060	59.809	63.977
166.667	22299.693	1429.999	89374.268	7387.794	60.000	2.035	150.151	17.699	1523.286	0.000	189593.369	815.921	0.010	0.046	59.566	63.973
180.833	22298.776	1429.999	89286.247	7380.720	59.999	2.907	143.464	17.696	1524.236	0.000	189442.785	815.862	0.004	0.032	58.902	63.961
195.000	22297.683	1429.999	88840.351	7344.294	59.999	4.021	100.198	17.669	1522.016	0.000	188666.187	815.563	0.001	0.016	55.611	63.896
209.167	22291.854	1429.999	84141.840	6972.336	59.991	5.373	11.750	17.059	1457.075	0.000	180922.282	812.251	0.000	0.005	35.378	63.249
223.333	22254.714	1429.999	74254.782	6231.937	59.967	6.904	1.529	13.769	1162.484	0.000	164697.743	804.274	0.000	0.002	20.309	62.009
237.500	22100.033	1429.999	64097.122	5504.291	59.918	8.558	0.318	7.763	688.110	0.000	147717.650	794.259	0.000	0.001	14.154	60.841
251.667	21536.839	1429.998	54410.780	4819.145	59.830	10.265	0.079	3.051	306.435	0.000	130857.062	782.264	0.000	0.001	10.876	59.762
265.833	19773.480	1429.993	45514.112	4182.091	59.675	11.679	0.021	1.019	118.622	0.000	113295.152	767.608	0.000	0.000	8.738	58.688
280.000	15702.599	1429.968	37951.222	3628.050	59.420	12.031	0.006	0.341	45.812	0.000	93878.466	748.693	0.000	0.000	7.088	57.473
294.167	9893.237	1429.855	32046.573	3186.767	59.036	10.644	0.002	0.122	18.776	0.000	74084.108	723.552	0.000	0.000	5.710	56.008
308.333	4841.371	1429.381	27221.530	2815.641	58.468	7.737	0.001	0.045	7.858	0.000	57371.478	691.752	0.000	0.000	4.607	54.355
322.500	1899.215	1427.289	22721.700	2449.730	57.576	4.480	0.000	0.016	3.146	0.000	44898.041	654.536	0.000	0.000	3.772	52.654
336.667	637.499	1417.608	18390.175	2072.603	56.133	2.109	0.000	0.005	1.178	0.000	35626.258	612.979	0.000	0.000	3.138	51.021
350.833	195.801	1372.642	14448.069	1705.289	53.834	0.865	0.000	0.002	0.418	0.000	28310.539	567.002	0.000	0.000	2.630	49.585
365.000	57.979	1189.343	11133.713	1376.550	50.364	0.332	0.000	0.000	0.145	0.000	22128.969	515.082	0.000	0.000	2.189	48.547
379.167	17.469	733.083	8596.788	1111.846	45.653	0.128	0.000	0.000	0.051	0.000	16578.061	453.439	0.000	0.000	1.766	48.124
393.333	5.295	264.685	6629.293	896.185	39.695	0.049	0.000	0.000	0.018	0.000	11960.877	384.110	0.000	0.000	1.382	48.816
407.500	1.505	63.281	4948.763	699.968	32.344	0.018	0.000	0.000	0.006	0.000	8588.824	316.484	0.000	0.000	1.081	50.907
421.667	0.399	12.545	3566.217	528.174	24.263	0.006	0.000	0.000	0.002	0.000	6136.521	254.036	0.000	0.000	0.844	53.152
435.833	0.100	2.295	2498.856	387.675	16.680	0.002	0.000	0.000	0.001	0.000	4318.835	197.745	0.000	0.000	0.652	53.802
450.000	0.024	0.397	1706.271	277.420	10.559	0.001	0.000	0.000	0.000	0.000	2982.160	149.011	0.000	0.000	0.497	52.633

**Table A.3: PHREEQC10 wt% NaCl-H<sub>2</sub>O raw results**

<b>Temperature</b>	<b>Cl-</b>	<b>Na+</b>	<b>Na+</b>	<b>NaCl</b>	<b>Adjusted NaCl (0.78)</b>
<b>C</b>	<b>mg/L</b>	<b>mg/L</b>	<b>Mole</b>	<b>mg/L</b>	<b>mg/L</b>
25	189700.0833	89470.64966	3.907015269	138503.6913	108014.6801
39.17	187789.1592	88558.01549	3.867162248	137090.9017	106912.8899
53.33	185613.2749	87547.34774	3.823028285	135526.3527	105692.7472
67.5	183197.6204	86407.96723	3.773273678	133762.5519	104317.2143
81.67	180554.7657	85161.42431	3.718839489	131832.8599	102812.3081
95.83	177712.0392	83809.85839	3.659819144	129740.5886	101180.6115
110	174628.3057	82355.55473	3.596312434	127489.2758	99424.88326
124.17	171336.2998	80803.02878	3.528516541	125085.9114	97550.57483
138.33	167838.0255	79153.22567	3.456472737	122531.9585	95558.82719
152.5	164141.1652	77409.76847	3.380339235	119833.0259	93454.01436
166.67	160245.1259	75572.37744	3.300103819	116988.6804	91235.79861
180.83	156152.6373	73642.34	3.215822707	114000.915	88905.73419
195	151883.9817	71620.0358	3.12751248	110870.3174	86464.27945
209.17	147398.7073	69505.0299	3.035154144	107596.2144	83910.90931
223.33	142709.3724	67293.80043	2.938593905	104173.1539	81241.37194
237.5	137789.9631	64974.0807	2.8372961	100582.1468	78440.85818
251.67	132621.4571	62525.87139	2.730387397	96792.23323	75485.22361
265.83	127133.4033	59938.46698	2.617400305	92786.8408	72361.54382
280	121199.3744	57140.80258	2.495231554	88455.95858	68984.02476
294.17	114636.5831	54046.70112	2.360117953	83666.18142	65248.62794
308.33	107009.0452	50444.14406	2.202801051	78089.29725	60899.39108
322.5	97427.89646	45927.58338	2.005571327	71097.50353	55446.71069
336.67	84088.60991	39632.4414	1.730674297	61352.40382	47846.8134
350.83	64668.47154	30479.38848	1.330977663	47183.15815	36796.66358
365	58642.92035	27639.44019	1.206962454	42786.81898	33368.0967
379.17	45304.9017	21352.99731	0.932445298	33055.1858	25778.70154
393.33	18069.5895	8516.515466	0.371900239	13183.86346	10281.68117
407.5	14652.64617	6906.049955	0.301574234	10690.80659	8337.42439
421.67	12921.16189	6089.970949	0.265937596	9427.48778	7352.201715
435.83	11784.84052	5554.402694	0.242550336	8598.409411	6705.629527
450	10949.55105	5161.626567	0.22539854	7990.378245	6231.445111

**Table A.4: PHREEQC produced water concentration raw results**

Temperature	NO3-	Na+	Pb	SO4-2	Mn (2)	Mg	Li	K	Fe (3)	Ba+2	Br-	Ca+2	Cl-	HCO3-	F-	Sr
C	mg/L	mg/L	mg/L	mg/L	mg/L	mg/L	mg/L	mg/L	mg/L	mg/L	mg/L	mg/L	mg/L	mg/L	mg/L	mg/L
25.00	249.56	89470.65	0.51	22.18	17.70	1429.59	60.03	7399.91	152.01	32.95	816.22	22351.73	189700.08	1.27	1.04	1539.85
39.17	247.01	88558.02	0.50	20.44	17.52	1415.00	59.42	7324.43	150.46	32.61	807.89	22123.73	187789.16	1.14	0.85	1524.14
53.33	244.15	87547.35	0.50	19.17	17.32	1398.61	58.73	7239.56	148.71	32.24	798.53	21870.08	185613.27	1.04	0.71	1506.48
67.50	240.97	86407.97	0.49	18.24	17.09	1380.41	57.96	7145.34	146.78	31.83	788.14	21588.11	183197.62	0.95	0.62	1486.88
81.67	237.50	85161.42	0.48	17.57	16.84	1360.49	57.13	7042.26	144.62	31.37	776.77	21279.29	180554.77	0.83	0.54	1465.43
95.83	233.73	83809.86	0.48	17.09	16.58	1338.90	56.22	6930.50	142.33	30.89	764.44	20946.73	177712.04	0.68	0.48	1442.17
110.00	229.67	82355.55	0.47	16.80	16.29	1315.67	55.25	6810.24	139.82	30.35	751.18	20585.79	174628.31	0.54	0.44	1417.14
124.17	225.34	80803.03	0.46	16.65	15.98	1290.86	54.20	6681.85	137.15	29.78	737.02	20200.20	171336.30	0.40	0.41	1390.43
138.33	220.78	79153.23	0.45	16.63	15.66	1264.51	53.10	6545.43	134.32	29.18	721.97	19790.19	167838.03	0.28	0.38	1362.04
152.50	215.92	77409.77	0.44	16.74	15.31	1236.66	51.93	6401.25	131.29	28.54	706.07	19354.29	164141.17	0.19	0.36	1332.04
166.67	210.79	75572.38	0.43	16.96	14.95	1207.30	50.70	6249.31	128.11	27.86	689.31	18894.89	160245.13	0.12	0.34	1300.42
180.83	205.41	73642.34	0.42	17.27	14.57	1176.47	49.40	6089.71	124.71	27.15	671.70	18412.34	156152.64	0.08	0.33	1267.21
195.00	199.73	71620.04	0.41	17.65	14.17	1144.16	48.04	5922.48	121.17	26.41	653.26	17904.51	151883.98	0.04	0.33	1232.41
209.17	193.84	69505.03	0.39	18.09	13.75	1110.37	46.63	5747.59	117.38	25.63	633.97	17373.64	147398.71	0.02	0.32	1196.02
223.33	187.67	67293.80	0.38	18.54	13.31	1075.05	45.14	5564.73	113.42	24.81	613.80	16818.85	142709.37	0.01	0.32	1157.97
237.50	181.17	64974.08	0.37	18.91	12.85	1038.11	43.59	5372.91	109.23	23.96	592.64	16235.08	137789.96	0.00	0.33	1118.05
251.67	174.37	62525.87	0.36	19.12	12.37	999.17	41.95	5171.37	104.78	23.06	570.41	15624.18	132621.46	0.00	0.33	1076.11
265.83	167.16	59938.47	0.34	18.96	11.86	957.82	40.22	4957.37	100.06	22.11	546.80	14977.63	127133.40	0.00	0.34	1031.58
280.00	159.36	57140.80	0.32	18.10	11.30	913.12	38.34	4725.98	94.97	21.07	521.28	14278.54	121199.37	0.00	0.35	983.43
294.17	150.73	54046.70	0.31	16.10	10.69	863.67	36.26	4470.08	89.41	19.93	493.05	13505.37	114636.58	0.00	0.36	930.18
308.33	140.70	50444.14	0.29	12.39	9.98	806.10	33.85	4172.12	83.07	18.60	460.19	12606.71	107009.05	0.00	0.37	868.18
322.50	128.11	45927.58	0.26	6.93	9.09	733.93	30.81	3798.56	75.35	16.94	418.99	11477.95	97427.90	0.00	0.38	790.44
336.67	110.49	39632.44	0.23	1.77	7.84	633.44	26.60	3278.49	65.04	14.62	361.62	9906.46	84088.61	0.00	0.40	682.22
350.83	84.77	30479.39	0.17	0.07	6.03	487.15	20.45	2521.32	50.39	11.24	278.11	7618.57	64668.47	0.00	0.39	524.66
365.00	76.82	27639.44	0.16	0.07	5.47	441.76	18.55	2286.40	45.51	10.20	252.19	6908.71	58642.92	0.00	0.28	475.78
379.17	59.31	21353.00	0.12	0.07	4.23	341.28	14.33	1766.37	35.00	7.88	194.83	5337.36	45304.90	0.00	0.17	367.56
393.33	23.63	8516.52	0.05	0.03	1.69	136.12	5.72	704.51	13.89	3.14	77.71	2128.77	18069.59	0.00	0.05	146.60
407.50	19.14	6906.05	0.04	0.03	1.37	110.38	4.63	571.28	11.19	2.55	63.01	1726.22	14652.65	0.00	0.03	118.88
421.67	16.85	6089.97	0.03	0.03	1.21	97.34	4.09	503.78	9.80	2.25	55.57	1522.24	12921.16	0.00	0.02	104.83
435.83	15.34	5554.40	0.03	0.03	1.10	88.78	3.73	459.47	8.86	2.05	50.68	1388.37	11784.84	0.00	0.01	95.61
450.00	14.22	5161.63	0.03	0.03	1.02	82.48	3.46	426.91	8.15	1.90	47.09	1289.96	10949.55	0.00	0.01	88.84



**Table A.5:** AspenPlus 10 wt% NaCl-H<sub>2</sub>O raw results

<b>Temperature</b>	<b>Na</b>	<b>Na</b>	<b>Cl</b>	<b>Cl</b>	<b>NaCl</b>
<b>°C</b>	<b>mol/L</b>	<b>mg/L</b>	<b>mol/L</b>	<b>mg/L</b>	<b>mg/L</b>
25	1.84844	42495.6	1.84821	65519	108015
42	1.83758	42246	1.83735	65134.1	107380
59	1.82334	41918.6	1.82311	64629.2	106548
76	1.80625	41525.7	1.80603	64023.8	105549
93	1.7867	41076.2	1.78648	63330.7	104407
110	1.76495	40576.2	1.76473	62559.7	103136
127	1.74115	40029	1.74093	61716	101745
144	1.71537	39436.4	1.71515	60802.1	100238
161	1.68761	38798.2	1.6874	59818.3	98616.5
178	1.65782	38113.3	1.65761	58762.3	96875.6
195	1.62588	37379	1.62567	57630	95009
212	1.59159	36590.7	1.59139	56414.8	93005.4
229	1.55471	35742.8	1.55452	55107.7	90850.5
246	1.51486	34826.6	1.51467	53695.1	88521.7
263	1.47149	33829.6	1.47131	52157.9	85987.5
280	1.42385	32734.3	1.42367	50469.1	83203.4
297	1.37073	31513.1	1.37056	48586.4	80099.4
314	1.31023	30122.2	1.31007	46442	76564.2
331	1.23908	28486.4	1.23892	43919.7	72406.2
348	1.15076	26456	1.15061	40789.1	67245.1
365	1.02448	23552.8	1.02435	36313.2	59866
382	0.90464	20797.7	0.90453	32065.5	52863.2
399	0.90464	20797.7	0.90453	32065.5	52863.2
416	0.90464	20797.7	0.90453	32065.5	52863.2
433	0.90464	20797.7	0.90453	32065.5	52863.2
450	0.90464	20797.7	0.90453	32065.5	52863.2

**Table A.6: AspenPlus produced water raw results**

Temperature	H2O	Na+	Cl-	Ca 2-	Mg 2+	K+	Li+	Ba 2+	Fe 2+	Mn 2+	Sr 2+	Pb 2+	Br-	SO4 2-	F-	HCO3-	NO3-
°C	mg/L	mg/L	mg/L	mg/L	mg/L	mg/L	mg/L	mg/L	mg/L	mg/L	mg/L	mg/L	mg/L	mg/L	mg/L	mg/L	mg/L
25	914895	81883.1	173647	20493.6	1308.3	6770.22	54.8936	30.1915	139.064	16.4681	1408.94	0.9149	746.554	180.234	30.1915	55.8085	58.5532
42	909523	81402.3	172627	20373.3	1300.62	6730.47	54.5713	30.0142	138.248	16.3714	1400.67	0.90952	742.171	179.176	30.0142	55.4808	58.2094
59	902473	80771.4	171289	20215.4	1290.54	6678.3	54.1483	29.7816	137.176	16.2445	1389.81	0.90247	736.418	177.787	29.7816	55.0508	57.7582
76	894016	80014.4	169684	20026	1278.44	6615.72	53.6409	29.5025	135.89	16.0922	1376.79	0.89402	729.517	176.121	29.5025	54.5349	57.217
93	884340	79148.4	167848	19809.2	1264.61	6544.12	53.0603	29.1832	134.42	15.9181	1361.88	0.88434	721.621	174.215	29.1832	53.9447	56.5977
110	873573	78184.8	165804	19568	1249.21	6464.44	52.4143	28.8279	132.783	15.7243	1345.3	0.87357	712.836	172.094	28.8279	53.2879	55.9086
127	861793	77130.4	163568	19304.2	1232.36	6377.26	51.7075	28.4391	130.993	15.5122	1327.16	0.86179	703.223	169.773	28.4391	52.5693	55.1547
144	849032	75988.4	161146	19018.3	1214.12	6282.84	50.9419	28.018	129.053	15.2825	1307.51	0.84903	692.81	167.259	28.018	51.7909	54.338
161	835294	74758.8	158539	18710.6	1194.47	6181.17	50.1176	27.5646	126.965	15.0352	1286.35	0.83529	681.6	164.553	27.5646	50.9529	53.4588
178	820548	73439	155740	18380.3	1173.38	6072.06	49.2328	27.078	124.723	14.7698	1263.64	0.82055	669.567	161.648	27.078	50.0534	52.515
195	804737	72023.9	152739	18026.1	1150.77	5955.05	48.2842	26.5563	122.32	14.4852	1239.29	0.80474	656.665	158.533	26.5563	49.0889	51.5031
212	787769	70505.3	149519	17646	1126.51	5829.49	47.2661	25.9963	119.741	14.1798	1213.16	0.78777	642.82	155.191	25.9963	48.0539	50.4172
229	769514	68871.5	146054	17237.1	1100.41	5694.4	46.1708	25.3939	116.966	13.8512	1185.05	0.76951	627.923	151.594	25.3939	46.9403	49.2488
246	749787	67105.9	142310	16795.2	1072.2	5548.42	44.9872	24.7429	113.968	13.4961	1154.67	0.74979	611.826	147.708	24.7429	45.737	47.9863
263	728325	65185.1	138236	16314.5	1041.5	5389.6	43.6994	24.0347	110.705	13.1098	1121.62	0.72833	594.313	143.48	24.0347	44.4278	46.6127
280	704742	63074.4	133760	15786.2	1007.78	5215.09	42.2845	23.2564	107.121	12.6853	1085.3	0.70474	575.069	138.834	23.2564	42.9892	45.1034
297	678450	60721.3	128770	15197.3	970.184	5020.53	40.707	22.3888	103.124	12.2121	1044.81	0.67845	553.615	133.655	22.3888	41.3854	43.4208
314	648508	58041.4	123087	14526.6	927.366	4798.96	38.9104	21.4007	98.5731	11.6731	998.702	0.64851	529.182	127.756	21.4007	39.5589	41.5044
331	613290	54889.4	116402	13737.7	877.004	4538.34	36.7973	20.2385	93.22	11.0392	944.466	0.61329	500.444	120.818	20.2385	37.4106	39.2505
348	569575	50977	108105	12758.5	814.492	4214.85	34.1744	18.7959	86.5753	10.2523	877.145	0.56958	464.773	112.206	18.7959	34.744	36.4527
365	507073	45383	96242.4	11358.4	725.114	3752.34	30.4243	16.7333	77.075	9.12731	780.892	0.50707	413.771	99.8932	16.7333	30.9314	32.4526
382	447758	40074.3	84984.4	10029.8	640.294	3313.41	26.8654	14.776	68.0591	8.05964	689.547	0.44776	365.37	88.2082	14.776	27.3132	28.6564
399	447758	40074.3	84984.4	10029.8	640.294	3313.41	26.8654	14.776	68.0591	8.05964	689.547	0.44776	365.37	88.2082	14.776	27.3132	28.6564
416	447758	40074.3	84984.4	10029.8	640.294	3313.41	26.8654	14.776	68.0591	8.05964	689.547	0.44776	365.37	88.2082	14.776	27.3132	28.6564
433	447758	40074.3	84984.4	10029.8	640.294	3313.41	26.8654	14.776	68.0591	8.05964	689.547	0.44776	365.37	88.2082	14.776	27.3132	28.6564
450	447758	40074.3	84984.4	10029.8	640.294	3313.41	26.8654	14.776	68.0591	8.05964	689.547	0.44776	365.37	88.2082	14.776	27.3132	28.6564

**Table A.7: SoWat simulation raw results (part 1)**

Temperature	X <sub>NaCl</sub>	Phases Present	L Density	L Molar Volume	L Cp	V Density	V Molar Volume	V Cp	S Density	S Molar Volume	S Cp
°C	Mole Fraction	L,V,S	kg/m <sup>3</sup>	cm <sup>3</sup> /mol	J/kg-K	kg/m <sup>3</sup>	cm <sup>3</sup> /mol	J/kg-K	kg/m <sup>3</sup>	cm <sup>3</sup> /mol	J/kg-K
20	0.033117828	L	1080.1	17.918	3652						
25	0.033117828	L	1078.1	17.951	3656.2						
50	0.033117828	L	1066.6	18.146	3664.9						
75	0.033117828	L	1052.9	18.382	3672.3						
100	0.033117828	L	1037.4	18.657	3690.1						
125	0.033117828	L	1020.1	18.973	3716.1						
150	0.033117828	L	1001	19.334	3748.3						
175	0.033117828	L	980.19	19.745	3788.6						
200	0.033117828	L	957.47	20.214	3841.3						
225	0.033117828	L	932.7	20.751	3912.6						
250	0.033117828	L	905.59	21.372	4010.5						
275	0.033117828	L	875.73	22.1	4146.2						
300	0.033117828	L	842.44	22.974	4338.6						
325	0.033117828	L	804.65	24.053	4625.6						
350	0.033117828	L	760.41	25.452	5099.4						
355	0.033117828	L	750.51	25.788	5235.1						
360	0.033117828	L	740.15	26.149	5392.7						
365	0.033117828	L	729.28	26.538	5578.2						
370	0.033117828	L	717.83	26.962	5800.9						
371	0.033117828	L	715.47	27.051	5850.9						
372	0.033117828	L	713.07	27.142	5903.1						
373	0.033117828	L	710.65	27.234	5957.6						
374	0.033117828	L	708.19	27.329	6014.5						
375	0.033117828	L	705.71	27.425	6074.1						
380	0.033117828	L	692.78	27.937	6419.4						
385	0.033117828	L	678.91	28.508	6873						
386	0.033117828	L	676	28.63	6981.7						
387	0.033117828	L	673.04	28.756	7098						
388	0.033117828	L	670.03	28.885	7222.7						
389	0.033117828	L	666.97	29.018	7356.9						
390	0.033117828	L+V	678.43	28.722	7046.4	181.22	99.477	19266			
391	0.033117828	L+V	695.2	28.301	6622	176.46	102.16	17738			
392	0.033117828	L+V	710.99	27.94	6269.3	172.23	104.67	16479			
393	0.033117828	L+V	725.92	27.627	5969.9	168.44	107.02	15423			
394	0.033117828	L+V	740.12	27.354	5711.6	165	109.24	14521			
395	0.033117828	L+V	753.66	27.114	5485.7	161.87	111.36	13743			
400	0.033117828	L+V	813.45	26.263	4666.4	149.36	120.67	11016			
405	0.033117828	L+V	863.74	25.769	4133.9	140.2	128.55	9357.8			
410	0.033117828	L+V	907.84	25.466	3744.3	133.02	135.48	8230.1			
415	0.033117828	L+V	947.68	25.28	3438	127.13	141.75	7407.2			
420	0.033117828	L+V	984.33	25.17	3186.1	122.17	147.51	6777.5			
425	0.033117828	L+V	1018.3	25.115	2973.5	117.88	152.87	6278.5			
430	0.033117828	L+V	1049.8	25.103	2791.6	114.12	157.9	5872.7			
435	0.033117828	L+V	1078.9	25.122	2634.4	110.78	162.67	5535.8			
440	0.033117828	L+V	1105.7	25.168	2497.8	107.77	167.21	5251.5			
441	0.033117828	L+V	1110.8	25.179	2472.6	107.2	168.09	5199.9			
442	0.033117828	L+V	1115.8	25.191	2448.1	106.64	168.97	5149.8			
443	0.033117828	S+V				105.96	170.06	5097.2	2045.2	551.55	984.1
444	0.033117828	S+V				105.43	170.91	5050.2	2044.9	554.34	984.5
445	0.033117828	S+V				104.91	171.77	5004.6	2044.5	557.1	984.8
446	0.033117828	S+V				104.39	172.61	4960.3	2044.2	559.84	985.2
447	0.033117828	S+V				103.89	173.45	4917.3	2043.9	562.56	985.6
448	0.033117828	S+V				103.39	174.28	4875.4	2043.5	565.26	985.9
449	0.033117828	S+V				102.9	175.1	4834.7	2043.2	567.93	986.3
450	0.033117828	S+V				102.43	175.92	4795.1	2042.9	570.59	986.7

**Table A.8:** SoWat simulation raw results (part 2)

Temperature	L	V	S	Mass Fraction L	Mass Fraction V	Mass Fraction S	Mass Weighted Cp	Mass Weighted Density
°C	X <sub>NaCl</sub>	X <sub>NaCl</sub>	X <sub>NaCl</sub>	YL	YV	YS	J/kg-K	kg/m <sup>3</sup>
20	0.033117828			1	0	0	3652	1080.1
25	0.033117828			1	0	0	3656.2	1078.1
50	0.033117828			1	0	0	3664.9	1066.6
75	0.033117828			1	0	0	3672.3	1052.9
100	0.033117828			1	0	0	3690.1	1037.4
125	0.033117828			1	0	0	3716.1	1020.1
150	0.033117828			1	0	0	3748.3	1001
175	0.033117828			1	0	0	3788.6	980.19
200	0.033117828			1	0	0	3841.3	957.47
225	0.033117828			1	0	0	3912.6	932.7
250	0.033117828			1	0	0	4010.5	905.59
275	0.033117828			1	0	0	4146.2	875.73
300	0.033117828			1	0	0	4338.6	842.44
325	0.033117828			1	0	0	4625.6	804.65
350	0.033117828			1	0	0	5099.4	760.41
355	0.033117828			1	0	0	5235.1	750.51
360	0.033117828			1	0	0	5392.7	740.15
365	0.033117828			1	0	0	5578.2	729.28
370	0.033117828			1	0	0	5800.9	717.83
371	0.033117828			1	0	0	5850.9	715.47
372	0.033117828			1	0	0	5903.1	713.07
373	0.033117828			1	0	0	5957.6	710.65
374	0.033117828			1	0	0	6014.5	708.19
375	0.033117828			1	0	0	6074.1	705.71
380	0.033117828			1	0	0	6419.4	692.78
385	0.033117828			1	0	0	6873	678.91
386	0.033117828			1	0	0	6981.7	676
387	0.033117828			1	0	0	7098	673.04
388	0.033117828			1	0	0	7222.7	670.03
389	0.033117828			1	0	0	7356.9	666.97
390	0.036372	3.10E-04		0.915945531	0.084054469	0	8073.511987	636.6372776
391	0.041056	2.97E-04		0.818592542	0.181407458	0	8638.525299	601.0966954
392	0.045756	2.85E-04		0.74112166	0.25887834	0	8912.370192	571.5167053
393	0.05046	2.74E-04		0.678149285	0.321850715	0	9012.386996	546.4946633
394	0.055158	2.63E-04		0.626052334	0.373947666	0	9005.854566	525.0552185
395	0.059842	2.54E-04		0.582304188	0.417695812	0	8934.739632	506.4717951
400	0.082836	2.15E-04		0.43959065	0.56040935	0	8224.77521	441.2877547
405	0.10494	1.89E-04		0.361512451	0.638487549	0	7469.295106	401.7687189
410	0.12625	1.70E-04		0.312159109	0.687840891	0	6829.81667	374.8871206
415	0.14698	1.56E-04		0.277889531	0.722110469	0	6304.200874	355.1522545
420	0.16722	1.45E-04		0.252630568	0.747369432	0	5870.202577	339.9779709
425	0.18699	1.36E-04		0.233239703	0.766760297	0	5507.642782	327.8936934
430	0.20622	1.28E-04		0.21794864	0.78205136	0	5201.178446	318.0501834
435	0.22483	1.21E-04		0.205645017	0.794354983	0	4939.141546	309.8690543
440	0.24274	1.13E-04		0.195589703	0.804410297	0	4712.904634	302.9548326
441	0.24623	1.12E-04		0.193801052	0.806198948	0	4671.346392	301.6987356
442	0.2497	1.10E-04		0.192072388	0.807927612	0	4630.878029	300.4717711
443		1.09E-04	1	0	0.900308365	0.099711018	4687.179408	299.3256491
444		1.06E-04	1	0	0.900303417	0.099711018	4644.875821	298.8180506
445		1.04E-04	1	0	0.90029863	0.099711018	4603.833925	298.3095063
446		1.01E-04	1	0	0.900293985	0.099711018	4563.963549	297.8109527
447		9.91E-05	1	0	0.900289285	0.099711018	4525.26469	297.3304042
448		9.70E-05	1	0	0.900285076	0.099711018	4487.557944	296.8399399
449		9.49E-05	1	0	0.900280806	0.099711018	4450.931595	296.3684476
450		9.29E-05	1	0	0.900276654	0.099711018	4415.296459	295.914977